#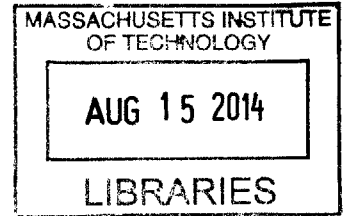 Numerical Fixed-Effectiveness and Fixed-Area Models of the Humidification Dehumidification Desalination System with Air Extractions and Injections

by

Karim Malek Chehayeb

B.Eng., Mechanical Engineering
American University of Beirut, Lebanon, 2012

Submitted to the Department of Mechanical Engineering
in partial fulfillment of the requirements for the degree of
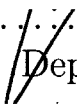
Master of Science in Mechanical Engineering

at the

MASSACHUSETTS INSTITUTE OF TECHNOLOGY

June 2014

Signature redacted

Author . . . .
Department of Mechanical Engineering
April 30, 2014

Signature redacted

Certified by . . . .
John H. Lienhard V
Collins Professor of Mechanical Engineering
Thesis Supervisor

Signature redacted

Accepted by . . . .
David E. Hardt
Chairman, Department Committee on Graduate Theses

Numerical Fixed-Effectiveness and Fixed-Area Models of the Humidification Dehumidification Desalination System with Air Extractions and Injections

by

Karim Malek Chehayeb

Abstract

The humidification dehumidification (HDH) desalination system can be advantageous in small-scale, off-grid applications. This system is very robust and can tolerate a wide range of feed salinities, making it a good candidate for treating produced water from hydraulically fractured natural gas wells. The main drawback of this technology has been its low energy efficiency, which results in high water production costs. This work focuses on the thermodynamic balancing of HDH. The first part uses a fixed-effectiveness approach to model the use of multiple air extractions and injections to thermodynamically balance the HDH system, so as to make it more energy efficient. The effect of the number of extractions on several performance parameters is studied. In addition, we study the effect of the enthalpy pinch, which is a measure of performance for a heat and mass exchanger, on these performance parameters. Further, we present results that can be used as guidelines in designing HDH systems. These results include the identification of appropriate temperatures for the extracted/injected air streams, the division of the heat duty between stages, and the value of the mass flow rate ratio in each stage at various values of enthalpy pinch. Fixing the effectiveness of the heat and mass exchangers allows them to be modeled without explicitly sizing the components and gives insight on how the cycle design can be improved. However, linking the findings of fixed-effectiveness models to actual systems can be challenging, as the performance of the components depends mainly on the available surface areas and the flow rates of the air and water streams. In the second part of this study, we present a robust numerical solution algorithm for a heat and mass transfer model of a complete humidification-dehumidification system consisting of a packed-bed humidifier and a multi-tray bubble column dehumidifier. We look at the effect of varying the water-to-air mass flow rate ratio on the energy efficiency of the system. In addition, we study the effect of the top and bottom temperatures on the performance of the system. We recommended the implementation a control system that varies the mass flow rate ratio in order to keep the system balanced in off-design

conditions, especially with varying top temperature. Finally we consider a single air extraction, and look at the effect of the location of extraction, and its direction. We define the criteria for achieving a completely balanced system.

Thesis Supervisor: John H. Lienhard V
Title: Collins Professor of Mechanical Engineering

Acknowledgments

This work would not have been possible without my advisor, Prof. John Lienhard. His guidance, expertise, and trust were always key in moving this work forward. I would like to thank him for giving me the chance to work on a topic that can have a huge influence on the world we live in.

I would like to thank Prakash Narayan for being a great mentor, starting in the summer of 2011 when I first came to MIT for a research internship. The trust he put in my abilities from the first day has been invaluable, and played a huge role in bringing me to where I am today.

I would also like to thank Prof. Syed Zubair for always showing interest in my work, and for providing me with some of his vast expertise. Big thanks to Farah Cheaib for her contribution to the work presented in Chapter 3 of this thesis. Many thanks to my friends, the members of the Lienhard research group, for their support and advice, and mainly for making our lab a great place to work and evolve.

I can never thank my family enough for all they have done for me throughout the years. Their hard work and love play a major role in making me who I am today.

Ruth, thanks for always being there for me. Huge thanks to my friends at MIT for making my time here truly special.

Contents

List of Figures

12

List of Tables

Nomenclature

Acronyms

GOR	Gained Output Ratio
HDH	Humidification Dehumidification
HE	Heat Exchanger
HME	Heat and Mass Exchanger
RR	Recovery Ratio

Symbols

A	area [m^2]
a	surface area per unit volume of packing[m^{-1}]
c_p	specific heat capacity at constant pressure [J/kg·K]
D	diameter [m]
g	gravitational acceleration [m/s^2]
H	height of humidifier [m]
$\dot{H}$	total enthalpy rate [W]
h	specific enthalpy [J/kg]
h^*	specific enthalpy [J/kg dry air]
h_t	heat transfer coefficient [W/m^2-K]
h_{fg}	specific enthalpy of vaporization [J/kg]
HCR	control volume based modified heat capacity rate ratio for HME devices [-]
K	mass transfer coefficient [kg/m^2-s]
k	thermal conductivity [W/m-K]
L	mass flow rate of water [kg/s]
Me	Merkel number, also KaV/L [-]
m_r, MR	water-to-air mass flow rate ratio [-]
$\dot{m}$	mass flow rate [kg/s]
N	number of extractions/injections [-]

N_t	number of trays [-]
Nu_D	Nusselt number based on the diameter [-]
P	absolute pressure [Pa]
Pr	Prandtl number [-]
$\dot{Q}$	heat transfer rate [W]
R	thermal resistance [K/W]
Re	Reynolds number [-]
T	temperature [°C]
V	packing volume [m^3]
V_g	gas superficial velocity [m/s]

Greek

Δ	difference or change
μ	dynamic viscosity [Pa s]
Ψ	enthalpy pinch [kJ/kg dry air]
ρ	density [kg/m^3]
ω	absolute humidity [kg water vapor per kg dry air]

Subscripts

a	moist air
c	cold stream
col	column
$cond$	condensate
deh	dehumidifier
da	dry air
h	hot stream
hum	humidifier
i	stage number
in	entering
f	liquid water
max	maximum
loc	defined locally
out	leaving
pw	pure water
tot	total
v	water vapor
w	seawater

Chapter 1

Motivation and background

1.1 Global problem: water scarcity

Water scarcity remains one of the major issues our world faces today. According to the United Nations Millennium Development Goals Report 2013, 783 million people still lack access to an improved source of drinking water, and more than 2.5 billion people still do not have access to improved sanitation facilities [1]. These numbers are expected to worsen with fast population growth and climate change [2–4].

Given that around 97% of water on Earth is saline, desalination, if done in a sustainable manner, could potentially unlock 'infinite' water resources. However, a major hurdle to using currently dominant desalination technologies to tackle water scarcity is the fact that 83% of the people without access to an improved drinking water source live in rural communities [1]. Most of these communities consist of 1,000 - 10,000 people, which would translate into a water need of around 10 - 100 m³/day if we consider a typical personal consumption of 10 L/person-day, whereas most of today's plants have capacities on the order of 100,000 m³/day. Providing these communities with fresh water requires systems that work well in small scale, can function properly without being connected to a reliable electricity grid, and do not need skilled labor for operation and maintenance. Most existing desalination technologies fail these requirements since they are currently designed for large scale operation, and consist of sophisticated components that require continuous maintenance and skilled labor for operation.

Another shortcoming of dominant desalination technologies is relatively new and follows the recent boom in hydraulic fracturing of oil and gas wells. Flowback and produced water from these wells can have salinities as high as 300,000 ppm compared to a salinity of 35,000 ppm for seawater. Treating highly saline water requires a technol-

ogy that is resistant to fouling which discourages the use of typical membrane-based systems such as Reverse Osmosis (RO), the world's leading desalination technology. RO is responsible for around 65% of the world's desalinated water capacity of 80.9 million m^3/day [5]. Although RO has an energy requirement which is within a factor of 2 or 3 of the thermodynamic minimum, its membranes are prone to fouling, and therefore face challenges when desalinating water only twice as saline as seawater. In addition, Multi-Effect Distillation (MED), a major thermal desalination technology, uses hot metal surfaces to heat the water in order to drive evaporation which makes it very likely to experience scaling at high salinities.

Humidification dehumidification (HDH) is a technology that could potentially work well in applications where conventional desalination technologies fail.

1.2 Humidification dehumidification desalination

1.2.1 Overview of HDH

Humidification dehumidification (HDH) is a distillation technology which imitates the rain cycle in an engineered setting by using a carrier gas, such as air [6–9], to transport water vapor between different compartments. The most basic system consists of a humidifier, a dehumidifier, and a heater. As shown in Fig. 1-1, cold air enters the humidifier where it is directly exposed to a hot stream of saline water, so its temperature increases, thus increasing its capacity to hold water vapor. Water from the saline water stream thus evaporates, making the air stream more humid. The humid air is then taken to the dehumidifier, where it is put in indirect contact with the cold incoming saline water stream. The temperature of the air decreases, causing some of the water vapor to condense, thus supplying a stream of pure water. Other configurations of HDH have been suggested and studied [6], but this work will focus on the cycle shown in Fig. 1-1, which can be described as closed-air, open-water, water-heated.

HDH is a promising technology for small scale desalination and is appropriate for water production in remote, off-grid locations where the water demand is not large enough to justify installing large scale plants since it can operate using low-grade heat sources such as solar irradiation [6, 10]. In addition, HDH systems do not require very sophisticated components and maintenance, making them appropriate for installation in communities where skilled labor is not readily available. Furthermore, HDH is a very robust technology, which, unlike membrane based technologies, can treat very
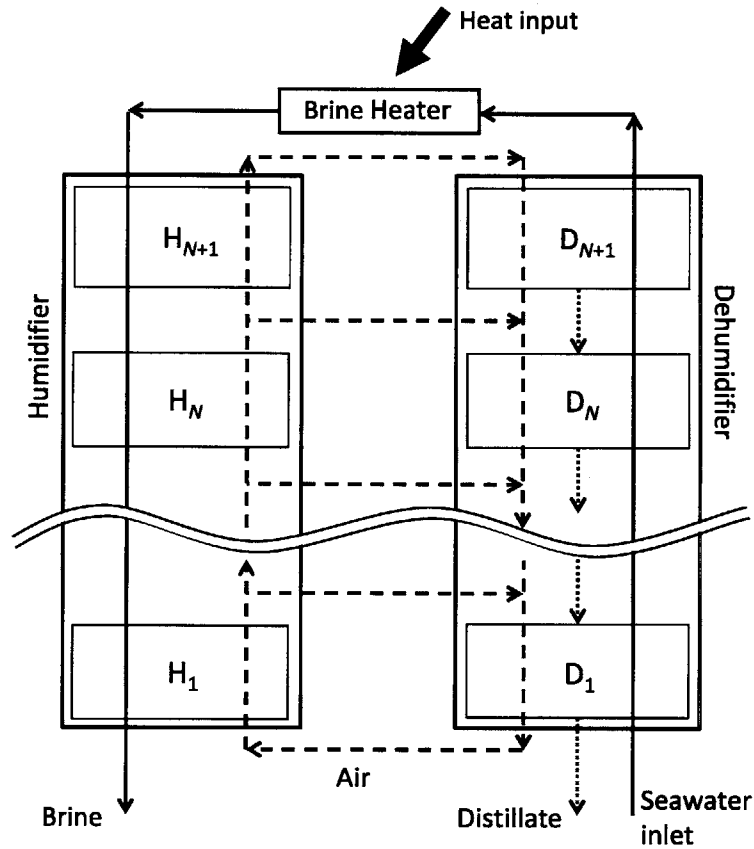
Figure 1-1: Schematic diagram of a water-heated, closed-air, open-water HDH system consisting of $N + 1$ stages separated by N air extractions from the humidifier to the dehumidifier.

saline water (many times saltier than seawater), which makes it a strong candidate for addressing the problem of produced water from oil and gas wells.

The major limitation of this technology is its high energy consumption. However, the energy requirements can be reduced through a careful understanding of the thermodynamics underpinning this technology so as to reduce the entropy generation within the operating cycle [11–13].

1.2.2 Thermodynamic balancing of HDH

It has been shown previously that the entropy production rate is at a minimum when the heat capacity rates of the interacting streams in a heat and mass exchanger are equal [14, 15]. This thermodynamically balanced system can be achieved by operation with an appropriate mass flow rate ratio that is a function of the top and bottom temperatures, and the performance of the heat and mass exchangers. In the HDH system presented in Fig. 1-1, the seawater inlet temperature is set by the ambient conditions, and the temperature of seawater at the humidifier inlet is set by the operator. The top and bottom temperatures of the air stream are then determined by the performance of the humidifier and that of the dehumidifier, which is why choosing the correct mass flow rate ratio can only be done iteratively.

The entropy generation rate can further by decreased through the variation of the mass flow rate ratio of the interacting streams (namely water and air) in each of the humidifier and dehumidifier which may be attained by mass extraction and injection between the two components at one or more internal locations [7]. This is true because the specific heat of moist air varies greatly with temperature whereas that of water remains constant. In this study, we consider air extractions from the humidifier to the dehumidifier as shown in Fig. 1-1.

Previous attempts to increase the energy efficiency of HDH desalination systems using mass extraction/injection have been reported in the literature. Müller-Holst [16, 17] suggested that entropy generation is minimized when the stream-to-stream temperature difference is kept constant throughout the system. In that study, it was proposed that a constant temperature pinch could be achieved by continuously adjusting the water and dry air volume flow rates. In addition, that study reported an optimized energy consumption of around 430 kJ/kg of fresh water.

Zamen et al. [18] proposed using a multi-stage process, where the water-to-air mass flow rate would be varied between stages. A temperature pinch was used to define the performance of the system, and the model got up to four stages. It was

reported that a two-stage system was the best configuration with the tested system since additional stages would not result in a substantial increase in efficiency. For a four-stage system with a temperature pinch of 4 °C, operating between 20 °C and 70 °C, the heat input was around 800 kJ/kg of fresh water.

McGovern et al. [19] studied the variation of the energy efficiency (represented by the gained output ratio, or GOR) and the recovery ratio with varying temperature pinch. The study reported an increase in GOR from 3.5 (heat input of around 675 kJ/kg of fresh water) in a system with no extraction to 14 (170 kJ/kg of fresh water) in a system with a single water extraction at effectively infinite heat and mass exchanger area with both systems at a feed temperature of 25 °C and a top moist air temperature of 70 °C. In addition, the recovery ratio increased from 7 % to 11 % with a single water extraction under the same conditions.

Thiel and Lienhard [20] suggested that in a heat and mass exchanger involving high concentrations of noncondensable gases, which is the case of the dehumidifier in any HDH system, the entropy generation is mainly due to mass transfer, and a balanced system is closer to a balanced humidity profile than a balanced temperature profile.

Narayan et al. [21] defined an enthalpy pinch, and used it in balancing devices with combined heat and mass transfer since a temperature pinch alone does not take the mass transfer into account. This parameter was used in defining balanced systems with no extraction, single extraction, and infinite extractions. In a subsequent experimental study, Narayan et al. [22] increased the GOR from 2.6 (heat input of around 900 kJ/kg of fresh water) to 4.0 (590 kJ/kg of fresh water) using a single air extraction with a system having an enthalpy pinch of 19 kJ/kg of dry air operating between 25 °C and 90 °C.

1.3   Goals of current study

This work focuses on the thermodynamic balancing of the humidification dehumidification desalination cycle through air extractions and injections. The first part of this study (Chapter 2) models a complete HDH system with multiple air extractions and injections from a fixed-effectiveness perspective by using the enthalpy pinch, as defined by Narayan et al. [21], as a measure of the size of the components used. This approach is useful since it allows the modeling of the heat and mass exchangers used without the need for a specific transport model, and allows the understanding of the thermodynamics of the cycle.

In Chapter 2, we present the model and its solution algorithm, and we study the effect of the enthalpy pinch and the number of extractions/injections on the performance of the system. In addition, we present results that can be used as guidelines in the design of HDH systems, such as optimal temperatures of the extractions/injections, optimal operating mass flow rate ratios in each stages, as well as the optimal division of the heat duty between the stages of the system.

A fixed-effectiveness model is a very useful tool for understanding the thermodynamics of the cycle; however, translating the results into practical system design is not straightforward. In a physical system, the parameter that is fixed is the available area in each of the components. Therefore, it was necessary to expand the knowledge gained from the fixed-effectiveness model by modeling the HDH system using heat and mass transfer models that allow component areas to be specified. The configuration we chose uses a multi-tray bubble column dehumidifier and a packed-bed humidifier. The use of multi-tray bubble column dehumidifiers in HDH desalination was suggested by Narayan et al. [23] for its ability to mitigate the negative effects of noncondensable gases on the condensation process. Subsequent studies by Tow et al. [24–26] have further developed the understanding of bubble column dehumidifiers.

In Chapter 3, we present the models used for each component as well the solution algorithms for these models and for the complete system with no extraction and with a single extraction. The approach used in the solution algorithm allows the modeling of fairly complex systems which would be impossible to do using simple simultaneous equations solvers. The results presented in Chapter 3 include the effect of the modified heat capacity rate ratio on performance, as well as that of top and bottom temperatures of the system. Conclusions are reached regarding ideal locations of extraction and the direction of extraction.

Chapter 2

A fixed-effectiveness model of multiple air extractions and injections for the thermodynamic balancing of HDH

In this chapter, which complements the previous paper by Narayan et al. [21], we model the use of multiple air extractions and injections to thermodynamically balance the HDH system, so as to make it more energy efficient. We examine the effect of a finite number of extractions on several performance parameters, such as energy efficiency, water recovery, and total heat duty. In addition, we study the effect of the enthalpy pinch, which is a measure of performance for a heat and mass exchanger, on these performance parameters. We also examine when it is useful to implement extractions and injections, and how many should be used for systems of different size. Finally, we present results that can be used as guidelines in designing HDH systems. These results include the identification of appropriate temperatures for the extracted/injected air streams, the division of the heat duty between stages, and the value of the mass flow rate ratio in each stage at various values of enthalpy pinch.

2.1 Modeling

2.1.1 Definition of a balanced system

Previous studies by Narayan et al. [14, 15] concluded that entropy generation is minimized at a fixed energy effectiveness when the modified heat capacity rate ratio

25
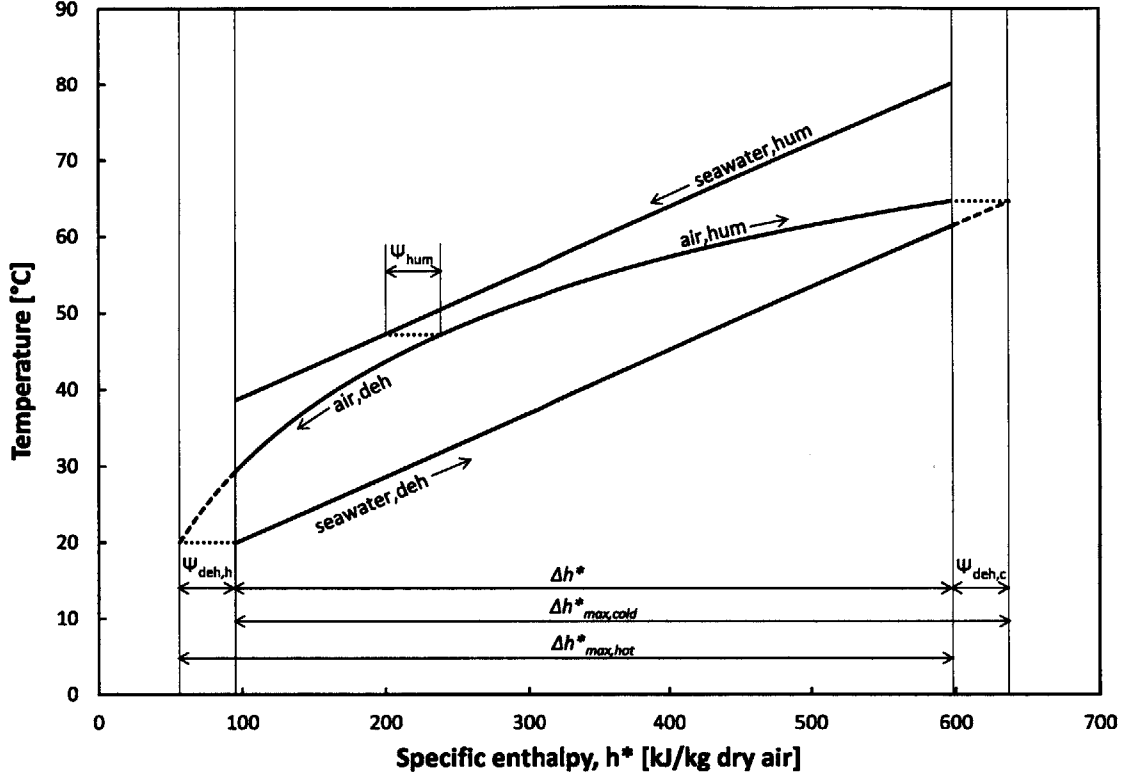
Figure 2-1: Temperature-enthalpy profile of a balanced system without extractions/injections with $T_{feed} = 20\,°C$, $T_{topbrine} = 80\,°C$, and $\Psi_{hum} = \Psi_{deh} = 20$ kJ/kg dry air.

(HCR) in the dehumidifier is equal to unity, where:

$$\text{HCR} = \frac{\Delta \dot{H}_{\text{max},cold}}{\Delta \dot{H}_{\text{max},hot}} \tag{2.1}$$

In Eq. 2.1, the numerator and denominator can both be divided by the mass flow rate of dry air, and, as shown in Fig. 2-1, the resulting equation can be written as follows:

$$\text{HCR} = \frac{\Delta h^*_{\text{max},cold}}{\Delta h^*_{\text{max},hot}} = \frac{\Delta h^* + \Psi_{deh,cold}}{\Delta h^* + \Psi_{deh,hot}} \tag{2.2}$$

where Ψ is the enthalpy pinch [21], which may be thought of as the minimum loss of enthalpy rate due to a finite device size. For HCR to be equal to unity in the dehumidifier, we need $\Psi_{deh,cold} = \Psi_{deh,hot}$. This means that in a balanced HDH system the enthalpy pinch point will be located at the inlet and outlet of the dehumidifier, and at a single intermediate location in the humidifier. The same definition is used for a system with multiple extractions and injections, where each stage (between two

26
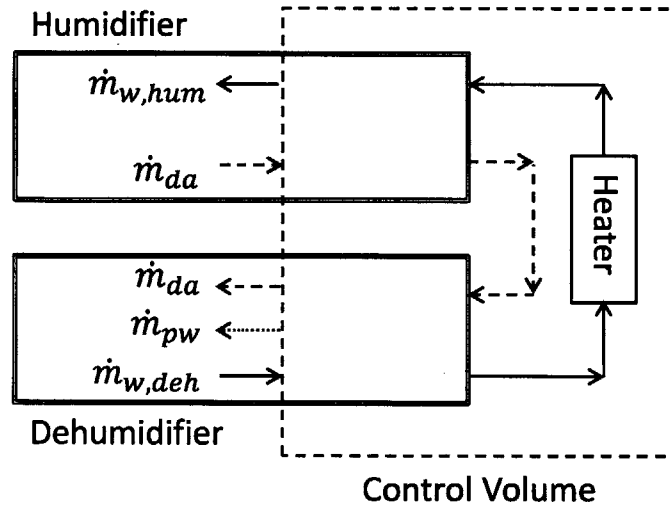
Figure 2-2: A control volume containing the heater, a section of the dehumidifier and the corresponding section of the humidifier.

consecutive extraction or injection points) satisfies these conditions.

2.1.2 Conservation equations and solution method

As explained in previous publications [19, 21], the HDH system can be modeled using temperature-enthalpy diagrams. These diagrams allow the representation of the process paths followed by each of the interacting streams, namely, moist air and seawater in the humidifier, and moist air, seawater, and distillate in the dehumidifier. Having the process paths defined allows the calculation of the enthalpy pinch at any location in the heat and mass exchangers. The enthalpy in these diagrams is expressed in kJ per kg of dry air since normalizing it in this fashion, as suggested by McGovern et al. [19], allows the representation of the process paths of air and water on the same diagram, and inherently satisfies the energy balance as will be shown in this section. The air, assumed to be saturated at all times, follows the air saturation curve, where the enthalpy is only a function of temperature.

Figure 2-2 shows a control volume containing the heater and portions of the humidifier and the dehumidifier. The control volume is chosen such that it intersects the humidifier and the dehumidifier in a location where the air is at the same temperature and mass flow rate in both components. The intersection of the control volume with both components corresponds to a vertical line (constant specific enthalpy of dry air) on the temperature-enthalpy profile. The water content in the air entering the control volume in the humidifier is the same as that in the air exiting the control

27

(a) Control volume in the dehumidifier

(b) Control volume in the humidifier

Figure 2-3: Diagrams showing the control volumes used in the conservation of mass and energy equations in (a) the dehumidifier and (b) the humidifier.

volume in the dehumidifier since the air is saturated and at the same temperature. A water mass balance on this control volume results in

$$\dot{m}_{w,hum} = \dot{m}_{w,deh} - \dot{m}_{pw,loc} \tag{2.3}$$

where the "loc" subscript denotes that the mass flow rate indicated is that of pure water condensed starting from the hot end of the dehumidifier up to the location in question. Note that, in the dehumidifier, the saline water is not in contact with the air so its mass flow rate is constant throughout the dehumidifier, and the saline water that enters the heater and the humidifier has the same mass flow rate as the feed saline water, $\dot{m}_w$. So at any location in the humidifier,

$$\dot{m}_{w,hum} = \dot{m}_w - \dot{m}_{pw,loc} \tag{2.4}$$

A more intuitive way to look at this result is that, at any location in the humidifier, the mass flow rate of saline water is the mass flow rate of water at the inlet of the humidifier minus the amount of water that has evaporated up to this location.

Figure 2-3(a) represents a control volume containing a small section of the dehu-

midifier. A water mass balance on this control volume results in

$$\dot{m}_{pw,1} - \dot{m}_{pw,2} = \dot{m}_{da}\left(\omega_2 - \omega_1\right) \tag{2.5}$$

In addition, an energy balance on the same control volume can be expressed as

$$\left(\dot{H}_2 - \dot{H}_1\right)_w - \left(\dot{H}_2 - \dot{H}_1\right)_{pw} = \left(\dot{H}_2 - \dot{H}_1\right)_a \tag{2.6}$$

or

$$\dot{m}_w c_{p,w}\left(T_2 - T_1\right)_w - \left[\left(\dot{m}c_p T\right)_{pw,2} - \left(\dot{m}c_p T\right)_{pw,1}\right] = \dot{m}_{da}\left(h_2^* - h_1^*\right) \tag{2.7}$$

For an infinitesimally small control volume, the change in the enthalpy rate of pure water is mainly due to temperature change, so the change in mass flow rate of pure water inside the control volume can be neglected, such that $\dot{m}_{pw,2} = \dot{m}_{pw,1} = \dot{m}_{pw,loc}$. Assuming that, at any location in the dehumidifier, the condensed water is at the same temperature as the saline water, and that the specific heat capacity of water is constant and the same for pure water and saline water, the energy balance simplifies to

$$\left(\dot{m}_w - \dot{m}_{pw,loc}\right) c_{p,w}\left(T_2 - T_1\right)_w = \dot{m}_{da}\left(h_2^* - h_1^*\right) \tag{2.8}$$

Dividing Eq. 2.8 by the product $\left(\dot{m}_w - \dot{m}_{pw,loc}\right) c_{p,w}\left(h_2^* - h_1^*\right)$, and taking the limit as $\left(h_2^* - h_1^*\right)$ goes to zero, we obtain the following expression for the slope of the process path followed by the water stream in the dehumidifier on the temperature-enthalpy diagram:

$$\frac{dT_w}{dh^*} = \frac{1}{m_r c_{p,w}} \tag{2.9}$$

where the mass flow rate ratio, m_r, is the ratio of the net mass flow rate of water to that of dry air:

$$m_r = \frac{\dot{m}_w - \dot{m}_{pw,loc}}{\dot{m}_{da}} \tag{2.10}$$

Similarly, an energy balance can be applied on the humidifier control volume shown in Fig. 2-3(b), and can be combined with Eq. 2.4 to give

$$\left(\dot{H}_2 - \dot{H}_1\right)_w = \left(\dot{H}_2 - \dot{H}_1\right)_a \tag{2.11}$$

and

$$\left(\dot{m}_w - \dot{m}_{pw,loc}\right) c_{p,w}\left(T_2 - T_1\right)_w = \dot{m}_{da}\left(h_2^* - h_1^*\right) \tag{2.12}$$

The resulting equation is the same as Eq. 2.8, which indicates that the slope of
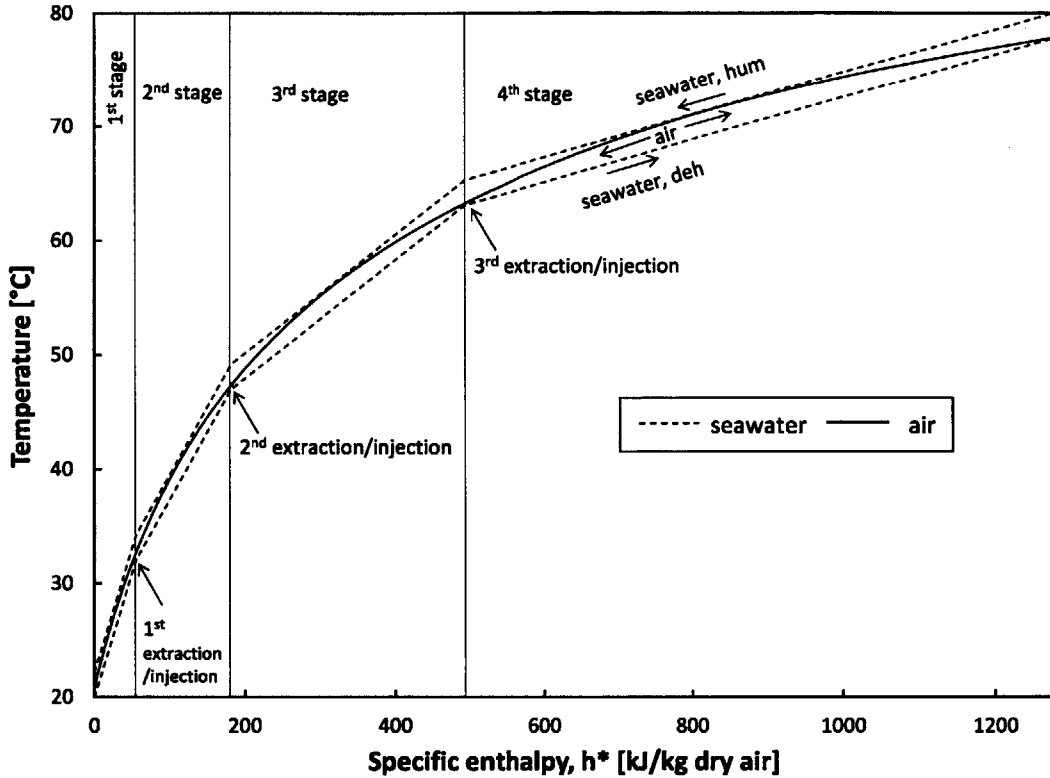
Figure 2-4: Temperature-enthalpy profile of a balanced system with 3 extractions/injections, $T_{feed} = 20\,°C$, $T_{topbrine} = 80\,°C$, and $\Psi = 3$ kJ/kg dry air.

the process path of water in the humidifier is also given by Eq. 2.9, and, on the temperature-enthalpy diagrams, the humidifier and dehumidifier lines should always be parallel. As a result of Eq. 2.9, varying the mass flow rate ratio through extractions of air from the humidifier to the dehumidifier allows the modification of the slope of the water process paths on the temperature-enthalpy diagram, and hence allows the balancing of the heat and mass exchangers.

In this chapter, the boundary conditions used in all simulations are a feed water temperature of 20 °C and a top brine temperature of 80 °C. The primary independent variables are the number of extractions, N, and the enthalpy pinch, Ψ. The algorithm used in this chapter is presented in the form of a flowchart in Fig. A-1 in the Appendix. The first part of the calculations is purely numerical and consists of finding the correct temperatures of the extracted/injected air streams that yield a balanced system, as defined in Section 2.1.1. After finding the appropriate temperature-enthalpy profile for a given N and Ψ, we can calculate all the parameters needed to evaluate the performance of the system. A typical balanced temperature-enthalpy profile is shown in Fig. 2-4, where $N = 3$ and $\Psi = 3$ kJ/kg dry air.

Equation 2.9 can be rearranged to calculate the mass flow rate ratio in the final stage of the system:

$$m_r = \frac{1}{\frac{dT_w}{dh^*} \times c_{p,w}} \tag{2.13}$$

As explained in Sections 2.1.3 and 2.2.2, the mass flow rate ratio is assumed constant in each stage. In addition, at the hot end of the dehumidifier, $\dot{m}_{pw,loc} = 0$ kg/s so the mass flow rate of dry air in the final stage can be calculated using Eq. 2.10. Given $\dot{m}_{da,N+1}$, the amount of pure water produced in the final stage can be calculated:

$$\dot{m}_{pw,N+1} = \dot{m}_{da,N+1}\Delta\omega_{N+1} \tag{2.14}$$

Equation 2.13 can then be used to calculate the mass flow rate ratio in the Nth stage, and, having calculated $\dot{m}_{pw,N+1}$, which is the local mass flow rate of pure water at the inlet of the Nth stage, $\dot{m}_{da,N}$ can be calculated using Eq. 2.10. The same procedure can be repeated to find the mass flow rate of dry air in each stage.

Additionally, the total mass flow rate of product water can be calculated:

$$\dot{m}_{pw,tot} = \sum_{stage,i=1}^{N+1} \dot{m}_{da,i}\Delta\omega_i \tag{2.15}$$

Finally, the total heat input into the system is calculated by applying the First Law of Thermodynamics on the heater:

$$\dot{Q}_{in} = \dot{m}_w\Delta h_w \tag{2.16}$$

2.1.3   Assumptions and approximations

- Specific heat capacity of water is assumed constant, evaluated at $50\,°C$, and a salinity of 35 ppt (maximum actual variation < 5 %)

- Temperature-enthalpy data for saturated air is input into the MATLAB code in the form of an array with a finite difference between consecutive data points. The discretization of the database is small enough such that the resulting uncertainty is reasonably small ($\ll$ 1 %)

- In the dehumidifier, pure water is produced at the temperature of seawater at the corresponding location. This means that pure water and seawater follow the same process path in the dehumidifier. The maximum error resulting from this assumption is small (< 2 %) and is discussed in an earlier publication [21].

31

- Air is assumed to be always saturated, which means the process path of air on the temperature-enthalpy diagrams is the same as the air saturation curve (discussed in previous publications, and shown to have an uncertainty $< 10\ \%$ [19, 21])

- An additional assumption to further simplify the modeling procedure of multiple extractions/injections is that of a constant mass flow rate ratio in each stage. This is discussed in detail in Section 2.2.2 of this chapter.

2.1.4 Performance parameters

In order to assess the performance of an HDH system, we need to first evaluate its energy efficiency. A common parameter used in thermal desalination systems is the Gained Output Ratio, or GOR, which is the ratio of the latent heat of vaporization of the product water to the net heat input to the system:

$$\text{GOR} = \frac{\dot{m}_{pw} h_{fg}}{\dot{Q}_{in}} \qquad (2.17)$$

GOR is a dimensionless quantity which measures the extent of reuse of the heat input. The most basic distillation system that uses heat to directly boil water without recovery of the heat of condensation would have at most a GOR of 1. In this chapter, h_{fg} is taken constant and equal to 2400 kJ/kg.

Another parameter of interest is the Recovery Ratio, RR. It is defined as the amount of pure water produced per unit amount of feed entering the system.

$$\text{RR} = \frac{\dot{m}_{pw}}{\dot{m}_w} \qquad (2.18)$$

A third parameter used in this chapter is the heat duty, which is the total energy transfer between the interacting streams summed over all stages of a single component type (humidifiers or dehumidifiers) per unit amount of water produced.

$$\dot{Q}_{duty} = \frac{\sum_{stage,i=1}^{N+1} \dot{m}_{da,i} \Delta h^*_i}{\dot{m}_{pw}} \qquad (2.19)$$

In a closed-air system, such as the one studied here, the heat duty is the same in both the humidifier and the dehumidifier. The heat duty, along with the driving force (e.g. temperature difference for a heat exchanger), determines the size of the heat and mass exchangers. Therefore, at a constant enthalpy pinch, the heat duty can be

32

used as a rough indicator of the initial cost of the system. It should be noted that the heat duty is different from (and larger than) the heat input, $\dot{Q}_{in}$.

2.1.5 Property packages

- The thermophysical properties of seawater were evaluated using the correlations developed by Sharqawy et al. [27].

- Thermophysical properties of pure water are evaluated using the IAPWS (International Association for Properties of Water and Steam) 1995 Formulation [28].

- Moist air properties are evaluated assuming an ideal mixture of air and steam using the formulations of Hyland and Wexler [29].

Moist air properties thus calculated are in close agreement with the data presented in ASHRAE Fundamentals [30] and pure water properties are equivalent to those found in NIST's property package, REFPROP [31].

2.2 Results and Discussion

2.2.1 Experimental validation

In a recent study, Narayan et al. [22] built an HDH system having an enthalpy pinch of 19 kJ/kg dry air at optimal operation. The GOR of the system without any extractions was 2.6, and that of a system with a single extraction/injection was 4.0. The system described in that study operated between 25 °C and 90 °C and had an uncertainty of ±5% on GOR. Performing the numerical calculations at these boundary conditions and at $\Psi = 19$ kJ/kg dry air, the calculated GOR was 2.3 for the case of no extraction (11 % difference) and 4.7 for that of a single extraction (17 % difference). The deviation of the experimental results from the numerical results presented in this chapter is expected since the experimental setup had some heat losses to the environment. The experimental system also had additional entropy generation due to mixing when injecting the air stream into the dehumidifier, and the ambient conditions could have varied slightly. In addition, the numerical study uses some simplifying assumptions, as explained in Section 2.1.3, which leads to a small error in the values of GOR. Nonetheless, the reported results are reasonably close to the experimental results, and serve the main purpose of showing trends in the variation

of the different performance parameters with varying enthalpy pinch and number of extractions/injections.

2.2.2 Effect of assuming fixed mass flow rate ratio

In the results reported in the following sections, the mass flow rate ratio, defined in Eq. 2.10, is kept constant in each stage of both the humidifier and the dehumidifier. This results from the assumption that the water flow rate is kept constant in each of these components. In other words, the effect of condensation on the flow rate of water in a dehumidifier stage and evaporation in the corresponding humidifier stage can be neglected since the mass flow rate of the condensed or evaporated water is very small compared to that of the mass flow rate of saline water. This approximation, along with that of a constant specific heat capacity of water, translates into a constant slope (Eq. 2.9), so the process path of water in each stage will be a straight line, making the numerical computation much simpler and faster.

In order to estimate the error caused by this approximation, additional calculations were done in which the mass flow rate ratio was actually varied to account for condensation and evaporation for the cases of no extraction and single extraction. The maximum error on the gained output ratio, GOR, was found to be around 1 % for the case of no extraction [Fig. 2-5(a)], and 2.5 % for that of single extraction [Fig. 2-5(b)]. As will be shown in Section 2.2.5, the recovery ratio converges to a maximum, and, after the first extraction, the increase in recovery ratio is limited. This, in turn, means that the error due to the assumption of constant mass flow rate ratio within each stage will not increase significantly for a higher number of extractions since condensation and evaporation are bounded by the total recovery.
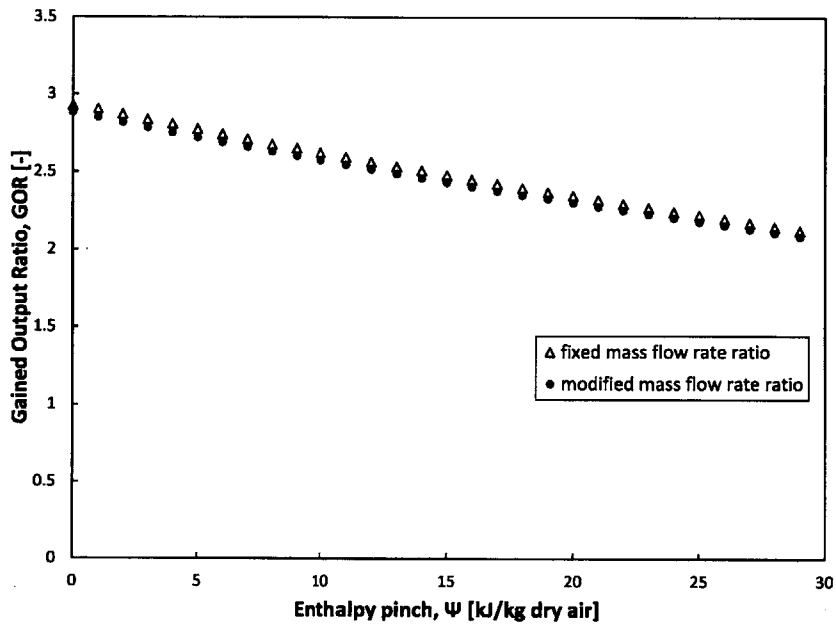
(a) Comparison of models with fixed and modified mass flow rate ratios for
$N = 0$
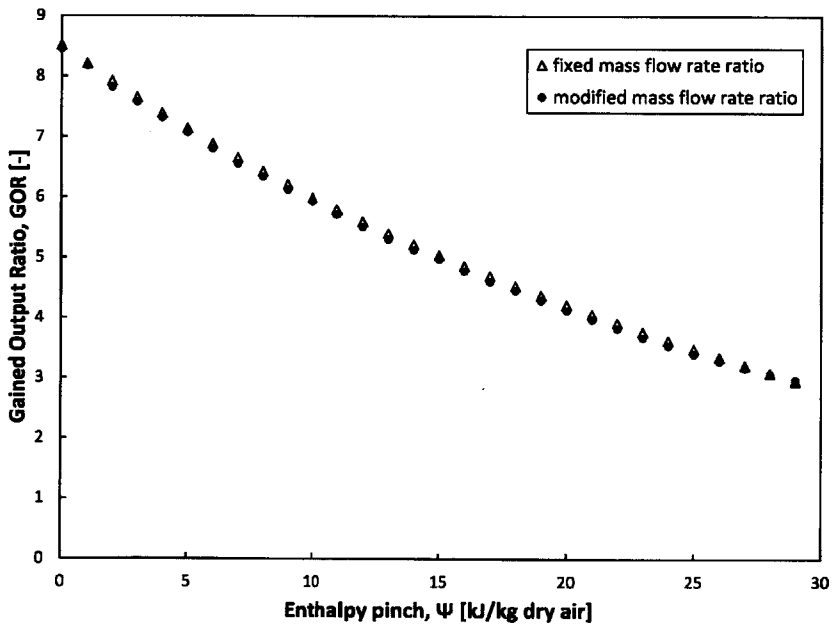
(b) Comparison of models with fixed and modified mass flow rate ratios for
$N = 1$

Figure 2-5: Effect of assuming fixed mass flow rate ratio on GOR for (a) $N = 0$ (b)
$N = 1$

35

2.2.3 Temperature of the extracted streams

As explained in Section 2.1.2, the appropriate temperatures of the extracted/injected air streams are determined by using a purely numerical approach. The correct temperature-enthalpy profile is the one that leads to a thermodynamically balanced system as defined in Section 2.1.1. Figure 2-6 presents the appropriate temperatures of the extracted/injected air streams at various Ψ and $N \leq 5$. Starting with $N = 5$ at $\Psi = 0$ kJ/kg dry air, it can be seen that, as the enthalpy pinch increases, the appropriate temperature of extraction/injection decreases. That is, if we have 5 extractions/injections (and therefore six balanced stages), as Ψ increases, the required temperature of each of these extractions/injections will decrease. A limiting enthalpy pinch for $N = 5$ is reached when the temperature of the first extraction point becomes equal to that of the air at the humidifier inlet (at $\Psi \approx 3.5$ kJ/kg dry air). In other words, the first extraction becomes redundant, thus reducing the number of effective extractions to $N = 4$ and the number of stages to five balanced stages. Similarly, at $\Psi \approx 8$ kJ/kg dry air, for a three extraction system, the first of the three extractions occurs at the temperature of the inlet, so we are reduced to 2 useful extractions that yield three balanced stages. What can be concluded from this graph is that at any enthalpy pinch there is only a limited number of extractions/injections that can yield a fully balanced system. A higher number of extractions for that enthalpy pinch would cause imbalance in the system, as well as raise capital cost. Therefore, for the boundary conditions studied, Fig. 2-6 presents the optimal temperatures of extraction/injection at any given enthalpy pinch for $N \leq 5$. Note that, at an enthalpy pinch higher than 35 kJ/kg dry air, the performance of the system does not improve if we extract/inject even once since the balanced system would be composed of a single balanced stage, which can be implemented simply by choosing the correct mass flow rate ratio (discussed in Section 2.2.8).

This brings us to the idea of continuous balancing proposed in an earlier publication [21], specifically using an infinite number of infinitesimal extractions/injections. It is now better understood why a continuously balanced component could be less efficient than a balanced system without any extractions/injections. In the model proposed for continuous extraction, only one component could be balanced at finite area. So as the enthalpy pinch increases we could have large entropy production rates in the "unbalanced" component, thus reducing the efficiency of the system. In the case of a finite number of extractions, both components of the system are balanced in each stage as explained in Section 2.1.1. Continuous extraction is therefore only

36
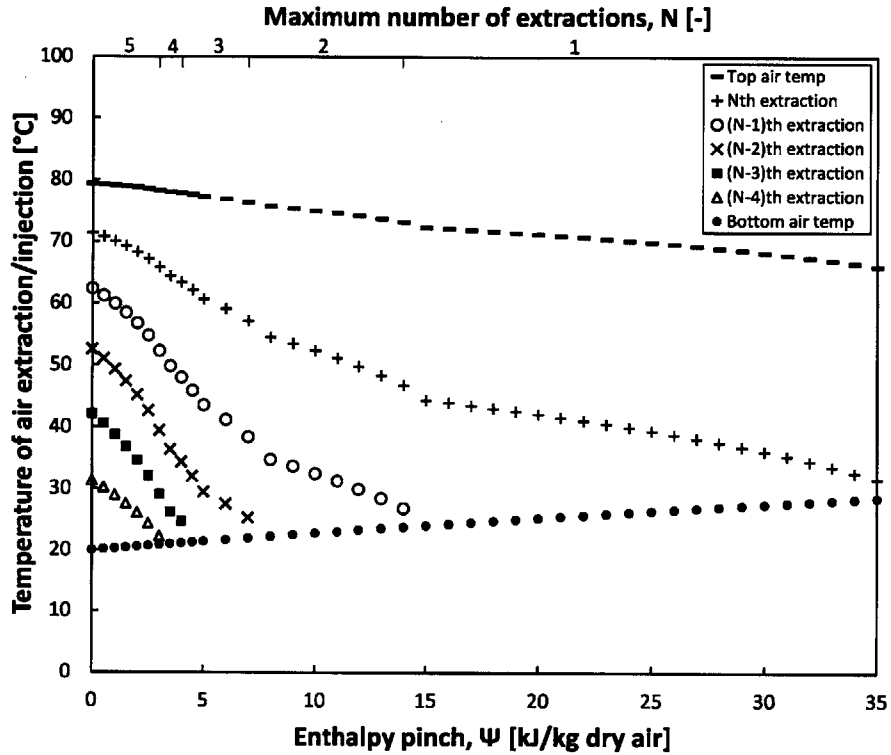
Figure 2-6: Optimal temperature of air extractions/injections for varying enthalpy pinch with $N \leq 5$, $T_{feed} = 20\,°C$, and $T_{topbrine} = 80\,°C$.

beneficial at infinite heat and mass exchanger surface area, i.e. at $\Psi = 0$ kJ/kg dry air.

Figure 2-7 presents the variation of the temperature of extraction/injection with N at infinite area. Since the approach used in this study is numerical, getting the initial guess value of the location of the extraction to be the closest possible to the correct value is critical in reducing the computing time. So, if the temperature of an extraction is known for the case of N extractions at a given enthalpy pinch, Fig. 2-7 shows that the temperature of the same extraction at $N + 1$ extractions will be lower.
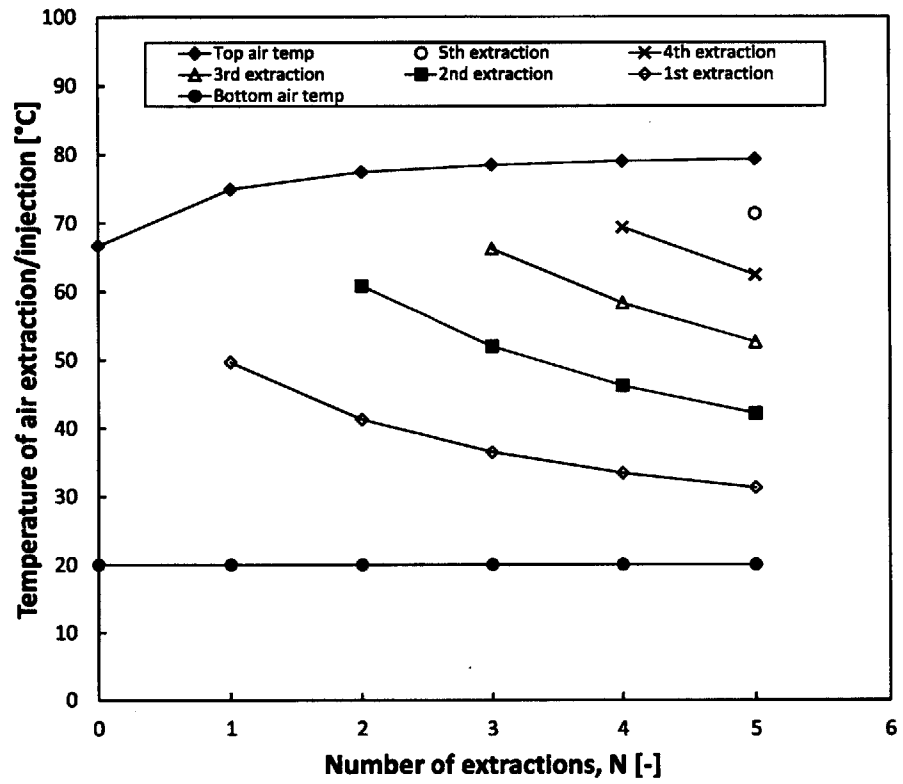
Figure 2-7: Temperature of air extractions/injections at infinite area ($\Psi = 0$ kJ/kg dry air) for varying number of extractions/injections, N.

2.2.4 Variation of GOR with enthalpy pinch and number of extractions

The variation of GOR with N and Ψ, presented in Fig. 2-8, can best be explained by looking back at the variation of the temperature of extractions with Ψ in Fig. 2-6. It can be seen that the variation of the temperature of the extractions is smooth with varying enthalpy pinch. So when the transition enthalpy pinch is reached, and the number of extractions is decreased by one, the temperature profile of the system does not vary much. In other words, when the optimal location of the first extraction becomes the inlet of the humidifier, the number of extractions is reduced by one while the temperature of the other extraction points is only varied slightly. For example, when the maximum number of extractions goes from 3 to 2 at $\Psi \approx 8\,\mathrm{kJ/kg}$ dry air, the 2nd and 3rd extractions remain at almost the same temperature. So the temperature profile of a system with three extractions at an enthalpy pinch just smaller than the transition enthalpy pinch will be the same as that of a system with two extractions at an enthalpy pinch just larger than the transition pinch. This means that the characteristics of these systems will be very close, which explains why the curves of GOR at various N intersect. Thus, at the transition enthalpy pinch between N and $N + 1$ extractions, the system with N extractions and that with $N + 1$ extractions have the same GOR, among other parameters, namely RR, heat duty, and mass flow rate ratio in each stage.

As expected, at a constant N, GOR decreases with increasing Ψ. This is true since the difference in both, temperature and humidity, is larger at larger Ψ, which means that the entropy generation is greater, and the energy efficiency is smaller. In addition, at a constant Ψ, the GOR is greater at a larger number of extractions since the process paths of the interacting streams become closer, and the driving forces for the heat and mass transfer become smaller, reducing the entropy generation and increasing the energy efficiency.

Another observation from Fig. 2-8 is that the effect of extracting is largest at infinite area where each additional extraction increases the efficiency by a significant amount. The larger the enthalpy pinch, the smaller the effect of additional extractions/injections. Also, when the enthalpy pinch is greater than 6 kJ/kg dry air, we notice that extractions/injections have diminishing returns as suggested by Zamen et al. [18]. That is, the increase in efficiency due an additional extraction is smaller than the increase due the previous extraction. For example, at $\Psi = 7$ kJ/kg dry air, the first extraction improves GOR by 3.9, the second by 3.6, and the third by 1.2.
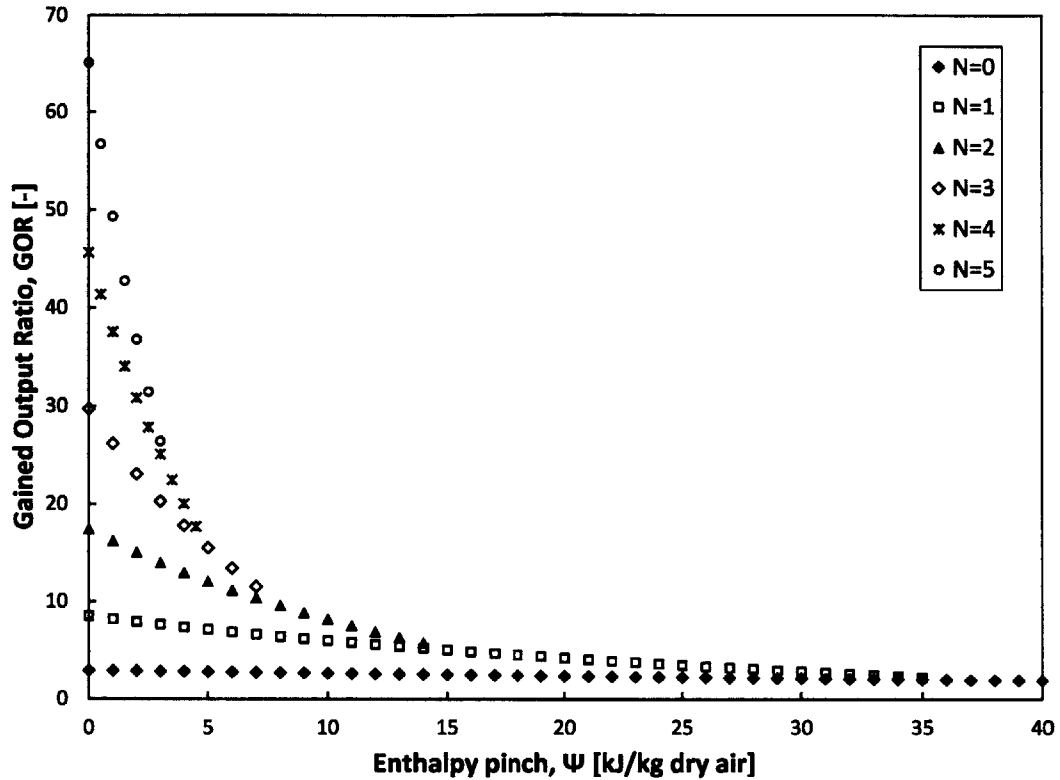
Figure 2-8: Variation of GOR with enthalpy pinch, Ψ, and number of extractions/injections, N. Boundary conditions: $T_{feed} = 20\,^{\circ}\text{C}$, $T_{topbrine} = 80\,^{\circ}\text{C}$.

This observation is not true for $\Psi \leq 6$ kJ/kg dry air where each additional extraction brings a significant increase in efficiency, in some cases even greater than that due to the previous extraction.

2.2.5 Variation of Recovery Ratio with enthalpy pinch and number of extractions

As can be seen in Fig. 2-9, for the same number of extractions/injections, the recovery ratio decreases with increasing enthalpy pinch, and, as was explained in Section 2.2.4, the recovery ratio of $N + 1$ extractions intersects that of N extractions at the transition enthalpy pinch. The recovery ratio increases with the number of extractions/injections; however, this increase becomes smaller with each additional extraction/injection. For a closed-air, open-water (CAOW) system operating between 20 °C and 80 °C, and balanced using air extractions/injections, the recovery ratio converges to a limit close to 7.6 % at infinite area as N goes to infinity.

When comparing Fig. 2-9 to Fig. 2-8, we notice that balancing through air ex-
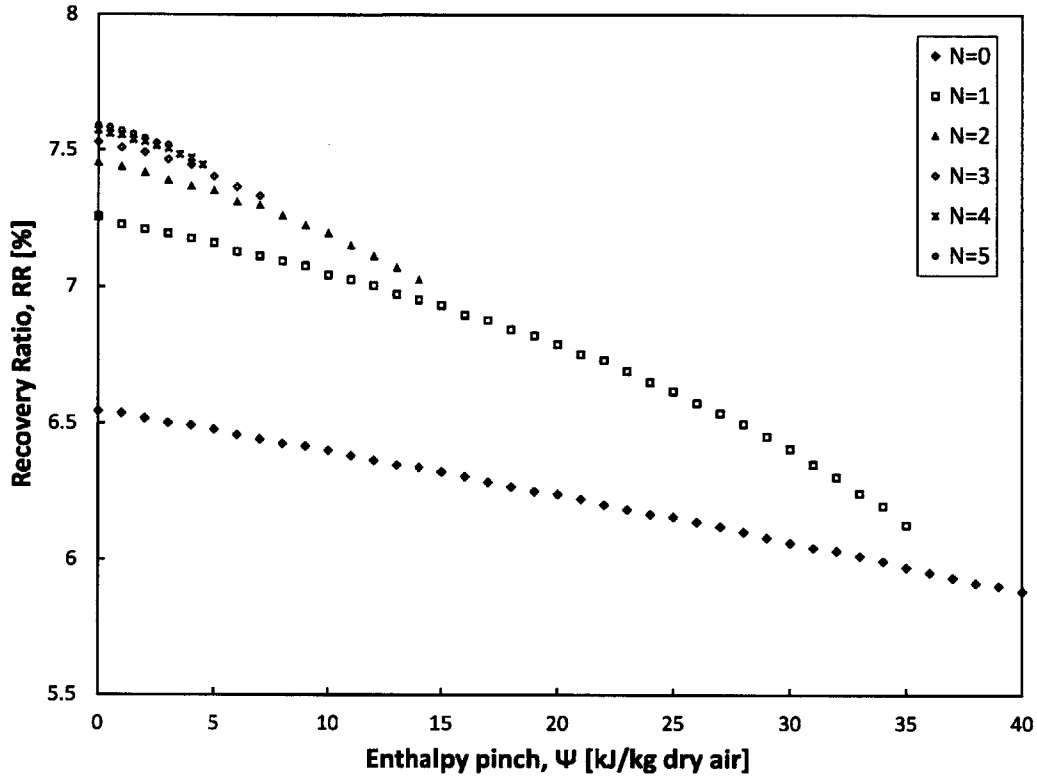
Figure 2-9: Variation of RR with enthalpy pinch, Ψ, and number of extractions/injections, N. Boundary conditions: $T_{feed} = 20\,°C$, $T_{topbrine} = 80\,°C$.

tractions and injections has a much larger effect on energy efficiency than on recovery ratio.

2.2.6 Variation of heat duty with enthalpy pinch and number of extractions

The variation of heat duty with N and Ψ, shown in Fig. 2-10, is similar to that of recovery ratio. The total heat duty decreases with increasing enthalpy pinch. Also, the heat duty increases with the number of extractions/injections until it reaches a limit of about 3050 kJ/kg of distillate for our boundary conditions at infinite area. It can be seen that the variation of the heat duty at $N \geq 3$ at Ψ close to 0 is not very smooth, but we should note that the variation is between 3020 and 3050 kJ/kg of distillate, which is less than 1 %, and falls within the numerical error range.

An important observation to be made is that a small increase in heat duty can lead to a large increase in GOR. For example, at $\Psi = 15$ kJ/kg dry air, the first extraction will double the GOR while only needing a 4 % increase in heat duty, which suggests

41
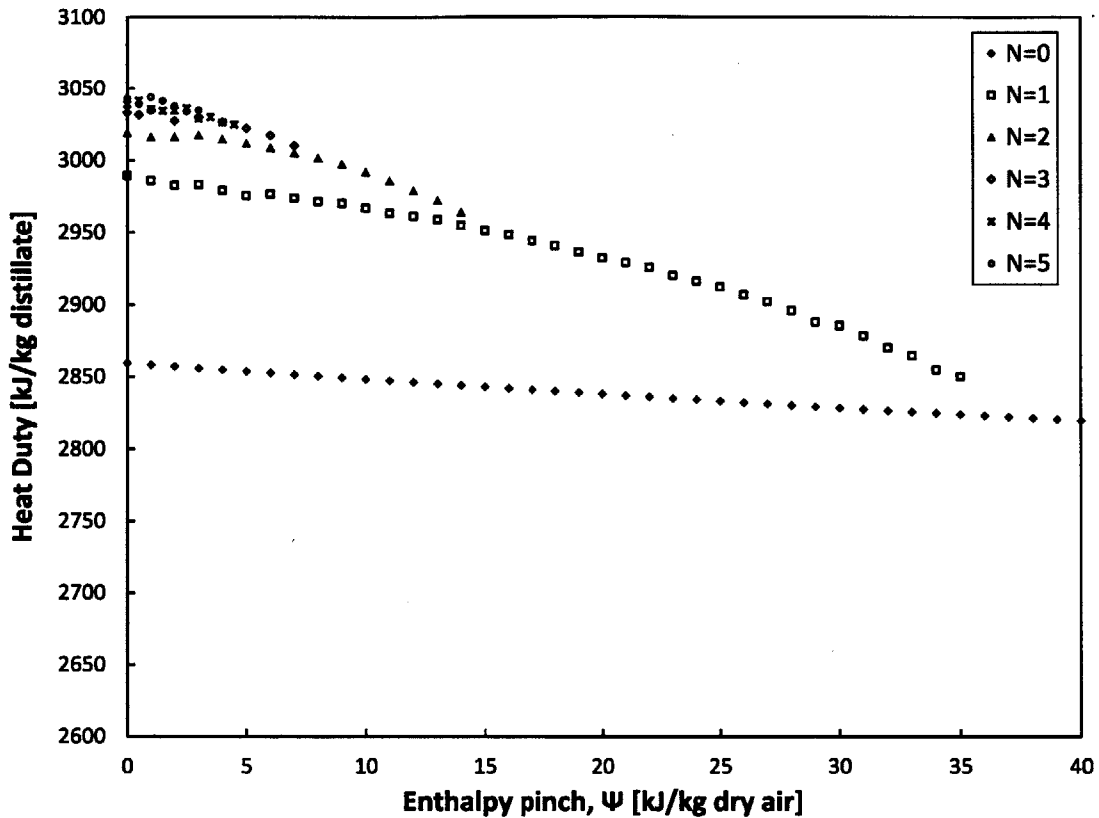
Figure 2-10: Variation of Heat Duty with enthalpy pinch, Ψ, and number of extractions/injections, N. Boundary conditions: $T_{feed} = 20\,°C$, $T_{topbrine} = 80\,°C$.

a significant increase in performance at only a modest increase in system cost. As noted in Section 2.2.4, GOR increases faster with N at Ψ close to 0, whereas the variation of heat duty with N becomes very small in that region. This means that the additional efficiency comes at a cheap price if we can achieve a low enthalpy pinch at an acceptable cost.

2.2.7 Division of heat duty between stages

The data presented in this section could be considered as a guideline in designing an HDH system. Figure 2-11(a) presents the division of the total heat duty between the different stages of the system at infinite area (which corresponds to $\Psi = 0$ kJ/kg dry air). As a rough estimate, the heat duty is almost divided equally between the different stages. The farther the system is from infinite area, the less uniform the division of the heat duty at high N, as shown in Fig. 2-11(b).

42
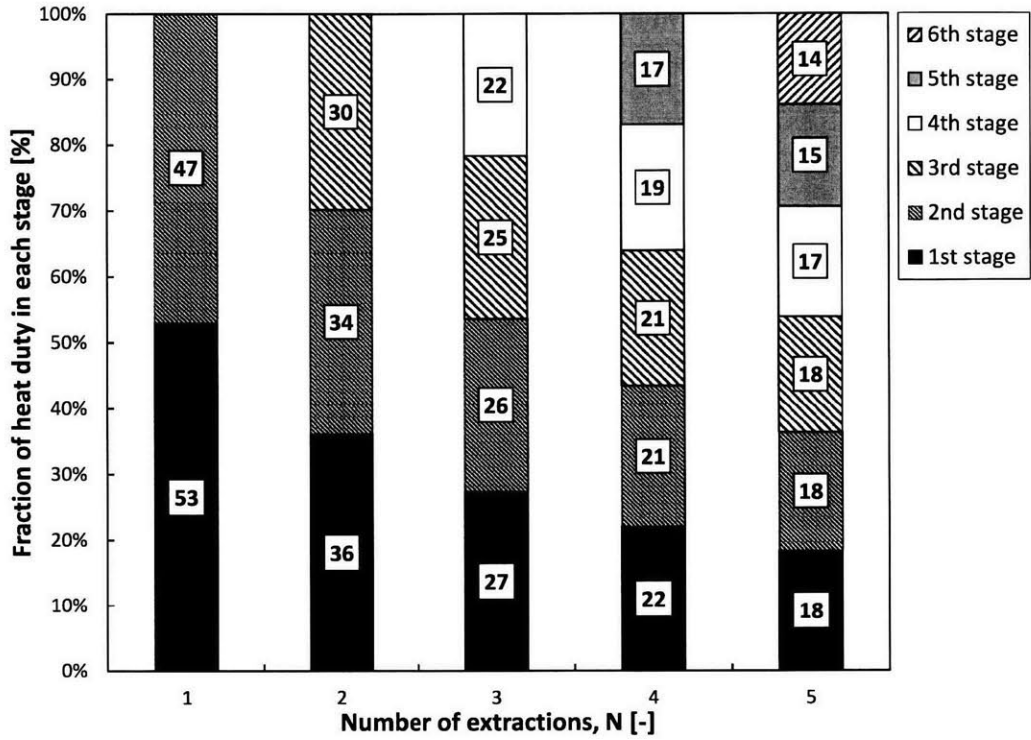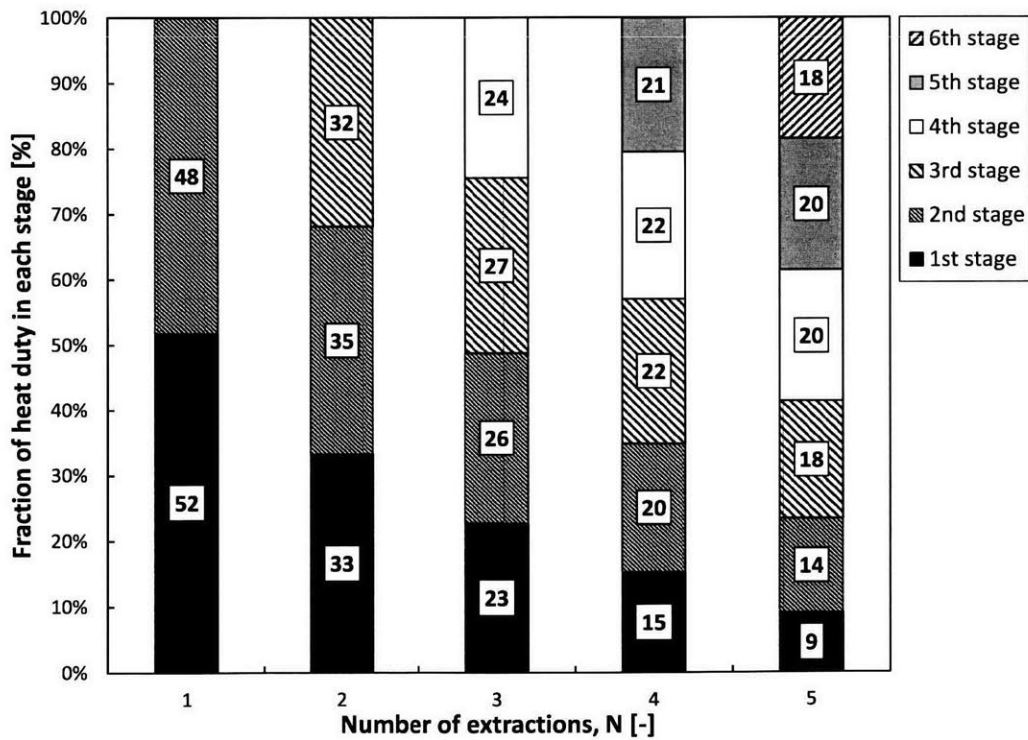
(a) $\Psi = 0$ kJ/kg dry air

(b) $\Psi = 2$ kJ/kg dry air

Figure 2-11: Distribution of heat duty between the stages of the system at various numbers of extractions/injections, N, at (a) $\Psi = 0$ kJ/kg dry air and (b) $\Psi = 2$ kJ/kg dry air. The percentage of the total heat duty in each stage is displayed in the corresponding column.
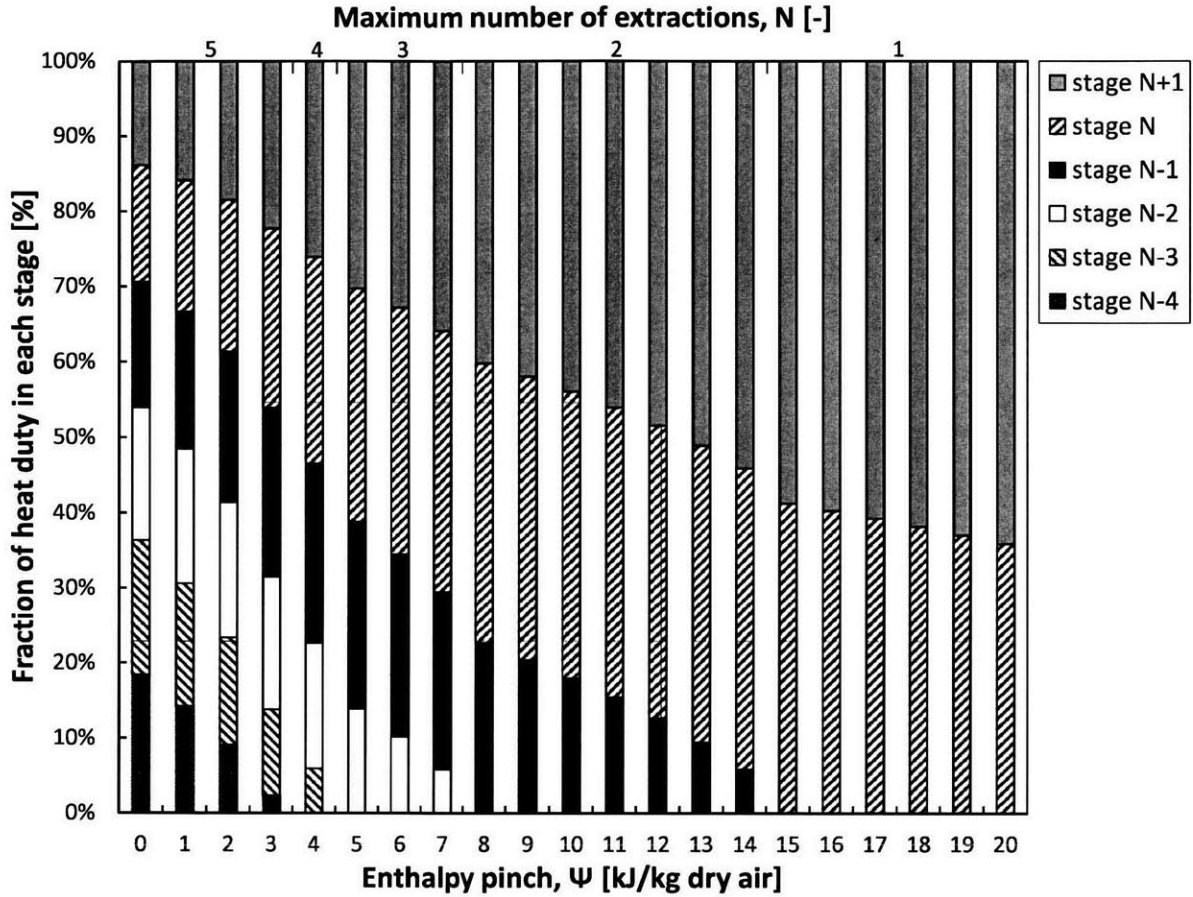
Figure 2-12: Optimal distribution of heat duty between the stages of the system at varying enthalpy pinch, Ψ, and $N \leq 5$.

The same results can be seen in Fig. 2-12, which presents the optimal division of heat duty between stages for various values of enthalpy pinch. This means that the cases presented show the maximum number of extractions possible at any given Ψ (where $N \leq 5$). Starting with six stages at $\Psi = 0$ kJ/kg dry air, the heat duty is almost divided equally between stages. As Ψ increases, the fraction of the heat duty in the first stage decreases before reaching 0 at the transition enthalpy pinch, and thus the number of extractions/injections is reduced by 1.

2.2.8 Optimal values for mass flow rate ratio for varying enthalpy pinch

Figure 2-13 shows the optimal value of the mass flow rate ratio in each stage at various values of enthalpy pinch. As expected, the mass flow rate ratio is always higher in
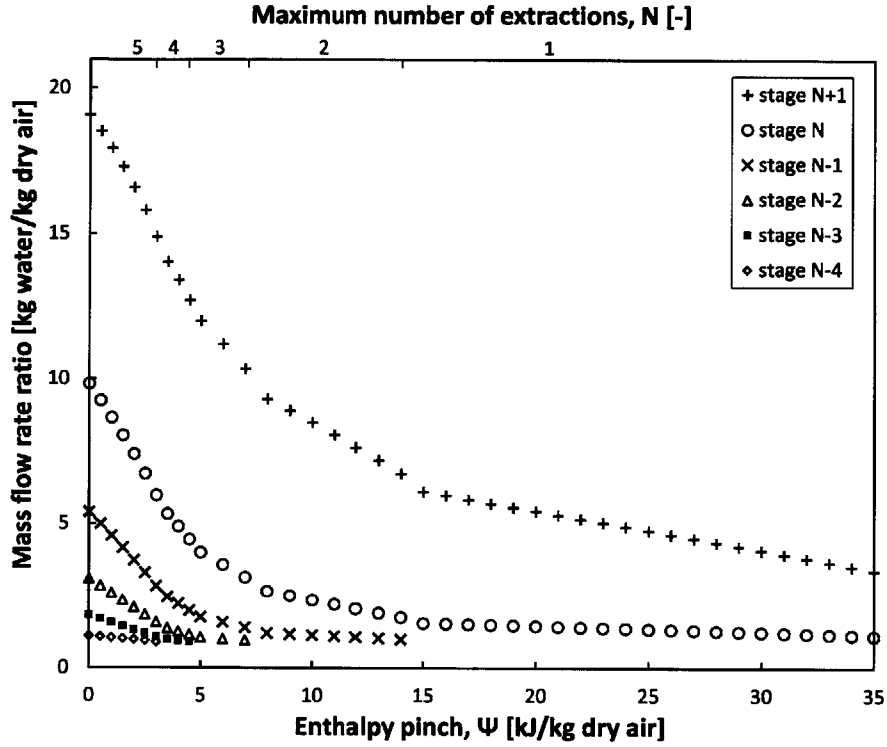
Figure 2-13: Optimal mass flow rate ratio at each stage in the system for varying enthalpy pinch, Ψ, and $N \leq 5$.

the hotter stages since we are extracting air from the humidifier and injecting it in the dehumidifier. So there is more air at the lower stages, and hence a lower mass flow rate ratio. In addition, the mass flow rate ratio decreases in each stage with increasing enthalpy pinch until a minimum m_r of around 1 is reached in the first stage at the transition enthalpy pinch. After some investigation, it was found that the mass flow rate ratio is close to 1 due the boundary condition $T_{feed} = 20\,^\circ\mathrm{C}$ since in that region $\frac{dT_a}{dh^*} \approx c_{p,w}$.

2.3 Conclusions

The effect of the number of extractions and the enthalpy pinch on various performance parameters of a closed-air, open-water humidification dehumidification system has been studied. The main conclusions of this chapter are the following:

1. At a given enthalpy pinch, we can only extract/inject beneficially a limited number of times.

2. Continuous extraction, as proposed in an earlier publication [21], can only fully

balance one component. Therefore, at a given enthalpy pinch, continuous extraction can be less beneficial than a finite number of extractions, which is able to balance both components.

3. Recovery ratio converges to a maximum as the number of extractions/injections increases.

4. Total heat duty converges to a maximum as the number of extractions/injections increases.

5. When modeling closed-air, open-water HDH systems with air extractions/injections, the change in mass flow rate ratio due to evaporation/condensation within a stage can be neglected.

6. A small increase in heat duty can lead to a large increase in energy efficiency, especially at a small enthalpy pinch.

7. The effect of balancing through extraction/injection is greater at smaller enthalpy pinch, where GOR increases faster with N and heat duty remains approximately constant. At larger enthalpy pinch (smaller heat and mass transfer surface area), balancing has diminishing returns.

8. Location of the injection points:

   (a) As the enthalpy pinch increases, the optimal temperature of the extracted/injected air stream decreases.

   (b) As the number of extractions/injections increases, the optimal temperature of the extracted/injected air stream decreases.

9. Balancing has a much smaller effect on recovery ratio than on energy efficiency.

In addition, this chapter presents results that can be used in designing HDH systems. These results include the optimal temperatures of the extractions/injections, the division of the heat duty between stages, and the value of the mass flow rate ratio in each stage for $0 \leq \Psi \leq 20$ kJ/kg dry air, and for $N \leq 5$.

Chapter 3

A transport model of an HDH system using packed-bed humidification and bubble column dehumidification

Previous studies in the literature have approached the issue of HDH's low energy efficiency through the thermodynamic balancing of the system; however, most theoretical work on the balancing of HDH has followed a fixed-effectiveness approach that does not explicitly consider transport processes in the components. Fixing the effectiveness of the heat and mass exchangers allows them to be modeled without explicitly sizing the components and gives insight on how the cycle design can be improved. However, linking the findings of fixed-effectiveness models to physical systems can be challenging, as the performance of the components depends mainly on the available surface areas and the flow rates of the air and water streams.

In this chapter, we present a robust numerical solution algorithm for a heat and mass transfer model of a complete humidification-dehumidification system consisting of a packed-bed humidifier and a multi-tray bubble column dehumidifier. We look at the effect of varying the water-to-air mass flow rate ratio on the energy efficiency of the system, and we compare the results to those reached following a fixed-effectiveness approach. In addition, we study the effect of the top and bottom temperatures on the performance of the system in an attempt to model operation under variable conditions. The importance of this robust solution method lies in its ability to model different configurations of the HDH desalination system, including the variation of the mass flow rate ratio through extractions and injections of either air or water,
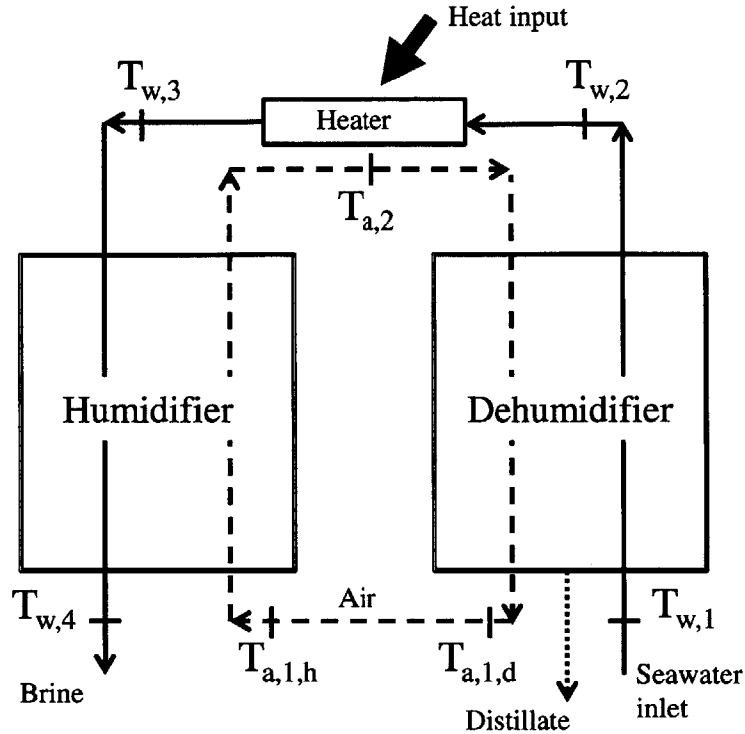
Figure 3-1: Schematic diagram representing an HDH system. Note that temperature labels are only used to explain the solution algorithm, and there is only one value of the air bottom temperature: $T_{a,1} = T_{a,1,d} = T_{a,1,h}$.

which would be impossible to achieve by using a simple simultaneous equation solver. We also present a detailed algorithm for the implementation of a single air extraction. We look at the effect of the heat capacity rate ratio of the different stages on system performance, and we study the effect of the location of extraction and its direction. We look at the criteria that define a balanced system, and give a physical interpretation of why this is the case.

3.1 Modeling

Establishing an accurate model of a complete humidification-dehumidification system allows us to simulate the effect of various parameters with significant practical importance. In addition, implementing models of the basic components of the system in MATLAB allows flexibility in varying the conditions of operation, and also allows us to model different configurations of these components. This section presents the models of the different components of the HDH system, and the algorithms used to solve them, and their implementation in a complete system without extraction and

48

with a single extraction.

3.1.1 Bubble column dehumidifier

The use of a short bubble column for dehumidification was first introduced by Narayan et al. [23] and was found to be very promising since it reduces the negative effect of the noncondensable gases on condensation. In traditional dehumidification systems, water vapor has to diffuse through an air layer, which increases the resistance to the mass transfer. In a bubble column, the location of condensation is the transiently formed bubble-water interface which has a very large specific area, giving it superior efficiency compared to alternative dehumidification systems [23, 24].

In a bubble column dehumidifier, cold saline water and hot moist air exchange heat and mass through a stationary column of fresh water. The saline water is circulated through a coil immersed in the column of fresh water, and the hot humid air is bubbled from the bottom of the column through a sparger. As the air passes through the column, it is cooled and dehumidified.

Governing equations

This study uses the model established by Tow and Lienhard [24–26] to evaluate the performance of the dehumidifier bubble column. This model is based on a resistance network between the hot air and cold saline water. To further simplify the resistance model, they assume perfect mixing in the column, meaning that the air always exits the dehumidifier at the column temperature, and that the air-side resistance to heat and mass transfer is negligible, leaving the model with just two resistances to the transfer of heat from the column to the cold saline water. The outer resistance, R_{out}, is between the column and the coil, and is determined using the correlation by Deckwer [32]. The inner resistance, R_{in}, is between the coil and the saline water, and is determined following the correlation developed by Mori and Nakayama [33, 34] since the coil used is curved. The correlations used in this study are summarized in Appendix B. Tow's model has been verified experimentally for various conditions [24].

For generality, and to be able to use the model in a multi-tray dehumidifier where the condensate from one column is bled into the following column, we assume that some fresh water also enters the column. Performing a water mass balance on the system allows us to calculate the mass flow rate of the condensate leaving the column:

$$\dot{m}_{\text{cond,out}} = \dot{m}_{\text{cond,in}} + \dot{m}_{\text{da}}\left(\omega_{\text{in}} - \omega_{\text{out}}\right) \tag{3.1}$$

Note that the condensate will be bled from the column (at the column temperature) in order to keep the process running at steady state. In addition, the energy balance can be written as

$$\dot{m}_{\mathrm{da}}\left(h_{\mathrm{a,in}} - h_{\mathrm{a,out}}\right) + \dot{m}_{\mathrm{cond,in}}h_{\mathrm{cond,in}} - \dot{m}_{\mathrm{cond,out}}h_{\mathrm{cond,out}} = \dot{m}_{\mathrm{w}}\left(h_{\mathrm{w,out}} - h_{\mathrm{w,in}}\right) \equiv \dot{Q}_1 \tag{3.2}$$

We denote the heat removed by the saline water, calculated using an energy balance, as $\dot{Q}_1$ for clarity in the solution method. A logarithmic mean temperature difference is defined since the saline water exchanges heat with the column which is at fixed temperature

$$\Delta T_{\mathrm{lm}} = \frac{T_{\mathrm{w,out}} - T_{\mathrm{w,in}}}{\ln\left(\frac{T_{\mathrm{col}} - T_{\mathrm{w,in}}}{T_{\mathrm{col}} - T_{\mathrm{w,out}}}\right)} \tag{3.3}$$

And the heat transfer to the saline water can be expressed as

$$\dot{Q}_2 = \frac{\Delta T_{\mathrm{lm}}}{R_{\mathrm{in}} + R_{\mathrm{out}}} \tag{3.4}$$

We note that performing an energy balance on the saline water implies that $\dot{Q}_1 = \dot{Q}_2$, and the only reason these two quantities are denoted differently is for clarity in discussing the solution method.

Solution method

The equations governing the bubble column dehumidifier are nonlinear due to the presence of the logarithmic mean temperature difference. This section presents a method to solve these nonlinear equations in a linear manner using a computer program such as MATLAB. In a typical single-tray bubble column dehumidifier, the inlet temperatures are specified. However, when simulating the multi-tray bubble column, described in Section 3.1.2, two other cases arise.

Case 1

We denote by Case 1 a single-tray bubble column where the flow rates and the inlet temperatures are specified. The detailed algorithm for the solution method is presented in Fig. C-1 in Appendix C, but a basic description of the approach will be presented here. The first step in the solution method is to guess the air outlet temperature using the bisection method. We know from the model that both the air and the condensate exit at the column temperature, so the only unknown left in this
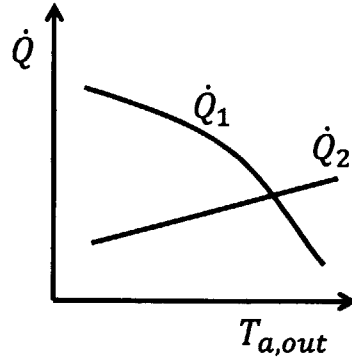
Figure 3-2: Variation of $\dot{Q}_1$ and $\dot{Q}_2$ with the guess values of $T_{a,out}$. The solution is the value of $T_{a,out}$ at the intersection of the two curves.

problem is the water outlet temperature, which can be calculated using Eq. 3.2. Next, the heat transfer that is governed by the size of the system, $\dot{Q}_2$, can be calculated using Eq. 3.4. Figure 3-2 shows the variation of $\dot{Q}_1$ and $\dot{Q}_2$ with $T_{a,out}$, which allows us to modify the guessed value of $T_{a,out}$ as explained in Fig. C-1.

Case 2

We denote by Case 2 the dehumidifier in which the air inlet temperature and the water outlet temperature are specified. This can be thought of as solving for the cold end of the system given the conditions at the hot end. The solution method for this case is almost identical to Case 1, the only difference being the use of Eq. 3.2 to calculate $T_{w,in}$ instead of $T_{w,out}$. The importance of Cases 2 and 3 will become apparent in Section 3.1.2.

Case 3

We denote by Case 3 the system in which $T_{a,out}$ and $T_{w,in}$ are specified. In other words, we are interested in determining the temperatures at the hot end of the system, given the conditions at the cold end. The solution method in this case is similar to Cases 1 and 2, but, instead of guessing $T_{a,out}$, we guess the value of $T_{w,out}$ and then calculate $\dot{Q}_1$ using Eq. 3.2 and $\dot{Q}_2$ using Eq. 3.4. From there, the calculation proceeds according to Fig. C-1. When the guessed values of $T_{w,out}$ converge, and we have $\dot{Q}_1 = \dot{Q}_2$, we can calculate $T_{a,in}$ from Eq. 3.2. This step can be problematic since the temperature appears in both $h_{a,in}$ and $h_{cond,in}$. We can solve for $T_{a,out}$ numerically, or we can choose to guess $T_{a,in}$ instead of $T_{w,in}$. However, since $T_{a,in}$ is higher than both inputs, $T_{w,in}$ and $T_{a,out}$, we need to find an appropriate maximum value. Case 3 will only be

51

used when modeling a multi-tray dehumidifier where we will know $T_{a,top}$ of the whole multi-tray dehumidifier, which can be set as the upper bound on $T_{a,in}$.

3.1.2 Multi-tray bubble column dehumidifier

One drawback to the use of a bubble column is that even though the water and air streams flow in a counterflow manner, both streams interact with the fresh water in the column which is at constant temperature. This means that, even at infinite coil length, the saline water will only reach the air outlet temperature. Tow discusses this phenomenon in detail before defining a parallel flow effectiveness as the appropriate performance metric [24]. However, the height of a single-tray bubble column can be made very small, and multiple trays, each at a different temperature, can be stacked to form a multi-tray bubble column which is no longer limited to the performance of a parallel flow device, as shown in Fig. 3-3, where the temperature profiles are plotted against the normalized enthalpy, which is the change in enthalpy from the cold end over the total enthalpy change.

The governing equations for a multi-tray bubble column are the equations of a single tray, discussed in Section 3.1.1, repeated for each tray, with additional equations for matching the boundary conditions between consecutive trays. One issue that makes solving these equations challenging is that the temperatures of water and air between the trays are unknown, as only the inlet temperatures are given. The system, therefore, has to be solved numerically. This is done by guessing one of the outlet temperatures and constructing the temperature profiles up to the other end by using the dehumidifier functions (Cases 2 and 3). The calculated inlet temperature is then compared to the specified value, and the guessed value is changed accordingly, as shown in detail in Fig. C-2.

In some cases, when the available coil area is large, high effectiveness makes the numerical analysis fail if the temperature is guessed at the wrong end. In order to explain this issue better, we first consider the modified heat capacity rate ratio (HCR) defined by Narayan et al. [7] as follows:

$$\text{HCR} = \frac{\Delta \dot{H}_{\text{max,cold}}}{\Delta \dot{H}_{\text{max,hot}}} \tag{3.5}$$

In the case of a multi-tray bubble column dehumidifier with no inflow of condensate, the cold stream consists of the saline feed water, and the hot stream consists of the moist air and the condensing fresh water stream. The modified heat capacity rate

(a) Single-tray bubble column.

(b) Five-tray bubble column.
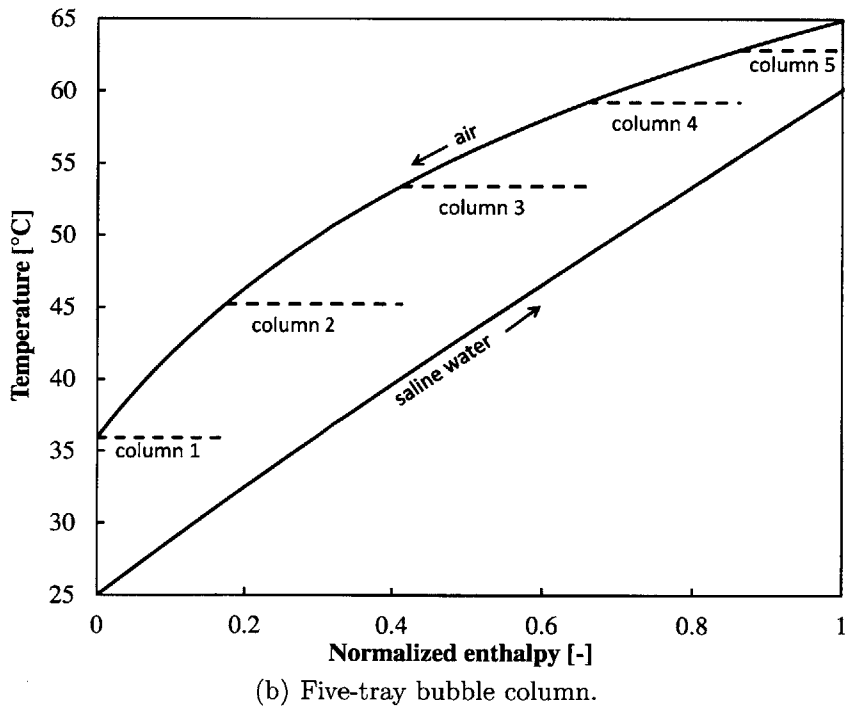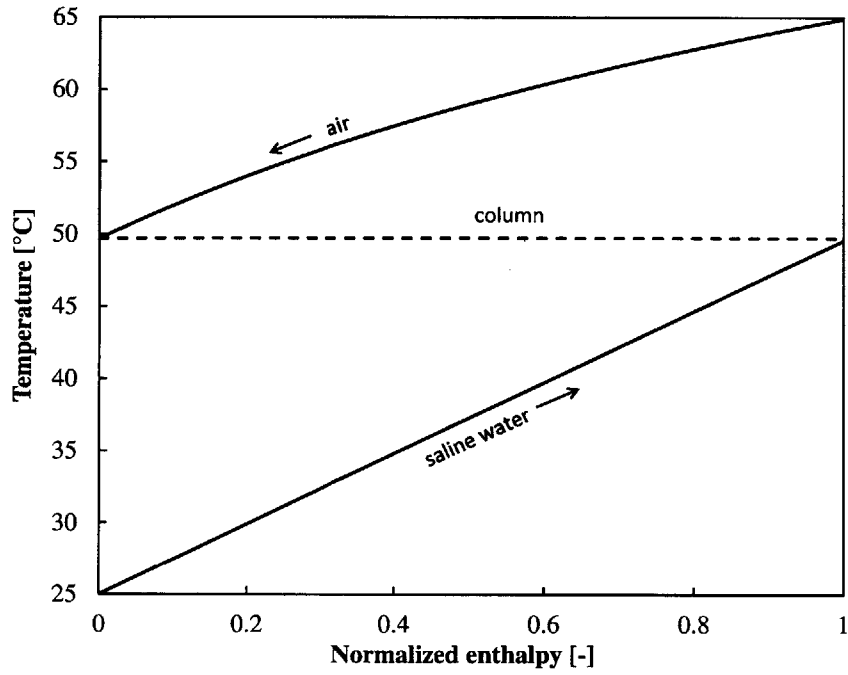
Figure 3-3: Comparison of the performance of a single-tray bubble column and a five-tray bubble column. Both dehumidifiers have the same size, and operate under the same conditions. In the multi-tray dehumidifier, the coil length is divided equally between the trays.

Table 3.1: Specifications of the system studied.

Operating conditions	
Top temperature, T_{top}	90 °C
Bottom temperature, T_{bottom}	25 °C
Feed mass flow rate, $\dot{m}_{\text{w,in}}$	0.242 kg/s
Humidifier geometry	
Height	3 m
Cross-sectional area	0.05 m^2
Fill surface area	226 m^2/m^3
Merkel number, Me	$0.967\left(\frac{\dot{m}_{\text{w}}}{\dot{m}_{\text{a}}}\right)^{-0.779} \times (3.28\ H)^{0.632}$
Minimum-maximum water loading	13.4-32 m^3/hr-m^2
Dehumidifier geometry	
Pipe length per tray	2.5 m
Number of trays	30
Pipe outer/inner diameter	9.5 mm/8.7 mm
Coil diameter	0.4 m

ratio in the dehumidifier can therefore be expressed as:

$$\text{HCR}_{\text{d}} = \frac{\dot{m}_{\text{w}}\left(h_{\text{w}}|_{T_{\text{a,in}}} - h_{\text{w}}|_{T_{\text{w,in}}}\right)}{\dot{m}_{\text{da}}\left(h_{\text{a}}|_{T_{\text{a,in}}} - h_{\text{a}}|_{T_{\text{w,in}}}\right) - \dot{m}_{\text{da}}\left(\omega|_{T_{\text{a,in}}} - \omega|_{T_{\text{w,in}}}\right)h_{\text{cond}}|_{T_{\text{w,in}}}} \qquad (3.6)$$

When the area of the system is large enough to get a high effectiveness, and HCR$_{\text{d}}$ is greater than unity, the air stream, having a lower heat capacity rate, will exit the heat and mass exchanger at a temperature close to the inlet temperature of the saline water. In addition, at the cold end of the system, the temperature variation will become very small since the driving force of the heat and mass exchange is small. This means that a small change in $T_{\text{a,out}}$ will result in a large change of the temperature profile on the hot side. This problem is resolved by building the profile starting from the hot side, so that $T_{\text{w,out}}$ is guessed. Depending upon the calculated value of $T_{\text{w,in}}$, a new $T_{\text{w,out}}$ guess value is picked, as explained in detail in Fig. C-2.

3.1.3 Packed-bed humidifier

The packed-bed humidifier in an HDH system is essentially the same as a cooling tower used in a power plant, but with a different purpose. A cooling tower, as its name suggests, is used to cool water through evaporation and the moist air is rejected back to the environment. In an HDH system, however, the humidifier serves to humidify the air that will later be dehumidified to produce fresh water.

Thanks to the widespread use of cooling towers, the packed-bed humidifier can

be modeled fairly accurately by using the most thorough model for cooling towers, namely the Poppe and Rögener model [35]. Kloppers and Kröger [36] have published a detailed algorithm to solve the equations of the model numerically using the fourth order Runge-Kutta method. The rest of this section briefly describes the governing equations for heat and mass transfer in the humidifier, and presents the algorithm used in finding their solution.

Governing equations and solution method

As explained by Kloppers and Kröger [36], determining the performance of the humidifier involves solving for the four main variables: the water temperature, T_w, the enthalpy of moist air, h_a, the absolute humidity, ω, and the Merkel number, Me, at different locations within the humidifier, where Me is a dimensionless parameter that captures the effect of the system size:

$$\text{Me} = \frac{KaV}{L} \tag{3.7}$$

The variation of the four variables along the humidifier can be expressed in terms of the change in water temperature:

$$\frac{dh_{\text{a}}}{dT_{\text{w}}} = f_1\left(T_{\text{w}}, h_{\text{a}}, \omega, \text{Me}\right) \tag{3.8}$$

$$\frac{d\omega}{dT_{\text{w}}} = f_2\left(T_{\text{w}}, h_{\text{a}}, \omega, \text{Me}\right) \tag{3.9}$$

$$\frac{d\text{Me}}{dT_{\text{w}}} = f_3\left(T_{\text{w}}, h_{\text{a}}, \omega, \text{Me}\right) \tag{3.10}$$

where f_1, f_2, and f_3 are functions given by Kloppers and Kröger [36], and are summarized in Appendix B. In order to determine the temperature profiles of air and water in the humidifier, these equations have to be solved numerically at small intervals. The algorithm is explained in Fig. C-3 in the Appendix, but some steps will be discussed here in greater detail. Given the water and air inlet temperatures, the first step is to guess the water outlet temperature using the bisection method. The humidifier is then divided into an appropriate number of intervals of constant water temperature change, ΔT_{w}. These intervals serve as a basis of solving Eq. 3.8, 3.9, and 3.10. At the cold end, the temperatures are known, the air properties, h_{a} and ω, are evaluated at saturation, and the Merkel number, Me, is set to 0. This gives us a complete set of boundary conditions at the cold end. Solving the differential equations numerically starting at the cold end allows us to build a complete profile

55

up until the hot end where the boundary conditions are checked, and the procedure is repeated with an appropriate new guess value for the water inlet temperature, as explained in Fig. C-3. For further details on the solution method, and on cooling towers in general, the reader should refer to Klopper's doctoral thesis [37].

The specifications of the fill used in this analysis were adopted from Brentwood Industries (model number: CF-1200MA) and are summarized in Table 3.1. We note that the Merkel number correlation is independent of the cross-sectional area of the fill, and that this area affects the performance in that it imposes upper and lower bounds on the mass flow rate of water. In our analysis, the value of the area was specified, and the value of the flow rate of water was taken between the allowable extremes to ensure a realistic operating flow rate.

3.1.4 Humidification dehumidification system without extractions

The full HDH system consists of a packed bed humidifier and a multi-tray bubble column dehumidifier. The governing equations are those mentioned above for each component. In addition, as shown in Fig. 3-1, the air temperatures have to match between the humidifier and the dehumidifier. The solution method for the system can be thought of as analogous to the real system reaching steady state operation. Starting with the bottom air temperature, $T_{a,1,h}$, equal to the bottom temperature of the system, the humidifier function is called, and $T_{a,2}$ is calculated. The obtained value of $T_{a,2}$ is then input into the multi-tray dehumidifier function, which returns a new value for $T_{a,1,d}$. If the error on $T_{a,1}$ is higher than acceptable, the procedure is repeated with the new temperature until we get $T_{a,1} = T_{a,1,d} = T_{a,1,h}$. The algorithm is summarized in the form of a flowchart in Fig. C-4.

3.1.5 Humidification dehumidification system with a single extraction

It has been previously proven than varying the water-to-air mass flow rate ratio can improve the performance of the system [21, 38] because the heat capacity of moist air varies greatly with temperature whereas that of water remains relatively constant. To keep the total heat capacity rates of the streams matched, their relative flow rates must vary.

Chapter 2 focused on the fixed-effectiveness modeling of extractions and injec-

tions, which was useful in understanding why they had a positive effect on system performance. To further understand how we can implement the variation of the mass flow rate ratio in actual system design, where the total area is fixed, we turn to modeling a single extraction in a system of fixed area.

Having modeled each component in the system separately, the algorithm used in modeling a system with a single extraction consists of combining models of the separate components and then matching the boundary conditions. Numerically this is not as straightforward as the algorithm for a system without extraction due to the fact that we now have two air flow rates to vary. What makes the modeling even more challenging is the fact that the two stages in the system are very interdependent. We cannot think of each stage as a system that can be solved separately since the intermediate temperatures are determined by the flow rates picked in each of the stages. In other words, varying the mass flow rate of air in the top stage while keeping the flow rate of air constant in the bottom stage will change the intermediate temperatures in the system, affecting the lower stage.

In modeling a system with a single extraction, the total areas of the dehumidifier and the humidifier, the top and bottom temperatures, and the feed flow rate are fixed. We have to first choose the location of the extraction, and we also have to decide on the flow rates of air in the two stages. In solving the system with these constraints, we would have to guess at least one intermediate temperature. One way to go around having to find the correct pair of mass flow rates was to specify instead the value of the intermediate water temperature in the dehumidifier, $T_{w,2}$, shown in Fig. 3-4. Fixing $T_{w,2}$ allows us to model the top stage as a system without extraction with fixed top and bottom temperatures, which means the top stage could be modeled using the N_0 function described in Section 3.1.4. Once $T_{w,2}$ is picked, we have to guess the air flow rate in the top stage, $\dot{m}_{da,2}$. We can set reasonable bounds on the mass flow rate ratio in the top stage from expertise gained in the fixed-effectiveness modeling presented in Chapter 2. After picking the flow rate of air in the top stage, we can run the N_0 function and calculate $T_{a,2}, T_{a,3}, T_{w,3}$, and $T_{w,5}$.

Let us now consider the dehumidifier of the first stage. The water inlet and outlet temperatures are known, and the top air temperature is known. We can find the appropriate flow rate of air that, given the inlet temperatures, would result in the desired $T_{w,2}$. By finding the appropriate $\dot{m}_{da,1}$, we also find $T_{a,1}$.

Finally, let us consider the humidifier in the first stage. The water and air inlet temperatures and flow rates are known. We can call the humidifier function, described in Section 3.1.3, with these inputs to calculate the outlet temperatures: $T_{w,6}$ and $T_{a,2,b}$.
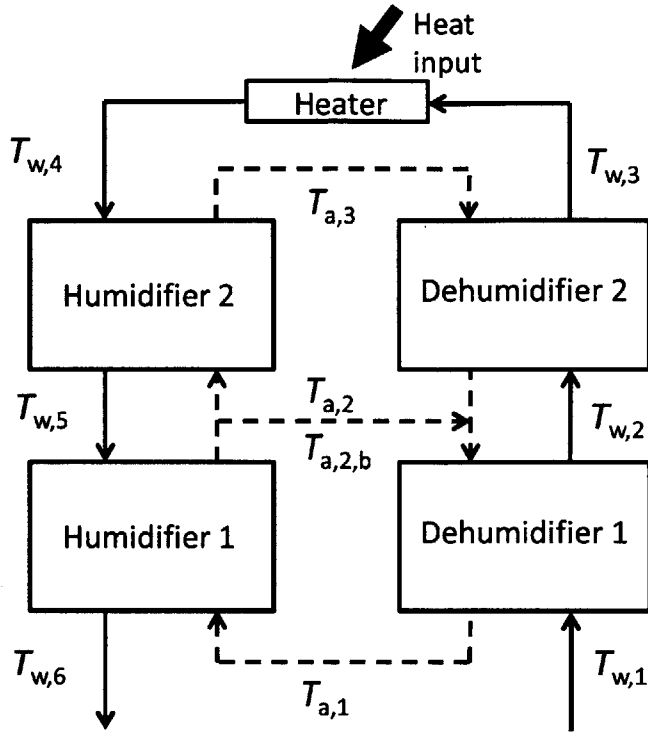
Figure 3-4: Schematic diagram representing an HDH system with a single extraction.

Note the added subscript 'b' since this temperature is not necessarily equal to $T_{a,2}$ calculated in the second stage. Knowing that these two temperatures must be equal, we can vary $\dot{m}_{da,2}$ according to Fig. 3-5.

By choosing to fix $T_{w,2}$ instead of the pair of flow rates of air, we greatly simplify the solution algorithm, and are sure to get convergence (unless the set value of $T_{w,2}$ is too high to be reached with the finite area available in stage 1, as discussed in greater detail in Section 3.3). The solution algorithm is summarized in the form of a flowchart in Fig. C-5 in Appendix C.

3.1.6   Performance parameters

A widely used measure of the energy efficiency of a thermal desalination system is the Gained Output Ratio, GOR, defined as

$$\text{GOR} = \frac{\dot{m}_{pw} h_{fg}}{\dot{Q}_{in}} \tag{3.11}$$

GOR measures the degree of reuse of the heat input. A desalination system that does not recover the heat of condensation will have at most a GOR of 1, which is achieved

58
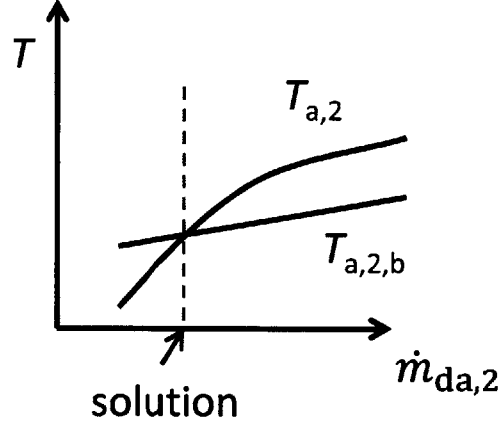
Figure 3-5: Variation of $T_{a,2}$ and $T_{a,2,b}$ with $\dot{m}_{da,2}$.

only if all of the heat input is used for vaporization. A system with a GOR of 3 uses the energy input effectively 3 times, or basically produces three times the quantity of water that the same heat input would produce in the basic system with a GOR of 1.

Another important measure of performance is the Recovery Ratio, RR, which is the ratio of fresh water produced to feed water:

$$\text{RR} = \frac{\dot{m}_{pw}}{\dot{m}_{w}} \tag{3.12}$$

3.2 Results and discussion for a system without extraction

The specifications of the system presented in this chapter are summarized in Table 3.1. The superficial air velocity in the dehumidifier was fixed at 10 cm/s (a value known to be in the regime for which the model was developed), and the cross-sectional area of the bubble column was varied according to the definition of superficial velocity:

$$V_g = \frac{\dot{m}_a}{\rho_a A_{col}} \tag{3.13}$$

3.2.1 Effect of the heat capacity rate ratio on performance

The first step of this study was to make sure the results of this fixed-area model matched those generated by the fixed-effectiveness model suggested by Narayan et al. [7]. The effect of HCR$_d$ (Eq. 3.5) on the performance of the system was studied in this section. Equation 3.6 shows that the value of HCR$_d$ depends on the bottom

59

temperature, the top air temperature, $T_{a,2}$, and the water-to-air mass flow rate ratio defined as

$$\mathrm{MR} = \frac{\dot{m}_w}{\dot{m}_{da}} \qquad (3.14)$$

Note that the top air temperature is not an input, but is rather determined by simulating the system, as explained in Section 3.1.4. In other words, the top air temperature depends on the top and bottom temperatures of the system, the mass flow rates of air and water, and the size of the system. For a system of fixed size, and given top and bottom temperatures, the value of $\mathrm{HCR_d}$ can be changed by varying the mass flow rate ratio.

As can be seen in Fig. 3-6(a), the GOR of a system with fixed area is maximized when $\mathrm{HCR_d}$ is equal to unity. In other words, the heat capacity rates of the interacting streams in the dehumidifier are equal. This result reiterates the importance of $\mathrm{HCR_d}$ in extracting the best performance from the HDH system.

Similarly, setting $\mathrm{HCR_d}$ to unity results in the highest possible recovery ratio, as shown in Fig. 3-6(b). The reason behind this behavior is that, when $\mathrm{HCR_d} = 1$, the effectiveness is at a minimum for this system, which means that the driving force will not become too small at either end of the exchanger. When $\mathrm{HCR_d} = 1$, at any point in the heat and mass exchanger there will be a finite driving force that will prompt the maximum possible heat and mass transfer. A high effectiveness is only desired when the system is balanced. It is a disadvantage to be limited by a small maximum heat duty, even if that value is reached. This is explained in greater detail in Section 3.3.1.

The importance of $\mathrm{HCR_d}$ raises the question on the role of $\mathrm{HCR_h}$ in balancing the HDH system. To answer this question, we look at Fig. 3-7, which shows the variation of GOR and RR with $\mathrm{HCR_h}$. We can clearly see a peak in GOR and RR at $\mathrm{HCR_h} = 3.3$, which corresponds to $\mathrm{HCR_d} = 1$. In fact, as $\mathrm{HCR_h}$ approaches unity, the performance keeps dropping because the dehumidifier is becoming less balanced. This trend can best be explained by looking at the temperature-enthalpy profiles of systems with $\mathrm{HCR_h} = 1$ and $\mathrm{HCR_d} = 1$, shown in Fig. 3-8. The air stream in the humidifier can at most reach saturation at the inlet temperature of the water, which, in this case, is 90 °C. Due to high water content in moist air at high temperatures, the change in specific enthalpy that can be achieved by the moist air stream is very large compared to the change in specific enthalpy of the water stream which is simply in the form of sensible heat. In order to get $\mathrm{HCR_h} = 1$, the mass flow rate ratio has to be very high to compensate for the difference in the maximum changes of specific
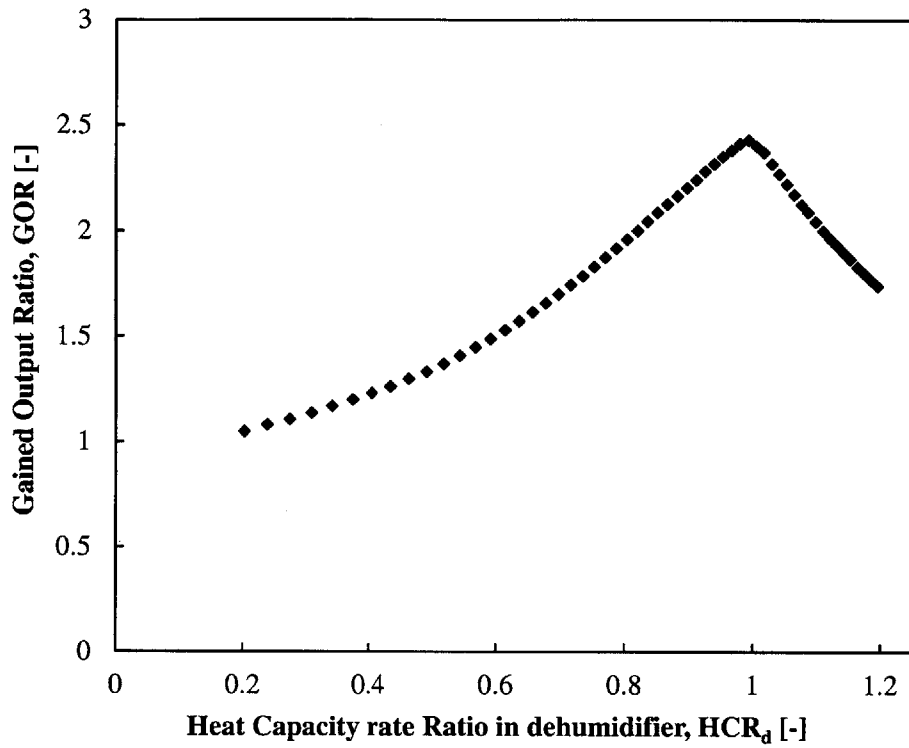
(a) Variation of GOR with the heat capacity rate ratio.
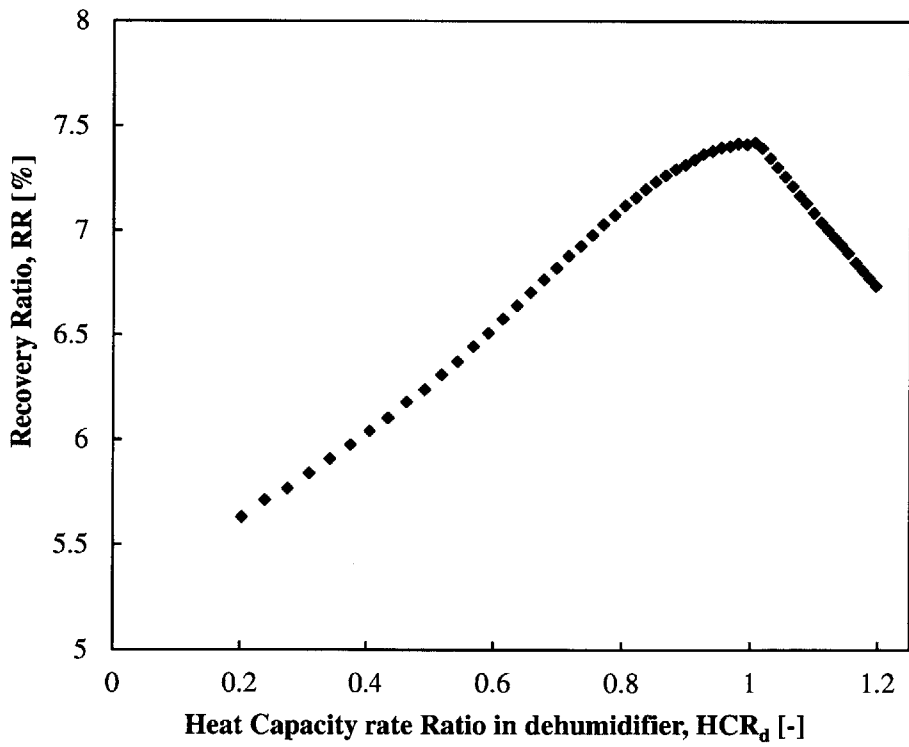
(b) Variation of RR with the heat capacity rate ratio.

Figure 3-6: Effect of HCR_d on performance.

enthalpy of the two streams. Setting $HCR_h = 1$ translates into the profile shown in Fig. 3-8(a), which shows large temperature differences between the interacting streams in the dehumidifier, generating more entropy in the dehumidifier than is saved by balancing the humidifier. The advantage of having $HCR_d = 1$ is apparent in Fig. 3-8(b), where the dehumidifier is balanced, thus minimizing the entropy produced in the dehumidifier, all while keeping the temperature differences in the humidifier acceptable.
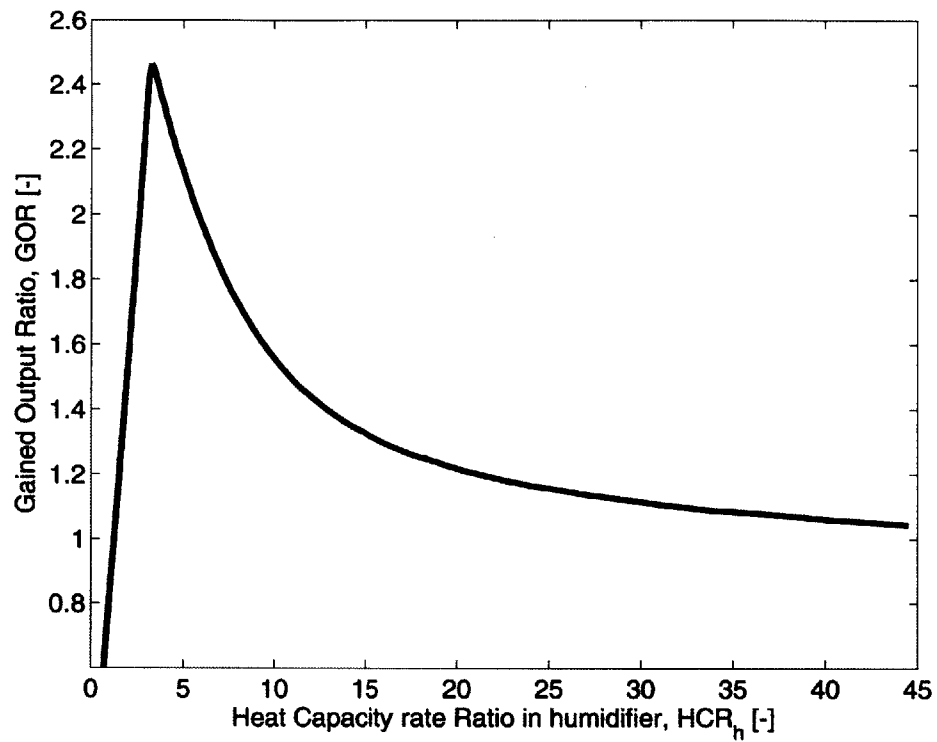
(a) Variation of GOR with the heat capacity rate ratio in the humidifier.
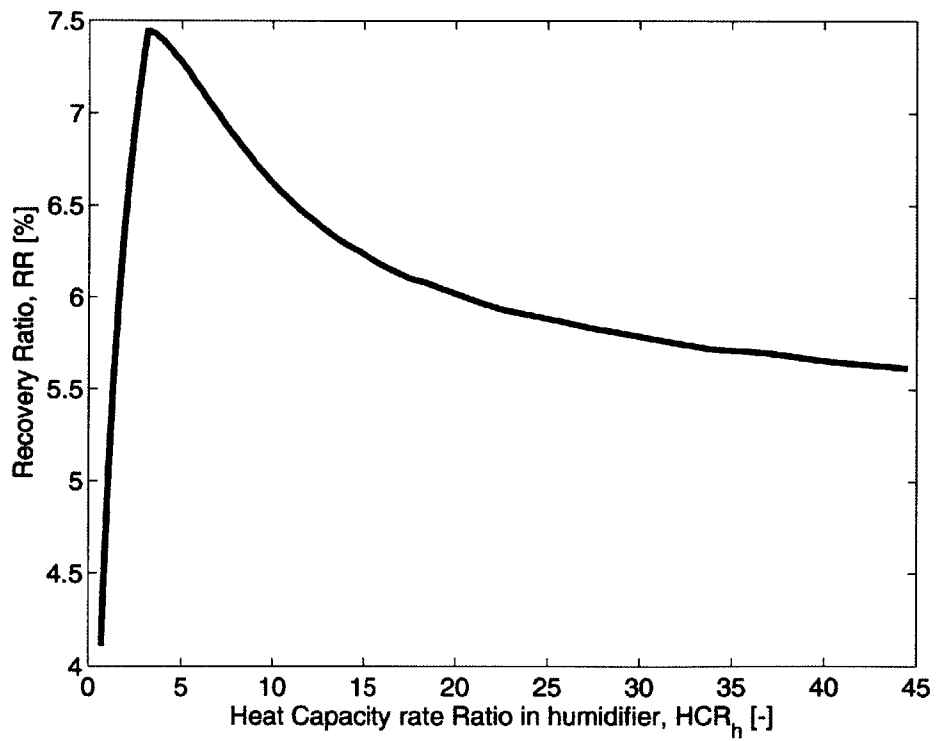
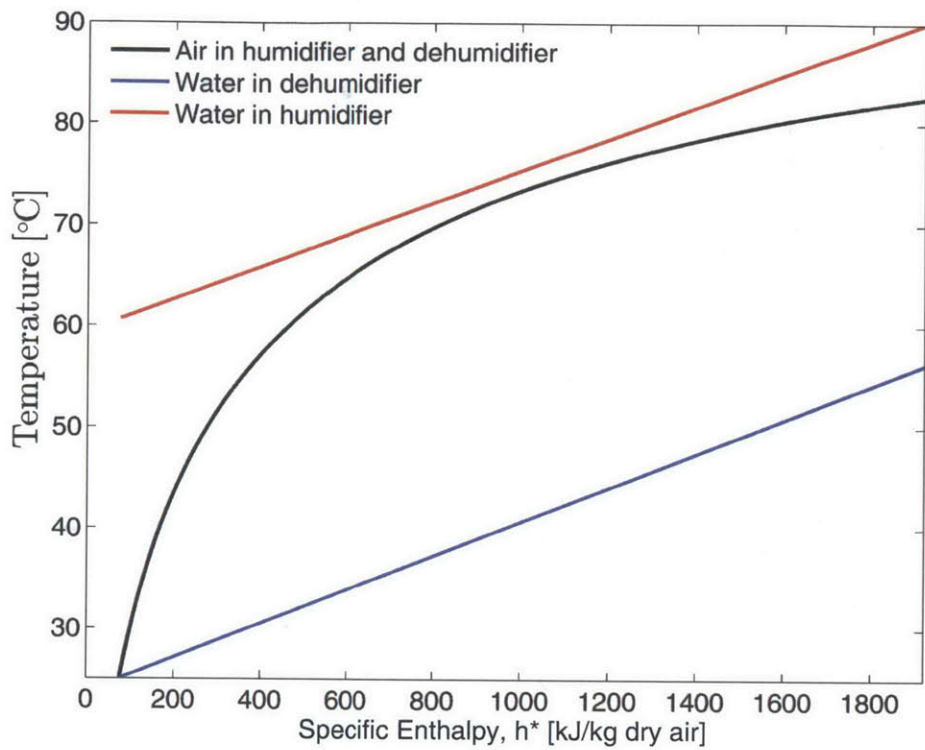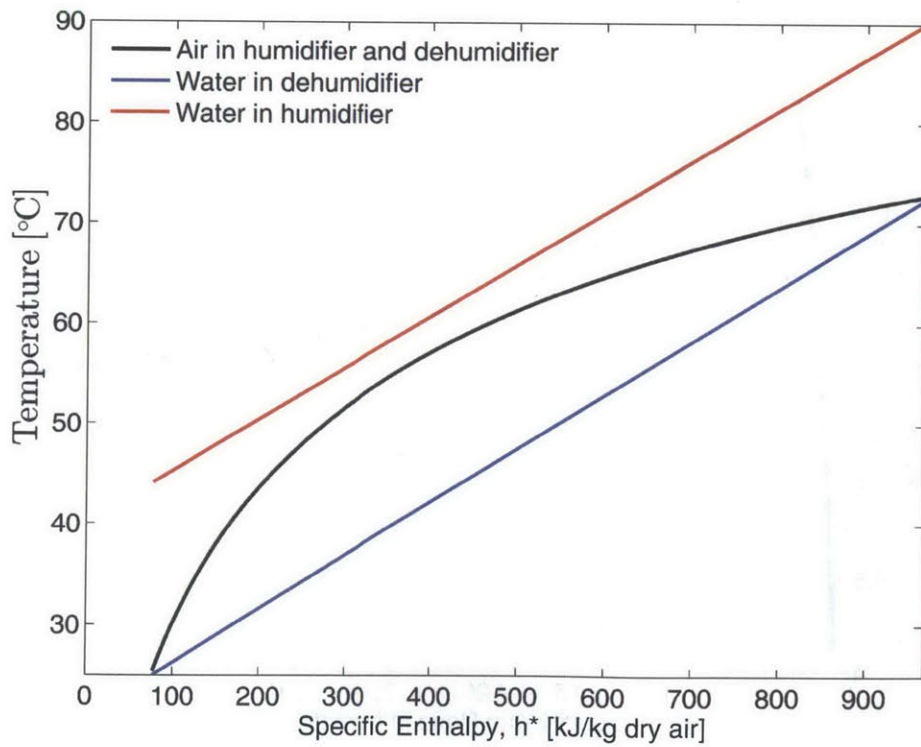

(b) Variation of RR with the heat capacity rate ratio in the humidifier.

Figure 3-7: Effect of HCR_h on performance.

(a) $HCR_h = 1$.

(b) $HCR_d = 1$.

Figure 3-8: Temperature-enthalpy profiles of systems with $HCR_h = 1$ and $HCR_d = 1$.

3.2.2 Effect of bottom temperature on system performance

This section simulates the same system described in Table 3.1 except with a varying bottom temperature. This is done in order to evaluate the effect of a changing ambient water temperature.

Variation of heat capacity rate ratio with bottom temperature

For a system designed to operate between 25 °C and 90 °C, it was shown in Section 3.2.1 that only one mass flow rate ratio (MR = 4.2) results in a balanced system, and thus the best performance. If we fix the mass flow rate ratio to the design value of 4.2, it can be seen in Fig. 3-9 that HCR_d will change from unity as the bottom temperature deviates from the design value of 25 °C, and the system will no longer be balanced, resulting in a drop in performance.

Variation of mass flow rate ratio with bottom temperature

When the bottom temperature changes from the design value, bringing HCR_d back to unity would require changing the operating mass flow rate ratio. Figure 3-10 presents the optimal operating mass flow rate ratio for this system at any bottom temperature. It can be seen that, when the bottom temperature increases, the mass flow rate ratio should also be increased to keep the system balanced. This result can be explained by looking back at Eq. 3.6. However, we should note that even though the variation of HCR_d with the bottom temperature is linear, the same cannot be said about the variation of MR since HCR_d depends on the top air temperature which is also a function of the MR.

Variation of GOR with bottom temperature

Figure 3-11(a) shows the variation of GOR with bottom temperature for two systems. The first system is designed to operate between 25 °C and 90 °C, meaning that its fixed MR only results in a balanced system at the design conditions. As the bottom temperature varies, as shown in Fig. 3-9, HCR_d will deviate from 1, and, as expected, GOR will drop. The other system allows for the variation of MR such that HCR_d is always equal to unity. We can see that the effect of increasing the bottom temperature while keeping $HCR_d = 1$ is to raise GOR. This is expected since, for the same area, the water can reach a higher temperature before entering the heater, and therefore the required heat input will drop, and GOR will increase. Also, comparing the two curves in Fig. 3-11(a), we can see the importance of balancing on the energy efficiency
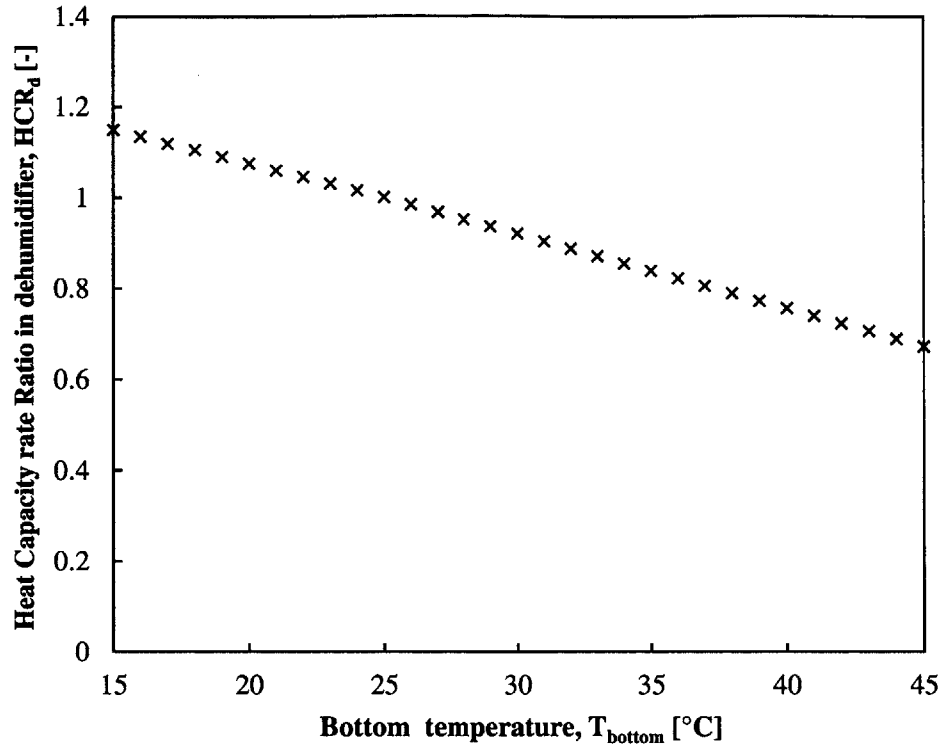
Figure 3-9: Variation of HCR$_d$ with bottom temperature for a system of fixed MR.
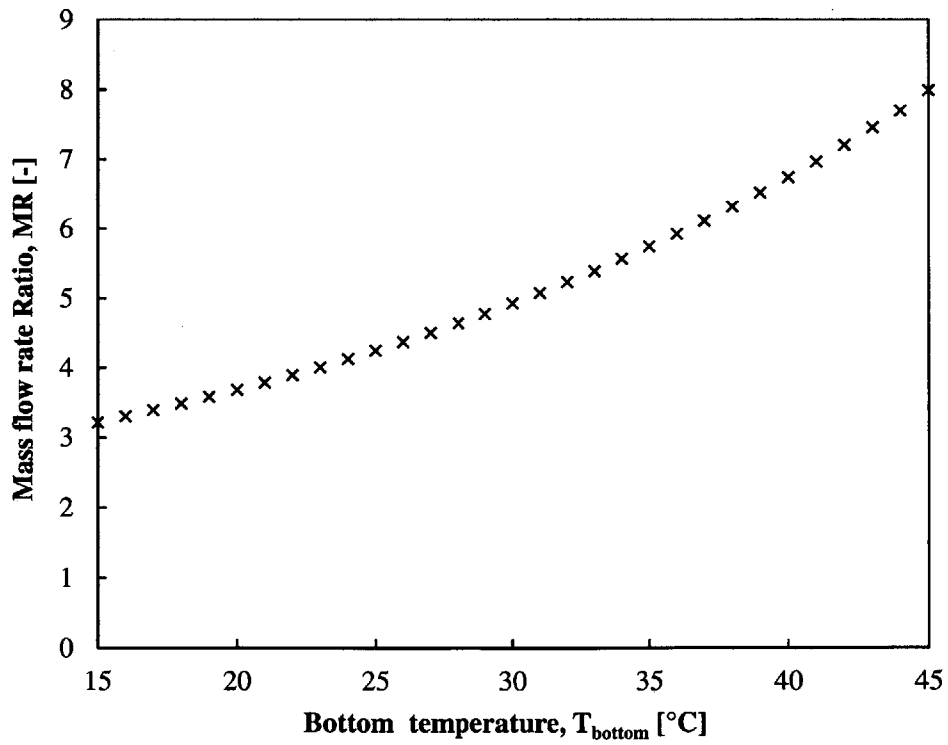
Figure 3-10: Variation of MR with bottom temperature for a system of HCR$_d$ = 1.

of the HDH cycle. If the system is installed in a location where the temperature of the water to be treated fluctuates greatly, it could be economical to install a control system that would vary the flow rate of the air stream to meet the MR profile shown in Fig. 3-10 in order to keep HCR_d equal to unity.

Variation of RR with bottom temperature

As can be seen in Fig. 3-11(b), the effect of balancing on RR is not as big as that on GOR. This observation indicates that the advantage of balancing is mainly to lower the heat input required to operate the system.

It is worth noting that satisfying $HCR_d = 1$ will always maximize the output of the system, while also increasing the energy efficiency. In fact, if we consider the cases where the bottom temperature is higher than $25\,^{\circ}C$, the required MR, shown in Fig. 3-10, will be higher than 4.2, and the flow rate of air will be lower, but the system will still produce more water and at a higher energy efficiency. This result shows that adding more air to the system will not necessarily produce more water, and will not necessarily provide the water with more preheating. If we consider the dehumidifier on its own, keeping the top air temperature fixed and increasing the flow rate of air will result in a higher water outlet temperature. But in an HDH system, varying the flow rate of air will not keep the top air temperature fixed. In fact, when the air flow rate is increased there is a possibility that the total amount of water produced will drop. If we consider the humidifier alone, fixing the bottom air temperature and increasing the flow rate of air will result in a lower top air temperature. Increasing the air flow rate means that the there will be more air in the dehumidifier, but it will enter at a lower temperature. Picking the correct flow rates is a balance between the humidifier and the dehumidifier, and it turns out that matching the heat capacity rates is the key in getting the best performance in terms of both energy efficiency and productivity.
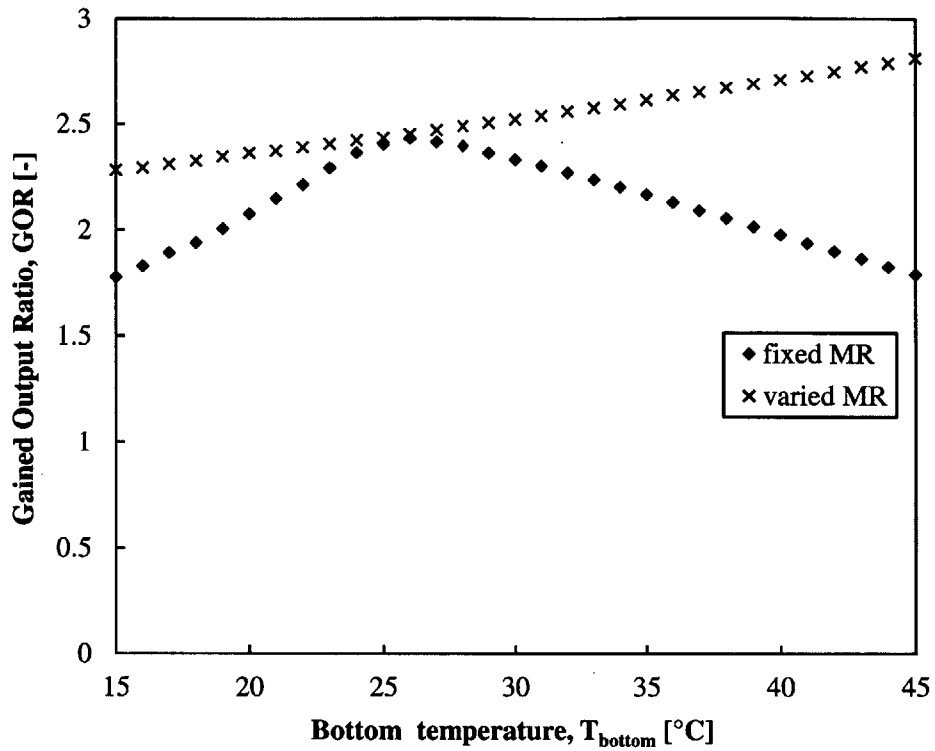
(a) Variation of GOR with bottom temperature.
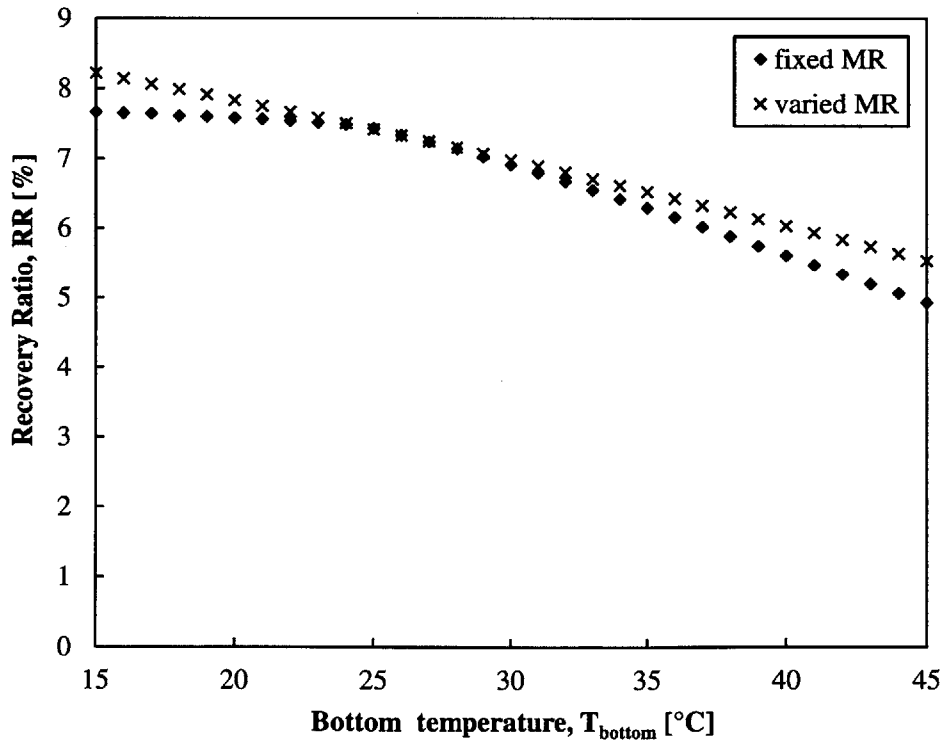
(b) Variation of RR with bottom temperature.

Figure 3-11: Effect of bottom temperature on performance for fixed MR and for a system that dynamically adjusts MR to hold $HCR_d = 1$.

3.2.3 Effect of top temperature on system performance

This section discusses the effect of the top temperature, which can vary if the heat source of the system is not constant. A typical application would be solar heating, where the solar irradiation will vary greatly during the daily operation of the system. The system studied has the specifications described in Table 3.1 except that the top temperature is allowed to vary.

Variation of heat capacity rate ratio with top temperature

Figure 3-12 shows the effect of the top temperature on HCR_d while keeping MR constant and equal to 4.2. We can see that, as the top temperature drops from the design value of 90 °C, HCR_d increases and deviates from unity, so we can expect the performance to drop.

Variation of mass flow rate ratio with top temperature

It follows from Eq. 3.6 that we would need to decrease MR as the top temperature drops from the design value in order to keep HCR_d equal to unity. The optimal MR at various top temperatures is shown in Fig. 3-13. Similar to the optimal MR profiles presented in Fig. 3-10 and 3-13, we could generate all possible combinations of top and bottom temperatures of interest, and find the optimal MR at each of these pairs, which could be then input into the control unit of the system. Even though the effect of the bottom temperature is not great on the performance of the system, if the top temperature also varies, the variation of MR should take into account both temperatures.

Variation of GOR with top temperature

Figure 3-14(a) shows the variation of the GOR of two systems with the top temperature. The first system is designed to operate between 25 °C and 90 °C, so has MR = 4.2 to get $HCR_d = 1$ at 25 °C and 90 °C. But as the top temperature varies, MR is kept constant, so the performance of the system drops. The second system is a dynamic system that adjusts its MR such that HCR_d is always equal to unity. We can see that, when the top temperature drops, the energy efficiency of the dynamic system actually increases slightly.

The difference between the dynamic and passive systems in terms of GOR is quite significant, which indicates that if an HDH system relies on a heating source that is not constant, such as solar heating, the system should be flexible in adopting different
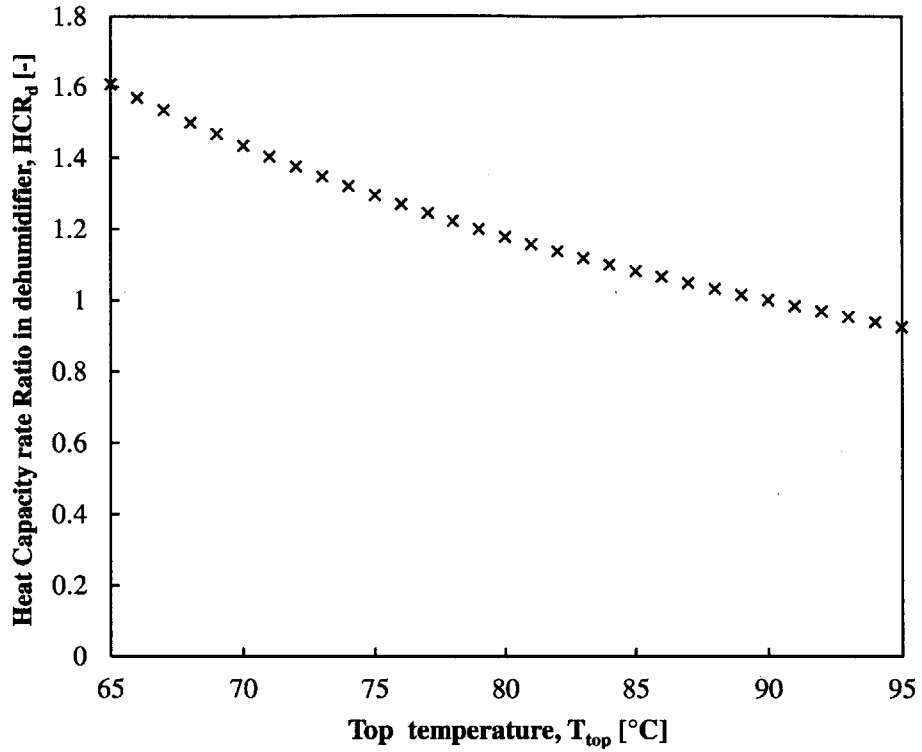
Figure 3-12: Variation of HCR$_d$ with top temperature for a system of fixed MR.
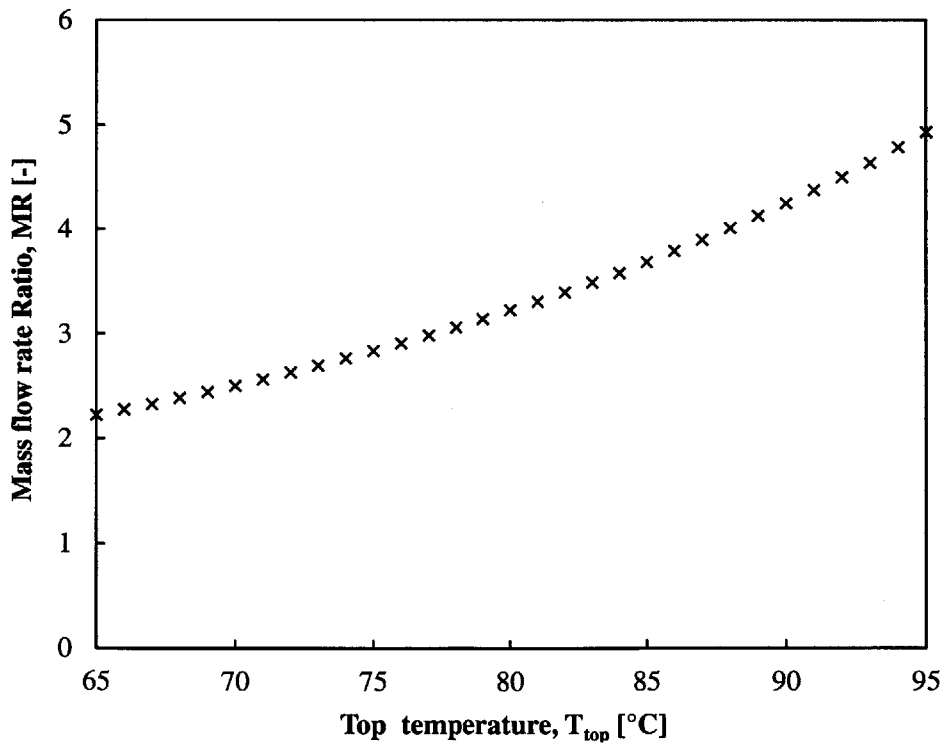
Figure 3-13: Variation of MR with top temperature for a system of fixed HCR$_d$ = 1.

70

mass flow rates of air to compensate for the change in top temperature. If a control system is not feasible, the system should be designed by taking into consideration the variation of the top temperature, and should operate at the MR that maximizes the total output over a certain period of time.

Variation of RR with top temperature

As shown in Fig. 3-14(b), the effect of the top temperature on the recovery ratio is very large even if the system operates under variable MR. The reason behind this strong dependence is the exponential relation between absolute humidity and temperature. Operating the system at a higher temperature allows a large quantity of water to evaporate in the humidifier, and then condense in the dehumidifier, giving rise to a high recovery. Although balancing does not have a substantial effect on recovery, it should be noted that, as seen in Fig. 3-14(a), it does have a substantial effect on the energy efficiency of the system.
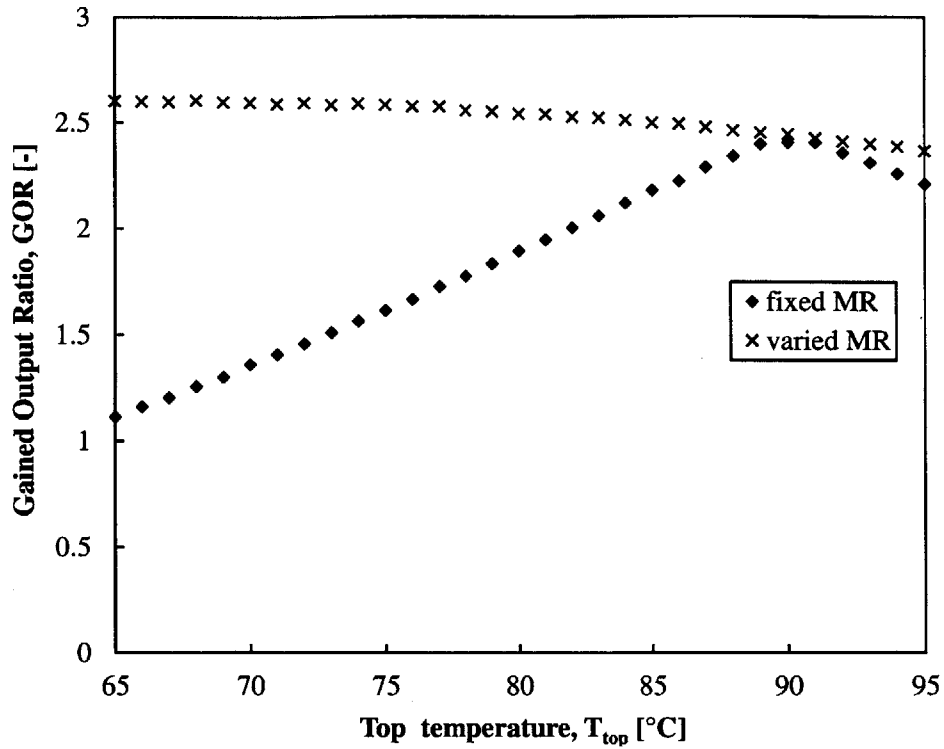
(a) Variation of GOR with top temperature.
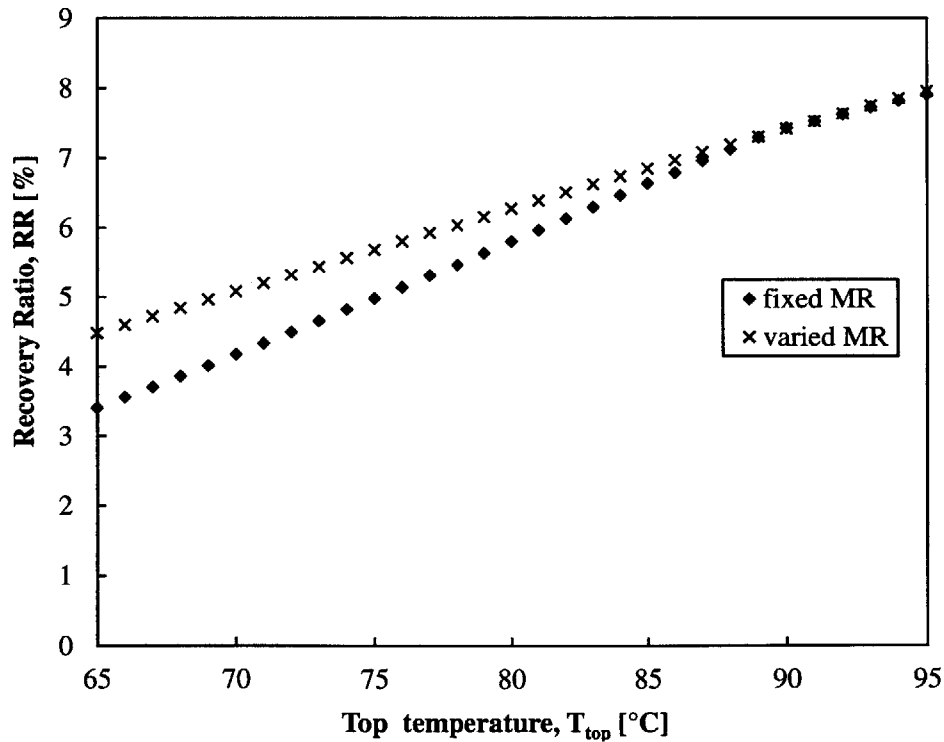
(b) Variation of RR with top temperature.

Figure 3-14: Effect of top temperature on performance for fixed MR and for a system that dynamically adjusts MR to hold $HCR_d = 1$.

3.3 Results and discussion for a system with a single extraction

As explained in Section 3.1.5, the areas of the components and the top and bottom temperatures are fixed at the values listed in Table. 3.1. Each different operating point presented in the results of this section corresponds to a specified location of extraction (number of trays in each stage) and a specified value of the intermediate temperature of the water in the dehumidifier, $T_{w,2}$. The number of trays in the first stage, $N_{t,1}$, is varied between 3 and 29, with $N_t = 30$. For example, if we set $N_{t,1} = 12$, this means $N_{t,2} = N_t - N_{t,1} = 18$. The available area in the humidifier is divided in the same proportions: $H_1 = H \times \frac{N_{t,1}}{N_t} = 1.2$ m, and the rest of the available humidifier height is in the second stage. At each location, $T_{w,2}$ is varied, and the correct pair of mass flow rates of dry air are calculated using the algorithm described in Section 3.1.5. $T_{w,2}$ is increased until the available area in the first stage is no longer sufficient to supply the appropriate heat duty. As shown in Fig. 3-15(a), the mass flow rate of dry air in the first stage required to heat the water to $T_{w,2}$ spikes at a certain $T_{w,2,\mathrm{max}}$. This is true because as $T_{w,2}$ increases, the mass flow rate of dry air in the second stages decreases, as shown in Fig. 3-15(a), so it is possible to get an effectiveness of 100% in the dehumidifier of the second stage. With the air being the stream with the smaller heat capacity rate, the temperature of the extracted air stream, $T_{a,2}$, becomes equal to $T_{w,2}$. This in turn means that the dehumidifier of the first stage must have an effectiveness of 100% with the water being the stream with the smaller heat capacity rate. In order to heat the water up to the desired $T_{w,2} \approx T_{a,2}$, the mass flow rate must be increased until the area available is no longer enough to accommodate the heat and mass transfer required.

As mentioned above, the mass flow rate of dry air in the second stages decreases with increasing $T_{w,2}$. In fact, at high $N_{t,1}$, $\dot{m}_{da,2}$ becomes the limiting factor as very low values are required as shown in Fig. 3-15(b). In simulating the system, extrema are imposed on the allowable values that the mass flow rates of dry air can take. In this simulation, based on knowledge gained from the results presented in Chapter 2 of this study, the mass flow rate ratio was chosen between 0.9 and 40. We note that these are conservative values to enable the simulation of the full operating range.
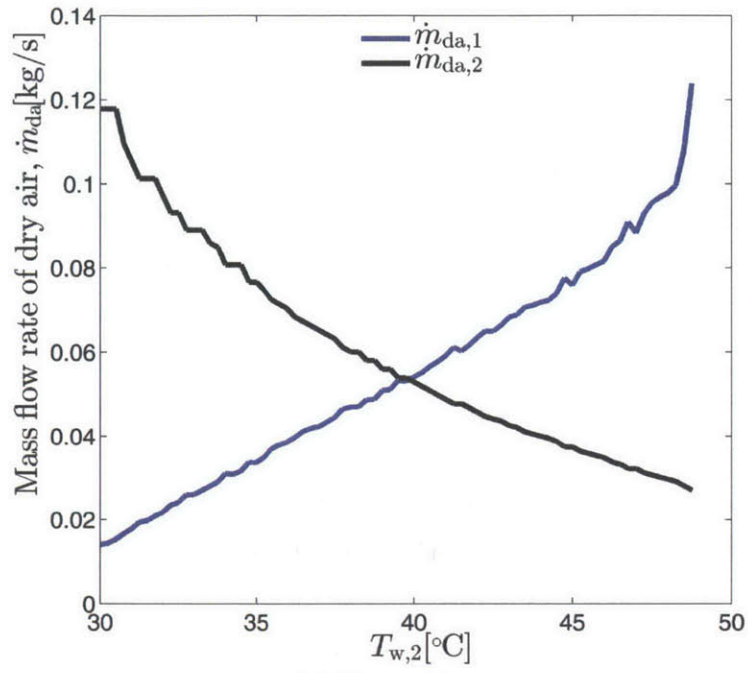
(a) $N_{t,1} = 14$.
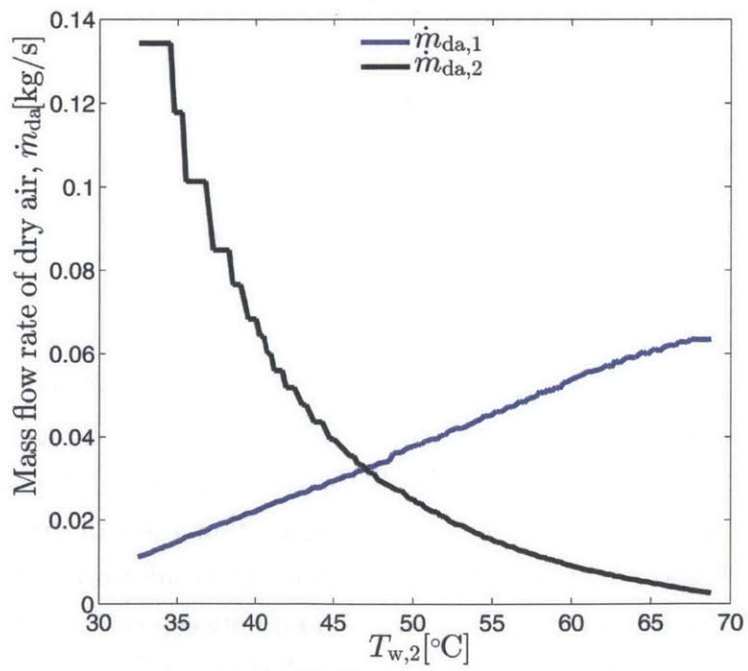
(b) $N_{t,1} = 27$.

Figure 3-15: Variation of $\dot{m}_{da,1}$ and $\dot{m}_{da,2}$ with $T_{w,2}$.

3.3.1 Effect of the heat capacity rate ratio on performance

This section studies the effect of the heat capacity rate ratio on the performance of the system, represented by the gained output ratio and the recovery ratio. We note that the data points are the same in Fig. 3-16(a), 3-16(b), and 3-17; however, to show the results clearly, the space was plotted in 3 different graphs. What is clear from Fig. 3-16(a) is that the point with the highest GOR has $HCR_{d,1} = 1$. In addition, Fig. 3-16(b) shows that the highest GOR is achieved when $HCR_{d,2} = 1$. Figure 3-17 represents the variation of GOR varies with both $HCR_{d,1}$ and $HCR_{d,2}$, and clearly shows that GOR is maximized when $HCR_{d,1} = HCR_{d,2} = 1$.

Setting $HCR_{d,1} = HCR_{d,2} = 1$ in a two-stage HDH system means that both stages are thermodynamically balanced. The best way to understand the importance of HCR_d on the performance of a heat and mass exchanger is to consider an exchanger of effectively infinite area. For example, if $\Delta \dot{H}_{max,w} > \Delta \dot{H}_{max,a}$, the air stream, being the stream with the lower maximum possible change in enthalpy rate, will reach the inlet state of the water stream. This will only allow the water stream to have $\Delta \dot{H}_w = \Delta \dot{H}_{max,a}$, meaning there was some loss in the possible change of enthalpy rate of that stream equal to the difference $\Delta \dot{H}_{max,w} - \Delta \dot{H}_{max,a}$. In a system where only one of the streams is important, we care about having an effectiveness close to 100%. But in a system like HDH where both the humidifier and the dehumidifier are coupled and are important for the performance of the system, we want to achieve the maximum possible change in the enthalpy rates of both streams (heat duty), and this can only be achieved by setting $HCR_d = 1$.

Equation 3.15, links the heat duty to the heat input into the system. This is done by applying an energy balance on the feed stream from the inlet of the dehumidifier to the inlet of the humidifier. In that control volume, some heat is added in the dehumidifier, denoted by $\dot{Q}_{duty}$, and the remaining energy required to reach the top temperature is added in the heater, denoted by $\dot{Q}_{in}$. In the system studied, the top and bottom temperatures are fixed, so the total heat input to the seawater stream required to take it from the bottom temperature to the top temperature is fixed. This means that, in order to minimize the heat input, we have to maximize the heat duty, which is done by setting $HCR_d = 1$.

$$\dot{m}_{w,in}\left(h_{w,top} - h_{w,bottom}\right) = \dot{Q}_{duty} + \dot{Q}_{in} = \text{constant} \qquad (3.15)$$

What this result means from a fixed-area perspective is that the use of the available area is maximized when we set $HCR_d = 1$. Consider a system of finite area
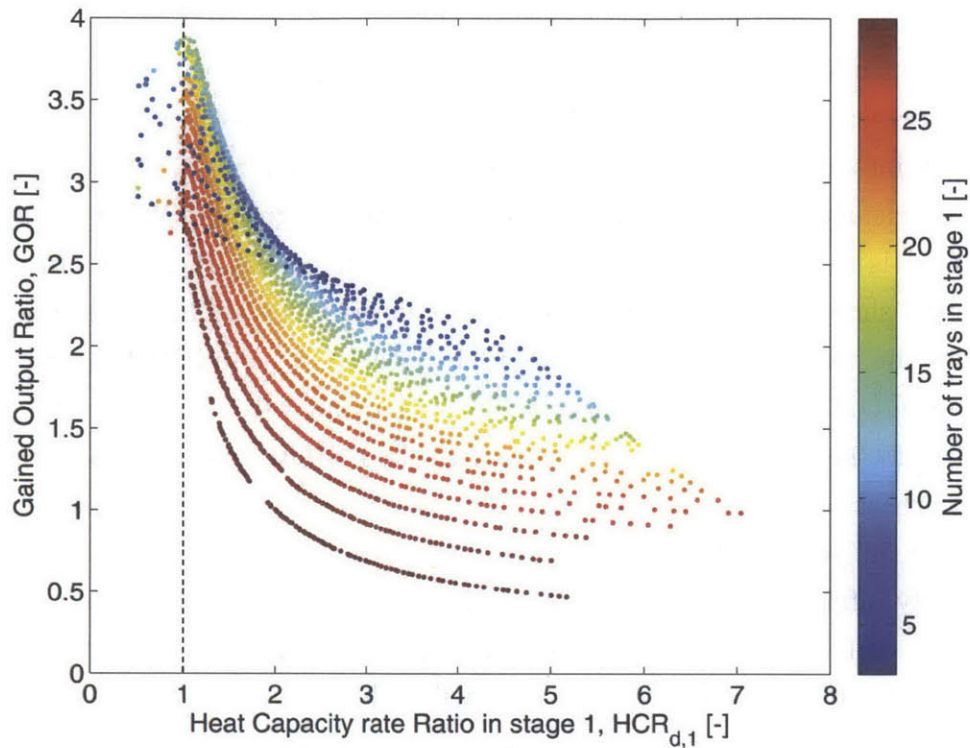
(a) Variation of GOR with $HCR_{d,1}$.
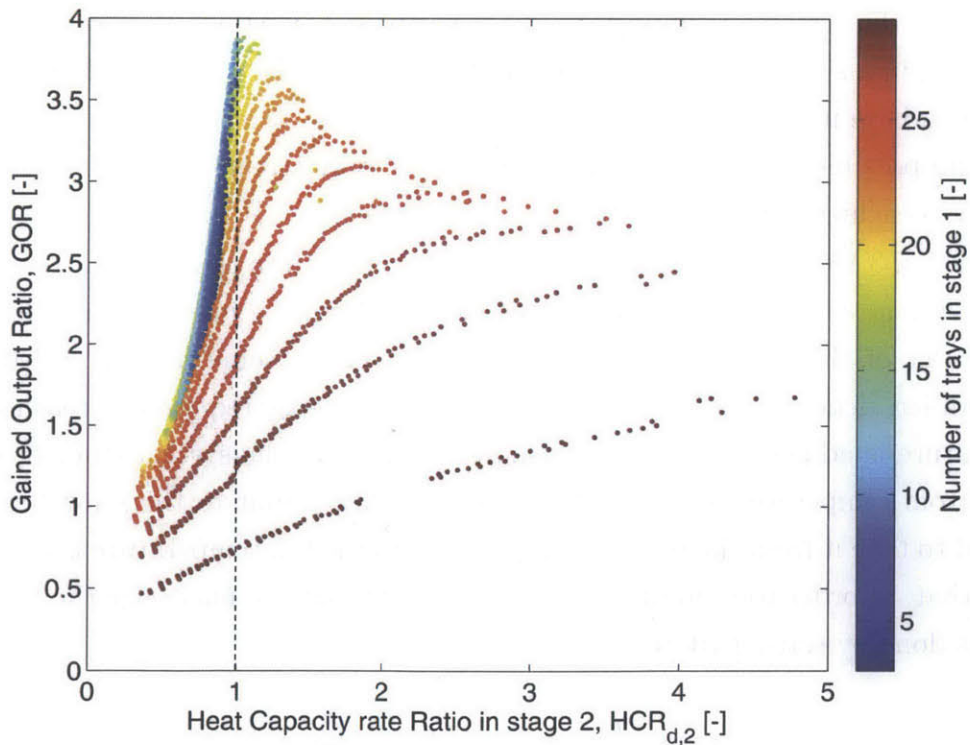
(b) Variation of GOR with $HCR_{d,2}$.

Figure 3-16: Variation of GOR with $HCR_{d,1}$ and $HCR_{d,2}$.
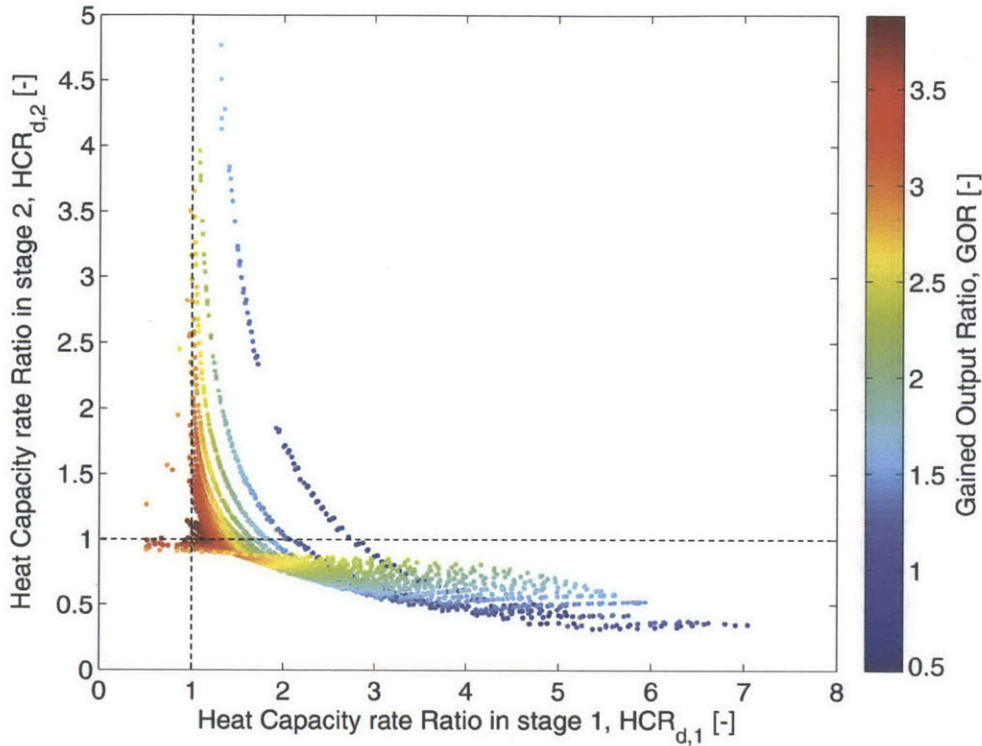
Figure 3-17: Variation of GOR with $HCR_{d,1}$ and $HCR_{d,2}$.

like the one studied here. If the flow rates are picked such that the system is not thermodynamically balanced, the stream with the lower heat capacity rate will reach a temperature close to that of the other stream. Knowing that the rate of heat and mass transfer is proportional to the driving force (ΔT for heat transfer and $\Delta \omega$ for mass transfer), the area at the end of the exchanger where the stream with the higher heat capacity rate enters will not result in a large heat and mass transfer since the driving force at that area will be small. If the system is balanced properly, the driving force will be kept relatively stable throughout the exchanger, and the total heat duty will be maximized.

Figure 3-18 shows the variation of GOR with $HCR_{h,1}$ and $HCR_{h,2}$. It is clear that HCR_h does not have an important effect on the performance of the system, and that HCR_d is the parameter that should be set to unity. As explained in Section 3.2.1, balancing the humidifier will cause great imbalance in the dehumidifier, causing the performance of the system to drop, whereas balancing the dehumidifier from a control volume perspective has little negative effect on the humidifier, and therefore serves to maximize the performance of the system.

Figure 3-19 shows the variation of GOR with recovery ratio. It can be clearly seen that GOR and RR vary in the same direction, meaning that optimizing operation

77
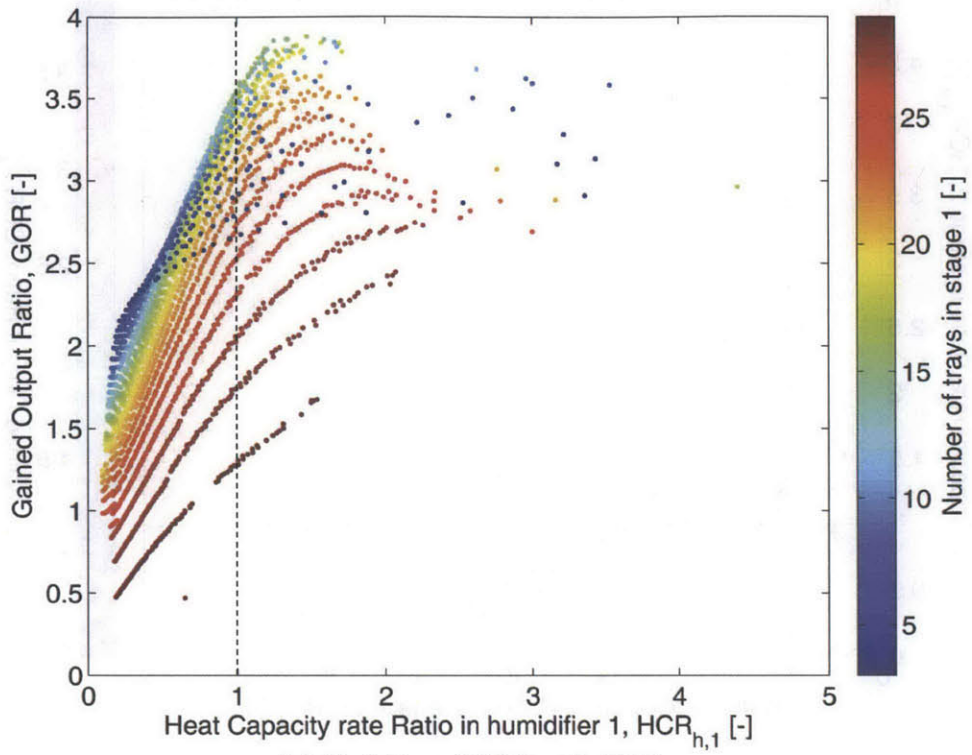
(a) Variation of GOR with $HCR_{h,1}$.
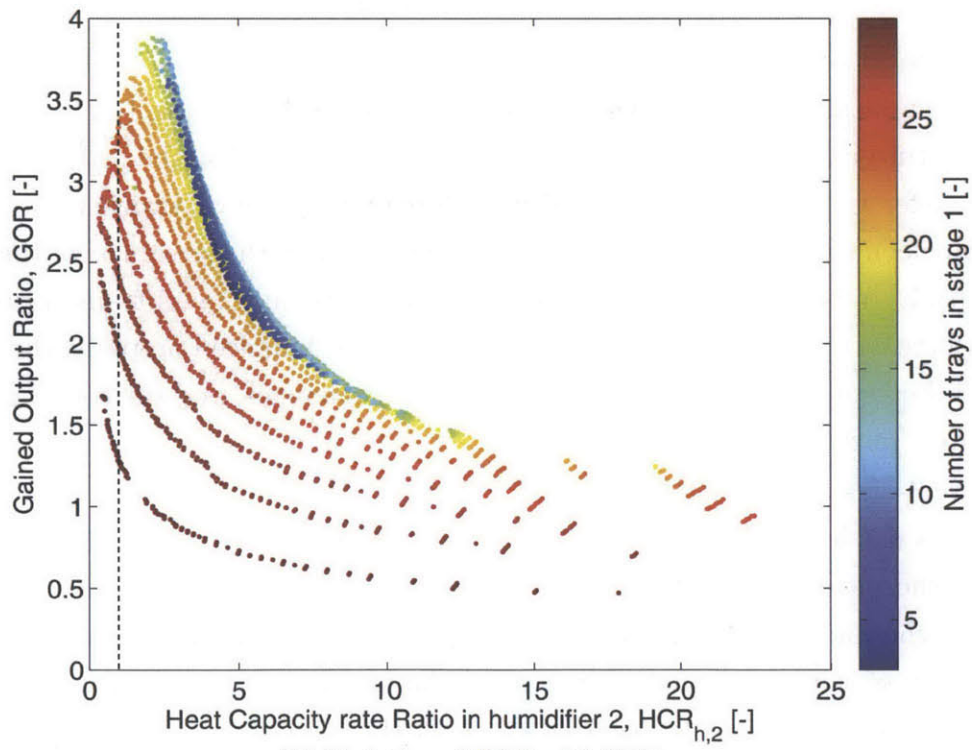
(b) Variation of GOR with $HCR_{h,2}$.

Figure 3-18: Variation of GOR with $HCR_{h,1}$ and $HCR_{h,2}$.
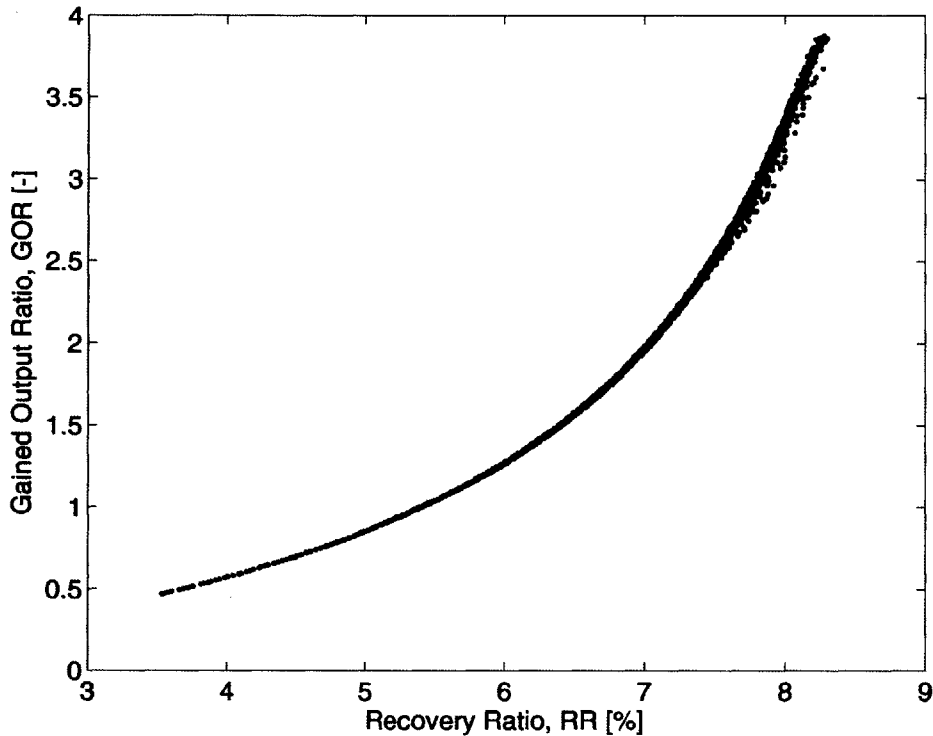
Figure 3-19: Variation of GOR with RR.

for energy efficiency will also maximize water production. The reason behind this agreement can be explained by looking back at Eq. 3.15. As explained above, GOR is maximized by minimizing the heat input, which is done by maximizing the heat duty. The heat duty is the same in the humidifier, where the air is heated and humidified. The larger the heat duty, the larger the flow rate of moist air, and the wider the range between the bottom and top air temperatures. Both of these consequences translate into a higher water production in the system. From a design perspective, this means that there is only one operating point that maximizes both the energy efficiency and the recovery ratio.

The highest GOR that could be reached with this available area without any extraction was 2.4, and this value was raised by 63% to 3.9 by using a single extraction. Similarly, the recovery ratio was increased from 7.4% to 8.2% due to the extraction.

3.3.2   Effect of location of extraction on performance

Figure 3-20 shows the variation of $HCR_{d,1}$ and $HCR_{d,2}$ with the number of trays in stages 1, $N_{t,1}$, or the location of the extraction. As shown in Section 3.3.1, it is desired to operate with the mass flow rates of dry air that result in $HCR_{d,1} =$

79

$HCR_{d,2} = 1$. As shown in Fig. 3-20, this is only possible at some of the locations of extraction, and possibly only at a single location of extraction. If only a small area is allotted to the first stage, we can see that this will result at best in $HCR_{d,1} = 1$ but $HCR_{d,2} < 1$. Similarly, if a very large area is allotted to the first stage, the best we can get is $HCR_{d,1} = 1$ but $HCR_{d,2} > 1$, or $HCR_{d,2} = 1$ but $HCR_{d,1} > 1$. In order to achieve complete balancing of the two stages, we need to choose the correct location of extraction, which will be a central location. In this study, the highest GOR was achieved by choosing $N_{t,1} = N_{t,2} = 15$, but one system size is not enough to make a conclusion regarding the exact relative location of the extraction.
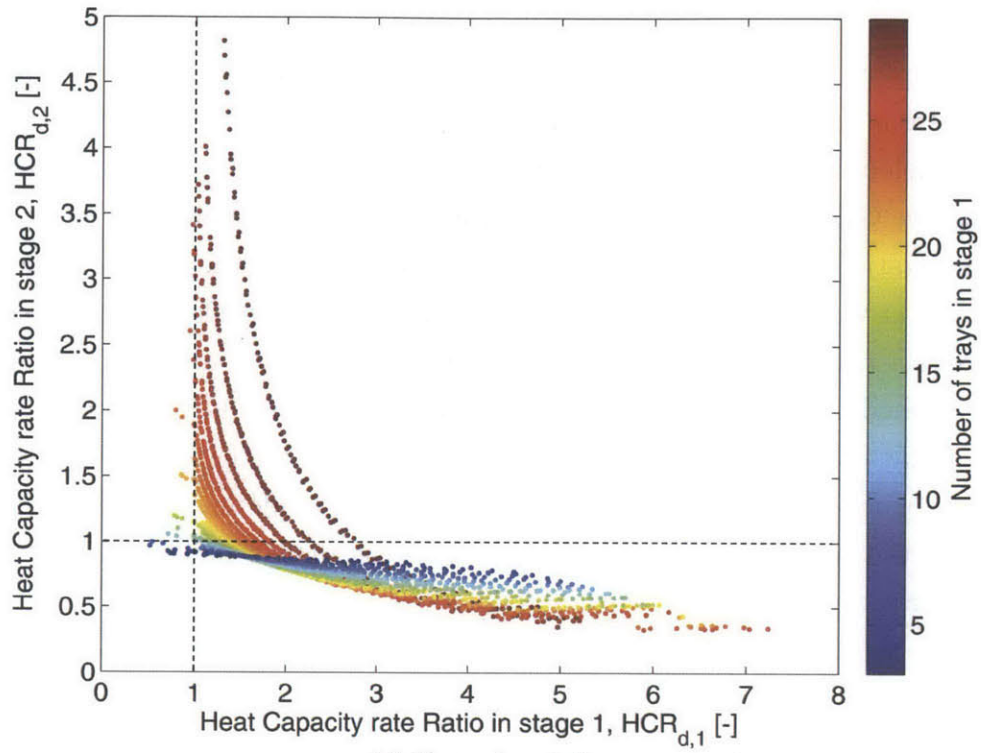
(a) General variation.
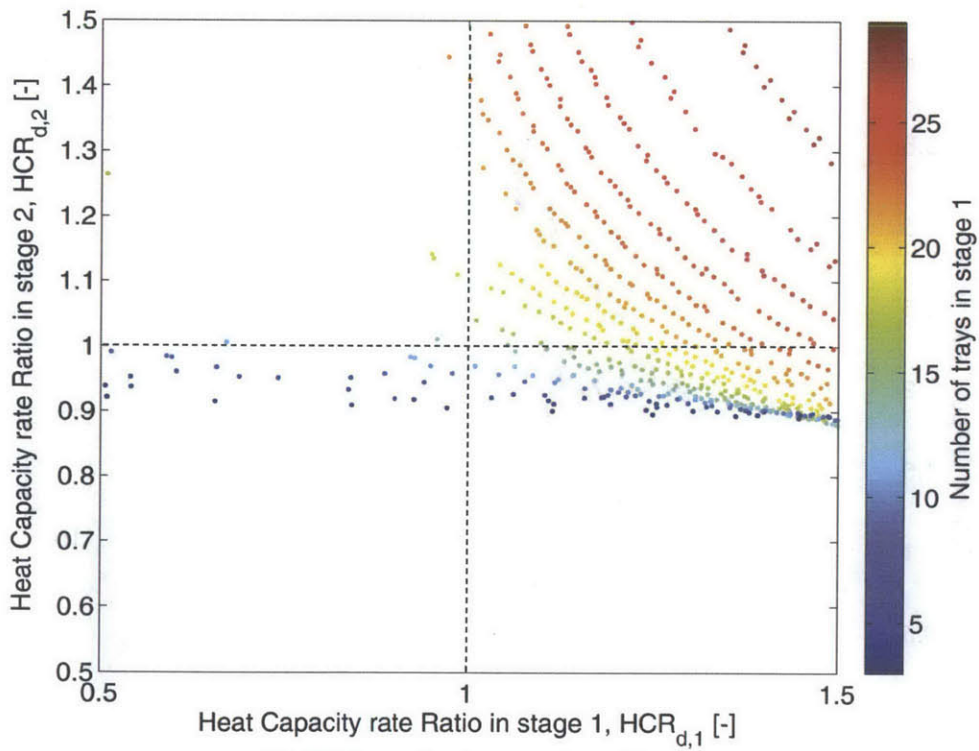
(b) With emphasis on region of interest.

Figure 3-20: Variation of $HCR_{d,1}$ and $HCR_{d,2}$ with the number of trays in stages 1 (location of extraction).

3.3.3 Direction of extraction

Figure 3-21 plots the GOR of the various operating points against the amount of air extracted from the humidifier to the dehumidifier. From this graph, it is clear that for the same location of extraction (represented by the color of the points), and for all locations, the GOR of a system with an extraction from the dehumidifier to the humidifier (negative value of amount extracted in the correct direction) is always worse than a system without extraction. This means that it is always more advantageous to not extract rather than extract in the wrong direction. A better performance can only be reached by extracting air from the humidifier to the dehumidifier.

This result can be explained by considering the heat capacities of water and saturated air (where $c_{\mathrm{p}} = \frac{\mathrm{d}h}{\mathrm{d}T}$). We first note that the specific heat of water is almost constant in the range of operation of HDH, whereas that of moist air varies greatly with temperature:

$$h_{\mathrm{a}}^* = h_{\mathrm{da}} + \omega h_{\mathrm{v}} \tag{3.16}$$

$$\frac{\mathrm{d}h_{\mathrm{a}}^*}{\mathrm{d}T} = c_{\mathrm{p,da}} + \frac{\mathrm{d}\left(\omega h_{\mathrm{v}}\right)}{\mathrm{d}T} \tag{3.17}$$
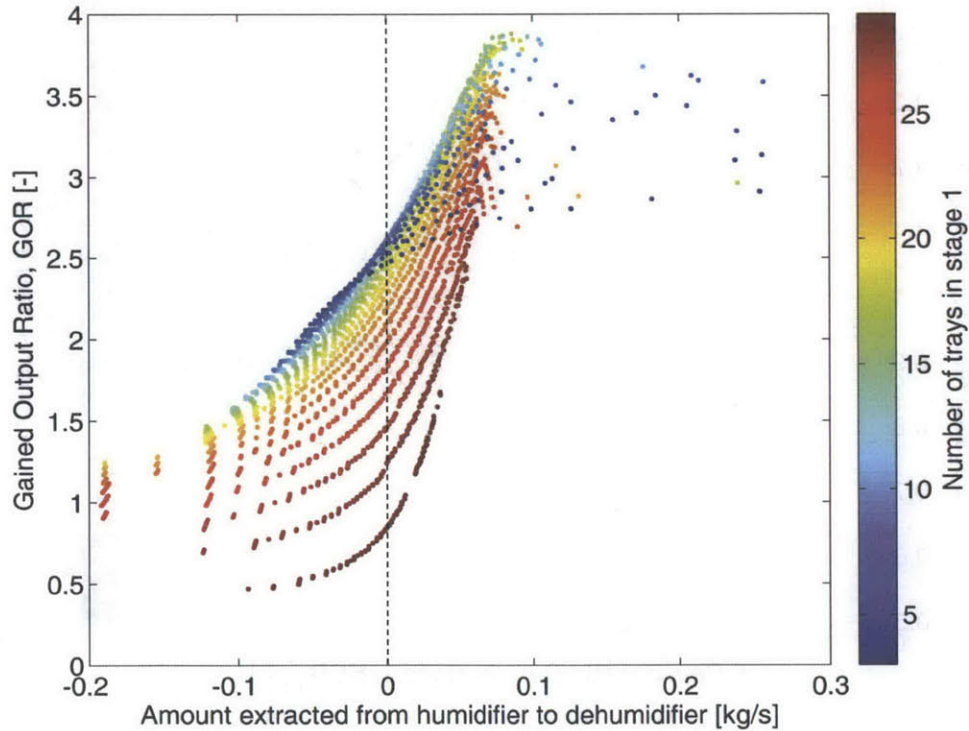
Figure 3-21: Variation of GOR with the amount extracted from humidifier to dehumidifier. Note that negative values indicate amount extracted in the other direction.

since the absolute humidity, ω varies exponentially with temperature. Given that we want to balance the total heat capacity rates of water and moist air, we need:

$$\dot{m}_{\mathrm{da}}\frac{\mathrm{d}h_{\mathrm{a}}^{*}}{\mathrm{d}T} = \dot{m}_{w}\frac{\mathrm{d}h_{w}}{\mathrm{d}T} \tag{3.18}$$

$$\mathrm{MR} = \frac{\dot{m}_{w}}{\dot{m}_{\mathrm{da}}} = \frac{1}{c_{\mathrm{p,w}}} \times \frac{\mathrm{d}h_{\mathrm{a}}^{*}}{\mathrm{d}T} \tag{3.19}$$

Given that $\frac{\mathrm{d}h_{\mathrm{a}}^{*}}{\mathrm{d}T}$ increases with temperature whereas c_{p} of water remains constant, the mass flow rate ratio has to increase with temperature in order to reach a better balanced system. This can be done by extracting either air or water from the humidifier to the dehumidifier so that the water-to-air mass flow rate ratio is lower in the colder stages.

Previous attempts to balance HDH systems with the closed-air, open-water, water-heated configuration might have resulted in cases where it was more beneficial to extract air or water from the dehumidifier to the humidifier [13, 39]. This was possible because the flow rates in the bottom stage were fixed at values that are essentially very far from the optimum, and extracting in the wrong direction would make the system perform better. This does not mean that the extraction in that direction is generally correct. It only means that extracting in that direction made the performance better for the specific flow rates that were fixed in the first stage. In fact, for that exact system, a much higher performance could be achieved by choosing the correct mass flow rates in both stages instead of fixing a single stage and varying the other stage. The flow rates in both stages must be treated as variables if overall optimal performance is to be reached. As seen in this chapter, the two stages are very interconnected, and the best system performance can only be achieved by simultaneously varying the flow rates in both stages.

To better visualize this idea, we consider the temperature-enthalpy profiles presented Fig. 3-22. Figure 3-22(a) presents the temperature-enthalpy profile for a system with an air extraction form the dehumidifier to the humidifier, resulting in a GOR of 2.0. If the system was operated at the mass flow rate ratio of the first stage without extraction, the system would achieve a GOR of 1.4. This is one case where extracting from the dehumidifier to the humidifier achieves a better performance, which could lead to the conclusion that it might be beneficial to extract in that direction. However, the same system could achieve a GOR of 2.4 by operating without extraction but with a proper mass flow rate ratio, as shown in Fig. 3-8(b), and the

performance could be improved even further by extracting air from the humidifier to the dehumidifier, resulting in the profile shown in Fig. 3-22(b), and a GOR of 3.9. Comparing the profiles presented in Fig. 3-22 leads to the conclusion that it is always desirable to extract from the humidifier to the dehumidifier. The values of the mass flow rate ratio in the two stages that gave the best performance for this system were $MR_1 = 2.4$ and $MR_2 = 8.9$. We note that for the case of no extraction the mass flow rate ratio that resulted in a balanced system was $MR = 4.2$. This proves that in going from a balanced system without extraction to a balanced system with a single extraction we must vary the flow rates in both stages, with the mass flow rate ratio in the first stage being lower than the case of no extraction, and the mass flow rate ratio in the second stage being higher than the case of no extraction.

An interesting conclusion that can be made from considering Fig. 3-22 is that better performance is achieved when the heat duty is better divided over the available area. In Fig. 3-22(a), the circles on the temperature profile of the air stream show the intermediate temperatures of the air stream between consecutive dehumidifier trays. At the cold end of the first stage, the spacing between the circles is very small, with some even overlapping, whereas, at the hot end of that stage, the spacing becomes much larger. This indicates that the trays at the cold end of the dehumidifier in the first stage achieve a very small heat duty since they only change the specific enthalpy of air by very small amounts, whereas the trays at the hot end are used to achieve much higher heat and mass transfer rates. This is due to the small driving force in the trays at the cold end. When the system is balanced properly, the trays used achieve comparable rates of heat and mass transfer throughout the system because the driving force is kept relatively constant. This can be seen in Fig. 3-22(b) with the circles almost equally spaced. This result is consistent with that reached in the fixed-effectiveness modeling presented in Chapter 2 concerning the equal division of the heat duty between stages. For stages with the same enthalpy pinch, that result translates roughly to requiring a relatively constant heat duty per unit available area throughout the system, which, assuming the heat and mass transfer coefficients are constant, means that the driving force is kept relatively stable. Therefore, an easy way to measure experimentally if the system is well balanced is by comparing the heat duty per unit area achieved at different locations in the system.
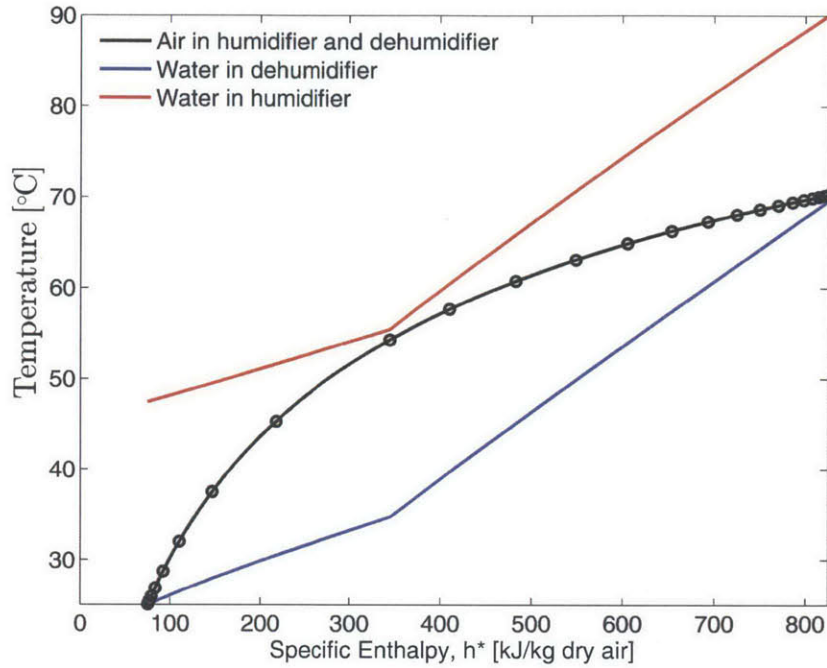
(a) Temperature-enthalpy profile for $MR_1 = 7.6$, $MR_2 = 3.0$. GOR $= 2.0$, RR $= 7.0\%$.
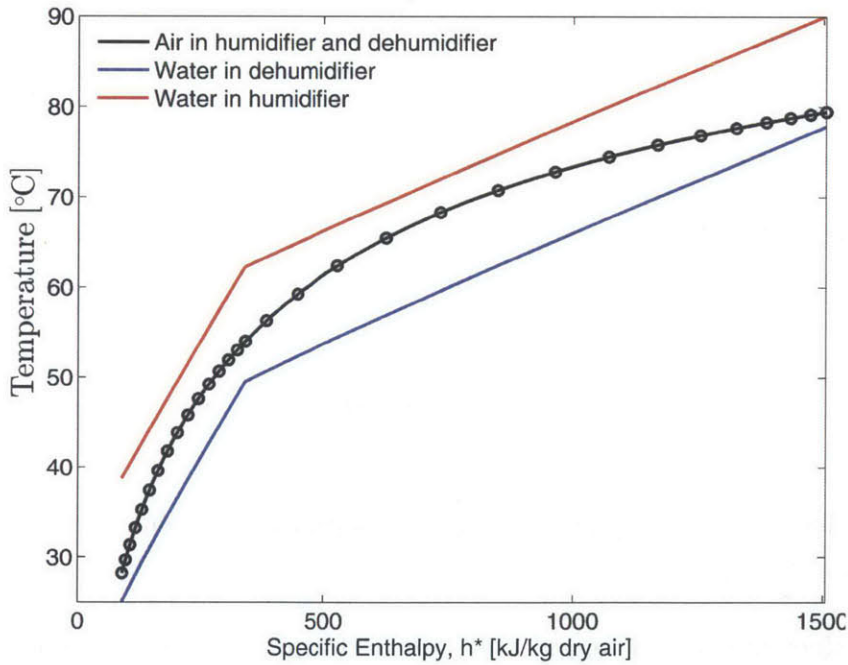
(b) Temperature-enthalpy profile for $MR_1 = 2.4$, $MR_2 = 8.9$. GOR $= 3.9$, RR $= 8.2\%$.

Figure 3-22: Temperature-enthalpy profiles of a system with (a) an extraction from the dehumidifier to the humidifier, and (b) an extraction from the humidifier to the dehumidifier. The dimensions of both systems are summarized in Table 3.1, and the extraction is such that $N_{t,1} = N_{t,2} = 15$.

3.4 Conclusions

This chapter presents a robust solution algorithm for a transport model of a complete HDH system with and without extraction/injection. The effects of operating in off-design conditions have been studied, and optimal mass flow rate ratios have been suggested for various top and bottom temperatures. The main conclusions drawn from this chapter are the following:

1. Thermodynamically balancing an HDH system of fixed area and without extraction is done by setting $HCR_d = 1$ and maximizes energy efficiency and water recovery.

2. HCR_h is not a useful predictor of system performance since its effect is masked by HCR_d.

3. A better balanced HDH system can be achieved by extracting air or water from the humidifier to the dehumidifier and setting $HCR_{d,1} = HCR_{d,2} = 1$.

4. The extractions in an HDH system should always be from the humidifier to the dehumidifier.

5. The location of the extraction is essential in achieving a balanced system, as only central locations make complete balancing possible.

6. It is recommended to implement a control system that varies the mass flow rate ratio in order to keep the system balanced in off-design conditions, especially with varying top temperature.

7. Better system performance is achieved when the heat duty is equally divided over the available area.

8. The effect of thermodynamic balancing is much larger on energy efficiency than on water recovery.

9. The effect of the top temperature on performance is much larger than that of the bottom temperature.

In addition, a physical explanation of the requirement that $HCR_{d,1} = HCR_{d,2} = 1$ is given.

Chapter 4

Recommendations

The work presented in Chapter 2 outlines a procedure for calculating the limits on the performance of HDH systems with a specified enthalpy pinch and a number of extractions/injections. It shows the improvement that can be made on the performance of a system through extractions/injections. In addition, it presents the range of optimal mass flow rate ratios in each stage which is essential in the understanding of balancing.

Chapter 3 presents algorithms for modeling HDH systems without extraction and with a single extraction. The algorithms presented are robust and can therefore simulate complex systems that would otherwise be impossible to simulate using simultaneous equation solvers. In addition, Chapter 3 specifies the condition of a balanced system with a single extraction and a fixed area as $HCR_{d,1} = HCR_{d,2} = 1$ and provides a physical explanation of why this is true.

4.1 Future work

4.1.1 Design procedure

The fixed-area model developed in Chapter 3 of this thesis can be used to simulate systems of various areas under various operating conditions. It can therefore be used in designing systems for specific water production needs. What is needed in addition to this working model is a clear design procedure that takes into account the desired water production rate, and determines the optimal use of component size.

87

4.1.2 Multiple extractions

The algorithms used in this study for systems of no extraction and single extraction can be extended to accommodate systems of multiple extractions. For a system of fixed area, the model for multiple extractions, along with a cost analysis can determine the optimal number of extractions to be implemented in the system.

4.1.3 Achieving a balanced system experimentally

The model presented in Chapter 3 of this study uses an HDH system that consists of a packed-bed humidifier and a multi-tray bubble column dehumidifier; however, the algorithms used to model systems without extraction and with a single extraction can be used for systems consisting of different component types. The model can therefore be used to understand the effect of the mass flow rates of air and water in the different stages on the temperatures of air and water at various locations in the system, which could be used to outline a procedure that can be used to experimentally determine the mass flow rates that result in a fully balanced system. This allows the operator to implement a control system that measures the temperatures of the streams at various locations, and vary the mass flow rates to achieve a balanced system. The same control system can then be implemented in the final design to account for variable conditions.

Appendix A

Solution algorithm for the fixed-effectiveness modeling
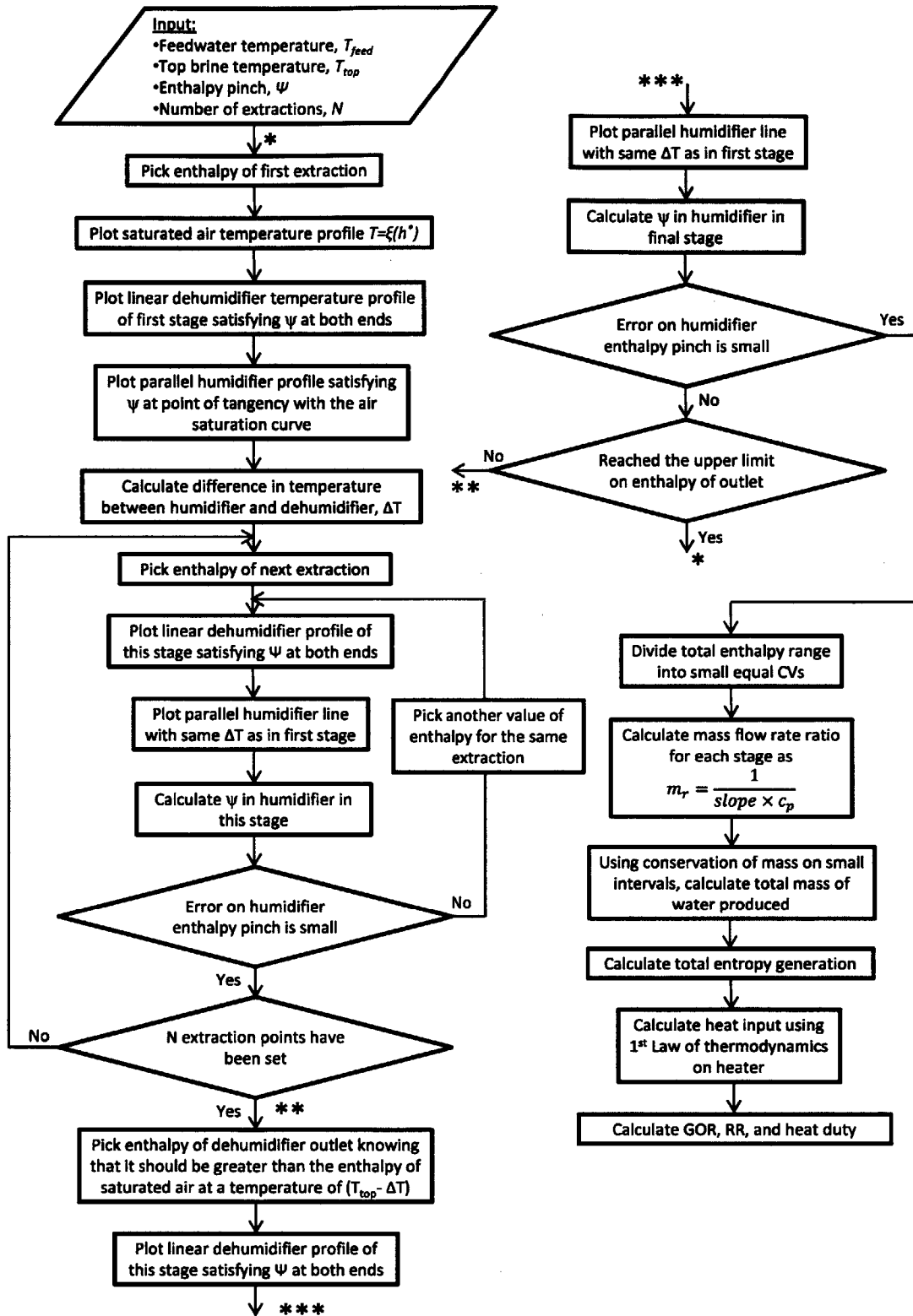
Figure A-1: Solution algorithm used in the fixed-effectiveness modeling presented in Chapter 2

Appendix B

Equations used in modeling the humidifier and dehumidifier

B.1 Bubble column dehumidifier

The following are the correlations used to model the resistances in the bubble column dehumidifier model:

For the outer resistance, $R_{\text{out}} = \frac{1}{h_t A_{out}}$, we used the correlation by Deckwer [32] in dimensional form, where h_t is the heat transfer coefficient:

$$h_t = 0.1 k_f^{1/2} \rho_f^{3/4} c_{p,f}^{1/2} \mu_f^{-1/4} g^{1/4} V_g^{1/4} \tag{B.1}$$

For the inner resistance, R_{in}, we used the correlations by Mori and Nakayama [33, 34]. In the laminar regime:

$$Nu_{\text{D}} = \frac{h_t D_{\text{in}}}{k} = 0.8636 \frac{K^{1/2}}{Z} \tag{B.2}$$

$$K = Re \left(\frac{D_{\text{in}}}{D_{\text{coil}}} \right)^{1/2} \tag{B.3}$$

$$Z = \frac{2}{11} \left(1 + \sqrt{1 + \frac{77}{4} Pr^{-2}} \right) \tag{B.4}$$

In the turbulent regime:

$$Nu_{\text{D}} = \frac{h_t D_{\text{in}}}{k} = \frac{1}{41} Pr^{0.4} Re^{5/6} \left(\frac{D_{\text{in}}}{D_{\text{coil}}} \right)^{1/12} \left\{ 1 + \frac{0.061}{\left[Re \left(\frac{D_{\text{in}}}{D_{\text{coil}}} \right)^{2.5} \right]^{1/6}} \right\} \tag{B.5}$$

B.2 Packed-bed humidifier equations

This section summarizes the equations used in modeling the packed-bed humidifier. These equations are taken from the work by Kloppers and Kröger [36], and describe the Poppe and Rögener model [35]. The solution procedure was also taken from Kloppers and Kröger [36], and greater detail can be found in Klopper's doctoral thesis [37].

B.2.1 Unsaturated air

The Lewis factor according to Bosnjakovic [40]:

$$Le_{\mathrm{f}} = 0.865^{0.667} \left(\frac{\omega_{\mathrm{sw}} + 0.622}{\omega + 0.622} - 1 \right) \left[\ln \left(\frac{\omega_{\mathrm{sw}} + 0.622}{\omega + 0.622} \right) \right]^{-1} \tag{B.6}$$

The variation of h_{a} with T_{w}, denoted in Chapter 3 as f_1:

$$\frac{\mathrm{d}h_{\mathrm{a}}}{\mathrm{d}T_{\mathrm{w}}} = \frac{\dot{m}_{\mathrm{w}} c_{\mathrm{p,w}}}{\dot{m}_{\mathrm{a}}}$$
$$\times \left(1 + \frac{(\omega_{\mathrm{sw}} - \omega)\, c_{\mathrm{p,w}} T_{\mathrm{w}}}{h_{\mathrm{a,sw}} - h_{\mathrm{a}} + (Le_{\mathrm{f}} - 1)\, [h_{\mathrm{a,sw}} - h_{\mathrm{a}} - (\omega_{\mathrm{sw}} - \omega)\, h_{\mathrm{v}}] - (\omega_{\mathrm{sw}} - \omega)\, c_{\mathrm{p,w}} T_{\mathrm{w}}} \right) \tag{B.7}$$

The variation of ω with T_{w}, denoted in Chapter 3 as f_2:

$$\frac{\mathrm{d}\omega}{\mathrm{d}T_{\mathrm{w}}} = \frac{\dot{m}_{\mathrm{w}} c_{\mathrm{p,w}}}{\dot{m}_{\mathrm{a}}}$$
$$\times \frac{\omega_{\mathrm{sw}} - \omega}{h_{\mathrm{a,sw}} - h_{\mathrm{a}} + (Le_{\mathrm{f}} - 1)\, [h_{\mathrm{a,sw}} - h_{\mathrm{a}} - (\omega_{\mathrm{sw}} - \omega)\, h_{\mathrm{v}}] - (\omega_{\mathrm{sw}} - \omega)\, c_{\mathrm{p,w}} T_{\mathrm{w}}} \tag{B.8}$$

The variation of Me with T_{w}, denoted in Chapter 3 as f_3:

$$\frac{\mathrm{d}Me}{\mathrm{d}T_{\mathrm{w}}} = \frac{c_{\mathrm{p,w}}}{h_{\mathrm{a,sw}} - h_{\mathrm{a}} + (Le_{\mathrm{f}} - 1)\, [h_{\mathrm{a,sw}} - h_{\mathrm{a}} - (\omega_{\mathrm{sw}} - \omega)\, h_{\mathrm{v}}] - (\omega_{\mathrm{sw}} - \omega)\, c_{\mathrm{p,w}} T_{\mathrm{w}}} \tag{B.9}$$

The subscript 'sw' means that the property is evaluated at saturation at the water temperature.

B.2.2 Supersaturated air

Lewis factor according to Bosnjakovic [40]

$$Le_{\mathrm{f}} = 0.865^{0.667} \left(\frac{\omega_{\mathrm{sw}} + 0.622}{\omega_{\mathrm{sa}} + 0.622} - 1 \right) \left[\ln \left(\frac{\omega_{\mathrm{sw}} + 0.622}{\omega_{\mathrm{sa}} + 0.622} \right) \right]^{-1} \qquad (\mathrm{B.10})$$

$$X = h_{\mathrm{a,sw}} - h_{\mathrm{a,ss}} + (Le_{\mathrm{f}} - 1) \left[h_{\mathrm{a,sw}} - h_{\mathrm{a,ss}} - (\omega_{\mathrm{sw}} - \omega_{\mathrm{sa}}) h_{\mathrm{v}} - (\omega_{\mathrm{sa}} - \omega) c_{\mathrm{p,w}} T_{\mathrm{w}} \right]$$
$$- (\omega_{\mathrm{sw}} - \omega) c_{\mathrm{p,w}} T_{\mathrm{w}}$$
$$(\mathrm{B.11})$$

f_1:

$$\frac{\mathrm{d} h_{\mathrm{a}}}{\mathrm{d} T_{\mathrm{w}}} = \frac{\dot{m}_{\mathrm{w}} c_{\mathrm{p,w}}}{\dot{m}_{\mathrm{a}}} \left(1 + \frac{(\omega_{\mathrm{sw}} - \omega_{\mathrm{sa}}) c_{\mathrm{p,w}} T_{\mathrm{w}}}{X} \right) \qquad (\mathrm{B.12})$$

f_2:

$$\frac{\mathrm{d} \omega}{\mathrm{d} T_{\mathrm{w}}} = \frac{\dot{m}_{\mathrm{w}} c_{\mathrm{p,w}}}{\dot{m}_{\mathrm{a}}} \left(\frac{\omega_{\mathrm{sw}} - \omega_{\mathrm{sa}}}{X} \right) \qquad (\mathrm{B.13})$$

f_3:

$$\frac{\mathrm{d} Me}{\mathrm{d} T_{\mathrm{w}}} = \frac{c_{\mathrm{p,w}}}{X} \qquad (\mathrm{B.14})$$

The subscript 'sa' means that the property is evaluated at saturation at the air temperature, and the subscript 'ss' denotes supersaturation.

Appendix C

Solution algorithms for the fixed-area modeling

Inputs:
- Water inlet temperature, $T_{w,in}$
- Air inlet temperature, $T_{a,in}$
- Inlet condensate flow rate, $\dot{m}_{cond,in}$
- Dehumidifier geometry

Set $T_{high}=T_{a,in}$ and $T_{low}=T_{w,in}$

Set $T_{a,out,guess} = \dfrac{T_{high}+T_{low}}{2}$

Calculate $\dot{Q}_1$ from 1st Law of Thermodynamics

Calculate $T_{w,out}$ from $\dot{Q}_1$

Evaluate R_i, R_o

Calculate ΔT_{lm}

Calculate $\dot{Q}_2$

$\dot{Q}_1 \approx \dot{Q}_2$

No

$\dot{Q}_1 > \dot{Q}_2$

Yes

$T_{low}=T_{a,out,guess}$

No

$T_{high}=T_{a,out,guess}$

Yes

Outputs:
- Water outlet temperature, $T_{w,out}$
- Air outlet temperature, $T_{a,out}$
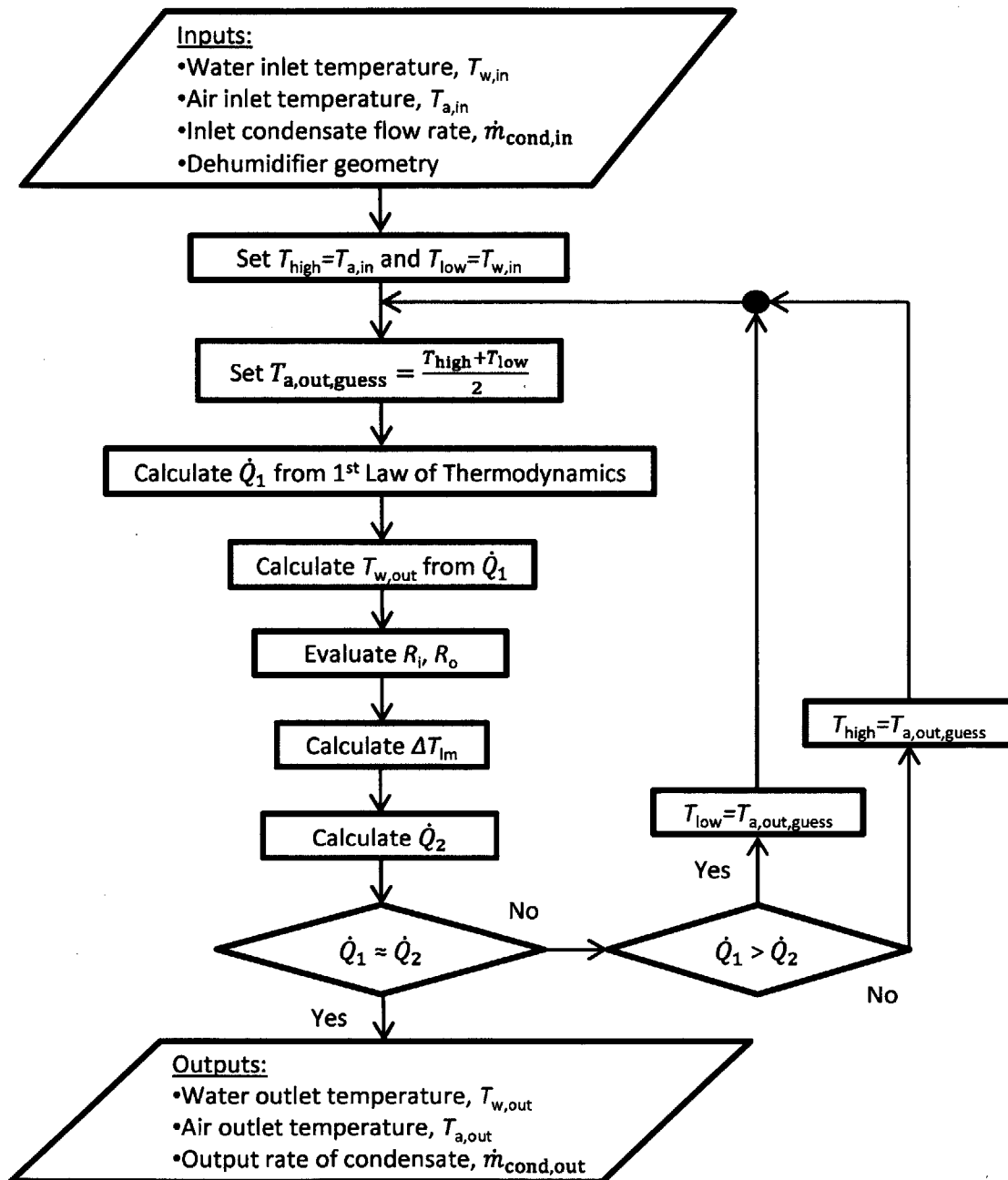- Output rate of condensate, $\dot{m}_{cond,out}$

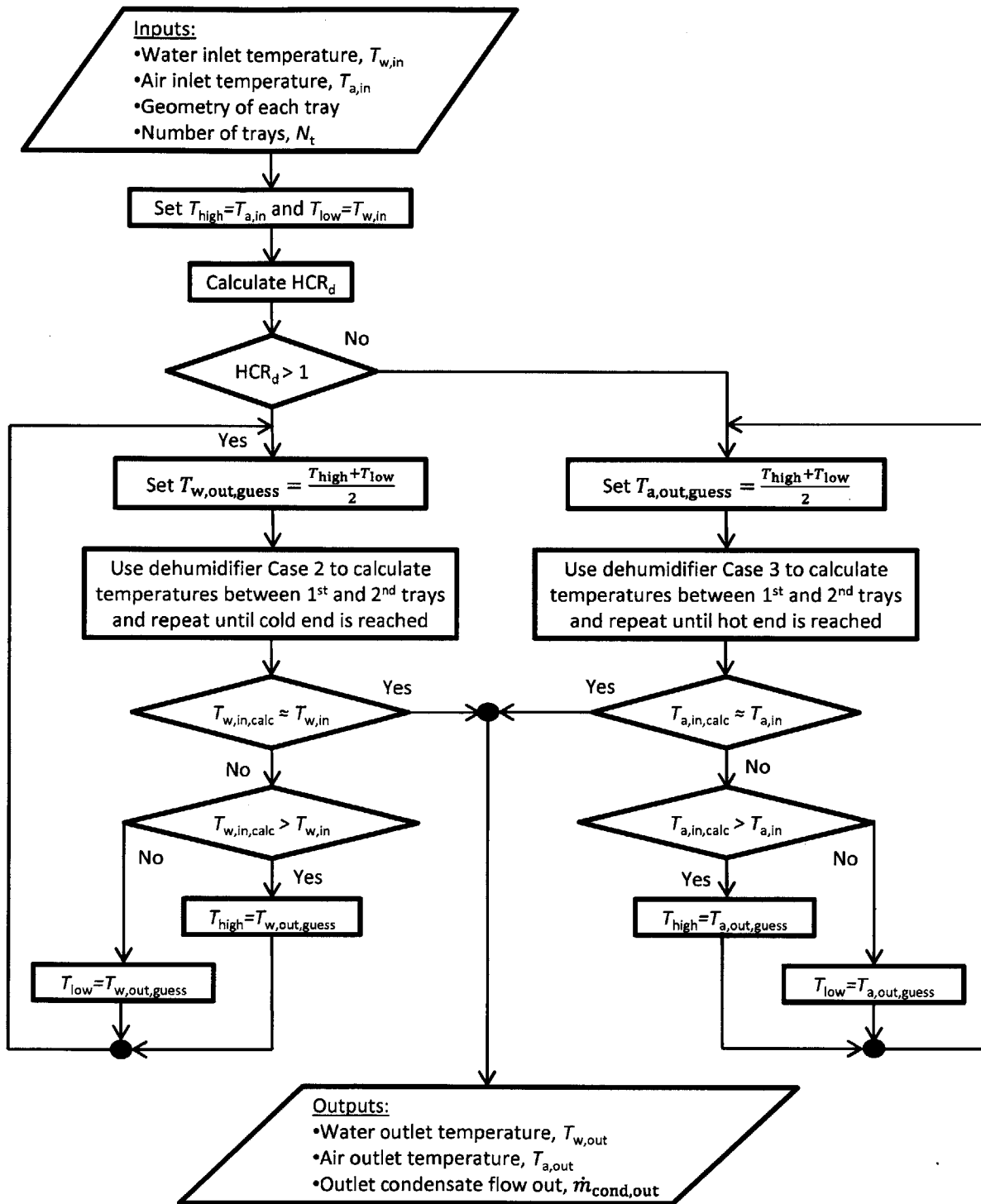Figure C-1: Solution algorithm for the bubble column dehumidifier.

Figure C-2: Solution algorithm for the multi-tray bubble column dehumidifier.
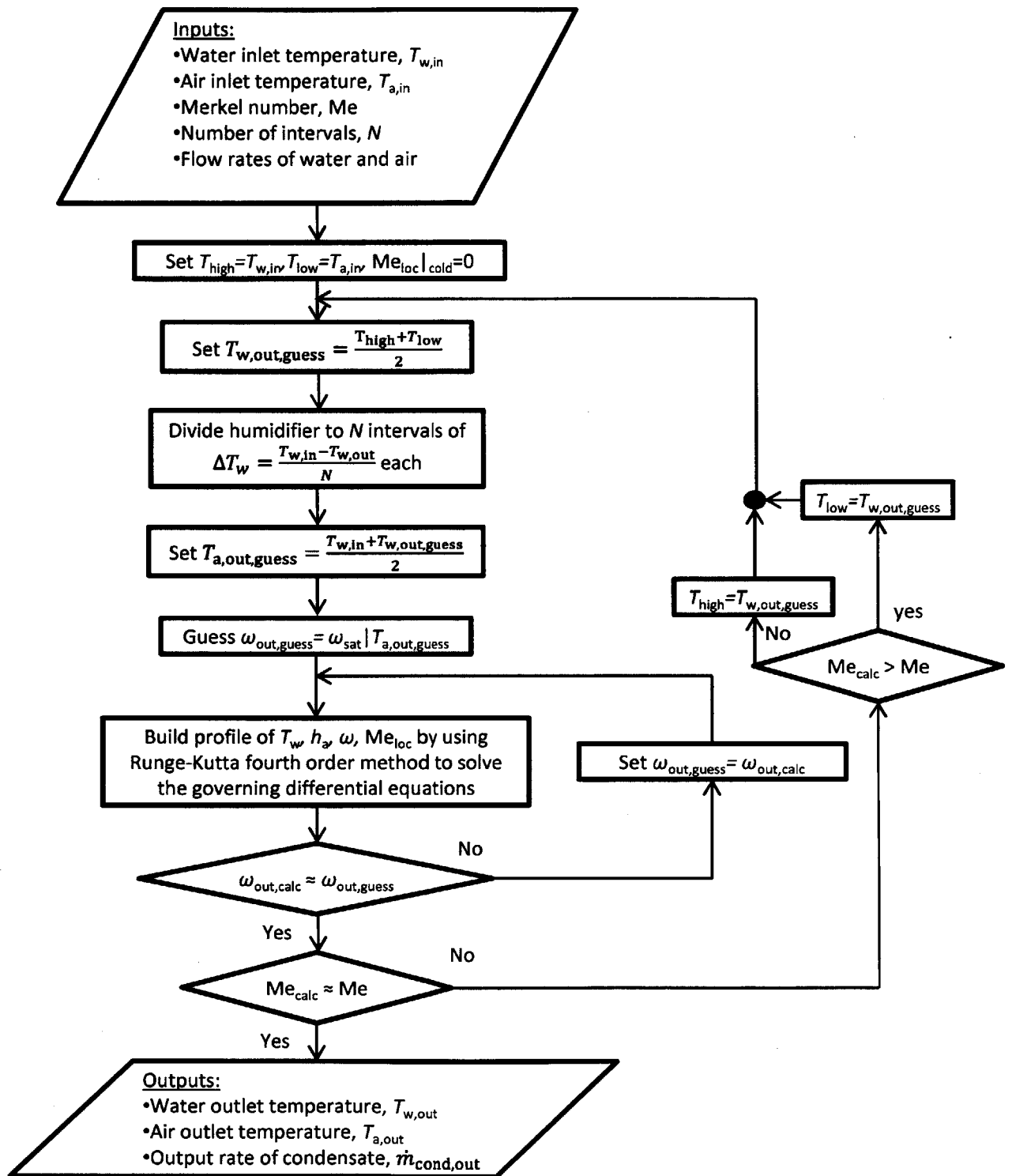
Figure C-3: Solution algorithm for the packed-bed humidifier.
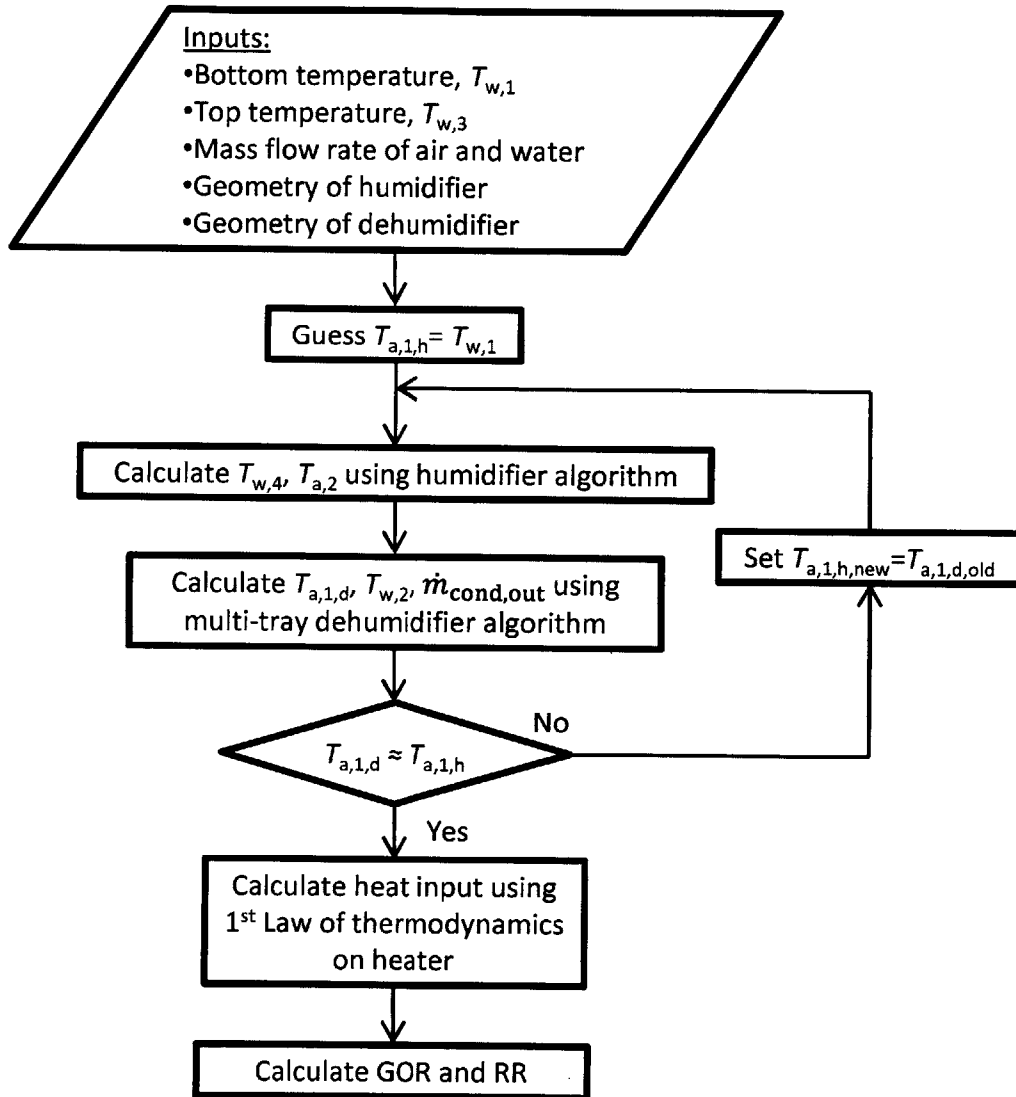
Figure C-4: Solution algorithm for the complete HDH system without extraction.

Inputs:
- Top temperature, T_{top}
- Bottom temperature, T_{bottom}
- Component areas
- Flow rate of water
- Location of extraction, $N_{t,1}$
- Intermediate water temperature, $T_{w,2}$

Set $\dot{m}_{da,2} = \dfrac{\dot{m}_{higher} + \dot{m}_{lower}}{2}$

Simulate top stage with N_0 function
Inputs: T_{top}, $T_{w,2}$, $\dot{m}_{da,2}$
Outputs: $T_{w,3}$, $T_{w,5}$, $T_{a,2}$, $T_{a,3}$

Find $\dot{m}_{da,1}$ that results in $T_{w,2}$ specified given $T_{a,2}$
and T_{bottom}
(this step can be made into a separate function)

Use humidifier function to calculate $T_{w,6}$ and
$T_{a,2b}$ given $T_{a,1}$, $\dot{m}_{da,1}$ and $T_{w,5}$

$\dot{m}_{lower} = \dot{m}_{da,2}$

$\dot{m}_{higher} = \dot{m}_{da,2}$

No

yes

$T_{a,2b} > T_{a,2}$

No

$T_{a,2b} \approx T_{a,2}$

Yes

Calculate performance parameters

Figure C-5: Solution algorithm for the complete HDH system with a single extraction.

100

Bibliography

[1] United Nations, *Millennium Development Goals Report 2013*. United Nations, New York, 2013.
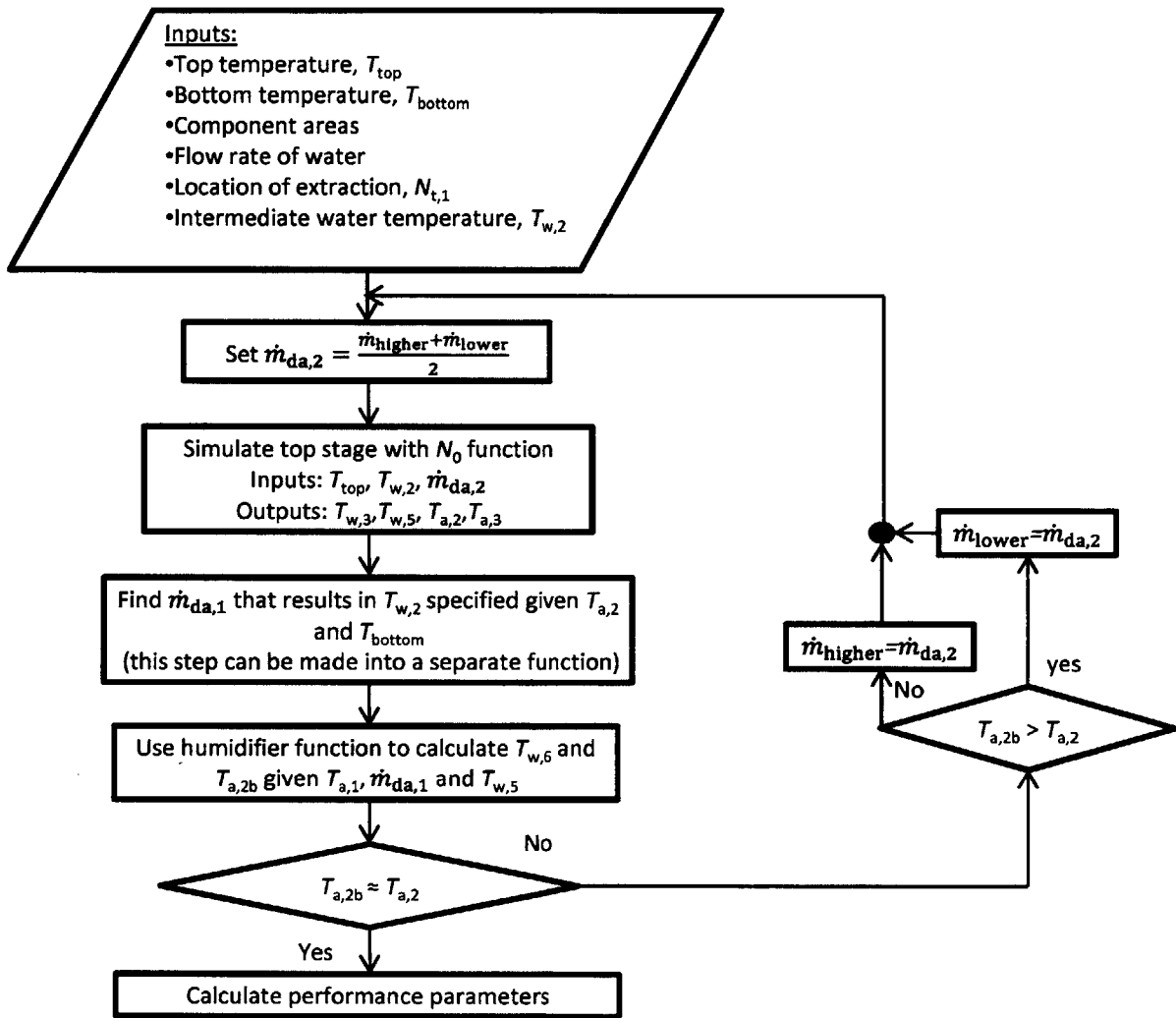
[2] J. Schewe, J. Heinke, D. Gerten, I. Haddeland, N. W. Arnell, D. B. Clark, R. Dankers, S. Eisner, B. M. Fekete, F. J. Colón-González, *et al.*, "Multimodel assessment of water scarcity under climate change," in *Proceedings of the National Academy of Sciences*, National Acad Sciences, 2013.

[3] S. Sherwood and Q. Fu, "A drier future?," *Science*, vol. 343, no. 6172, pp. 737–739, 2014.

[4] C. Prudhomme, I. Giuntoli, E. L. Robinson, D. B. Clark, N. W. Arnell, R. Dankers, B. M. Fekete, W. Franssen, D. Gerten, S. N. Gosling, *et al.*, "Hydrological droughts in the 21st century, hotspots and uncertainties from a global multimodel ensemble experiment," in *Proceedings of the National Academy of Sciences*, National Acad Sciences, 2013.

[5] International Desalination Association, IDA, *IDA desalination yearbook 2013-2014*. Media analytics Ltd., 2013.

[6] G. P. Narayan, M. H. Sharqawy, E. K. Summers, J. H. Lienhard V, S. M. Zubair, and M. A. Antar, "The potential of solar-driven humidification-dehumidification desalination for small-scale decentralized water production," *Renewable and Sustainable Energy Reviews*, vol. 14, pp. 1187–1201, 2010.

[7] G. P. Narayan, M. H. Sharqawy, J. H. Lienhard V, and S. M. Zubair, "Thermodynamic analysis of humidification dehumidification desalination cycles," *Desalination and Water Treatment*, vol. 16, pp. 339–353, 2010.

[8] K. Bourouni, M. Chaibi, and L. Tadrist, "Water desalination by humidification and dehumidification of air: state of the art," *Desalination*, vol. 137, pp. 167–176, 2001.

[9] G. P. Narayan and J. H. Lienhard V, "Humidification-dehumidification desalination," in *Desalination: Water from Water*, Salem, MA: Scrivener Publishing, 2014.

[10] H. Ettouney, "Design and analysis of humidification dehumidification desalination process," *Desalination*, vol. 183, no. 13, pp. 341 – 352, 2005.

[11] K. H. Mistry, A. Mitsos, and J. H. Lienhard V, "Optimal operating conditions and configurations for humidification-dehumidification desalination cycles," *International Journal of Thermal Sciences*, vol. 50, pp. 779–789, 2011.

[12] J. A. Miller, "Numerical balancing in a humdification dehumidification desalination system," Master's thesis, Massachusetts Institute of Technology, 2011.

[13] J. A. Miller and J. H. Lienhard V, "Impact of extraction on a humidification dehumidification desalination system," *Desalination*, vol. 313, pp. 87 – 96, 2013.

[14] G. P. Narayan, J. H. Lienhard V, and S. M. Zubair, "Entropy generation minimization of combined heat and mass transfer devices," *International Journal of Thermal Sciences*, vol. 49, pp. 2057–66, 2010.

[15] G. P. Narayan, K. H. Mistry, M. H. Sharqawy, S. M. Zubair, and J. H. Lienhard V, "Energy effectiveness of simultaneous heat and mass exchange devices," *Frontiers in Heat and Mass Transfer*, vol. 1, no. 2, pp. 1–13, 2010.

[16] H. Müller-Holst, *Solar thermal desalination using the Multiple Effect Humidification (MEH) method in Solar Desalination for the 21st Century*, ch. 15, pp. 215–25. NATO Security through Science Series, Springer, Dordrecht, 2007.

[17] H. Müller-Holst, *Mehrfacheffekt-Feuchtluftdestillation bei Umgebungsdruck - Verfahrensoptimierung und Anwendungen*. PhD thesis, Technische Universität Berlin, 2002.

[18] M. Zamen, S. M. Soufari, and M. Amidpour, "Improvement of solar humdification-dehumidification desalination using multi-stage process," *Chemical Engineering Transactions*, vol. 25, pp. 1091–1096, 2011.

[19] R. K. McGovern, G. P. Thiel, G. P. Narayan, S. M. Zubair, and J. H. Lienhard V, "Performance limits of zero and single extraction humidification-dehumidification desalination systems," *Applied Energy*, vol. 102, pp. 1081 – 1090, 2013.

[20] G. P. Thiel and J. H. Lienhard V, "Entropy generation in condensation in the presence of high concentrations of noncondensable gases," *International Journal of Heat and Mass Transfer*, vol. 55, pp. 5133–5147, May 2012.

[21] G. P. Narayan, K. M. Chehayeb, R. K. McGovern, G. P. Thiel, S. M. Zubair, and J. H. Lienhard V, "Thermodynamic balancing of the humidification dehumidification desalination system by mass extraction and injection," *International Journal of Heat and Mass Transfer*, vol. 57, pp. 756 – 770, 2013.

[22] G. P. Narayan, M. G. St. John, S. M. Zubair, and J. H. Lienhard V, "Thermal design of the humidification dehumidification desalination system: An experimental investigation," *International Journal of Heat and Mass Transfer*, vol. 58, pp. 740 – 748, 2013.

[23] G. P. Narayan, M. H. Sharqawy, S. Lam, S. K. Das, and J. H. Lienhard V, "Bubble columns for condensation at high concentrations of noncondensable gas: Heat-transfer model and experiments," *AIChE Journal*, vol. 59, no. 5, pp. 1780–1790, 2013.

[24] E. W. Tow and J. H. Lienhard V, "Experiments and modeling of bubble column dehumidifier performance," *International Journal of Thermal Sciences*, vol. 80, pp. 65 – 75, 2014.

[25] E. W. Tow and J. H. Lienhard V, "Analytical modeling of a bubble column dehumidifier," in *Proceedings of the ASME 2013 Summer Heat Transfer Conference*, no. HT2013-17763, Minneapolis, MN, July 2013.

[26] E. W. Tow and J. H. Lienhard V, "Heat flux and effectiveness in bubble column dehumidifiers for HDH desalination," in *IDA World Congress on Desalination and Water Reuse*, Tianjin, China, October 2013.

[27] M. H. Sharqawy, J. H. Lienhard V, and S. M. Zubair, "Thermophysical properties of seawater: A review of existing correlations and data," *Desalination and Water Treatment*, vol. 16, pp. 354–80, 2010.

[28] S. Pruss and W. Wagner, "The IAPWS formulation 1995 for the thermodynamic properties of ordinary water substance for general and scientific use," *Journal of Physical and Chemical Reference Data*, vol. 31, pp. 387–535, 2002.

[29] R. W. Hyland and A. Wexler, "Formulations for the Thermodynamic Properties of Dry Air from 173.15 K to 473.15 K, and of Saturated Moist Air From 173.15 K to 372.15 K, at Pressures to 5 MPa," *ASHRAE Transactions*, vol. Part 2A (RP-216), no. 2794, pp. 520–535, 1983b.

[30] D. J. Wessel, *ASHRAE Fundamentals Handbook 2001 (SI Edition)*. American Society of Heating, Refrigerating, and Air-Conditioning Engineers, 2001.

[31] E. W. Lemmon, M. L. Huber, and M. O. McLinden, "Standard reference database 23: Reference fluid thermodynamic and transport properties," tech. rep., NIST - REFPROP, Version 8.0 (2007).

[32] W.-D. Deckwer, "On the mechanism of heat transfer in bubble column reactors," *Chemical Engineering Science*, vol. 35, no. 6, pp. 1341–1346, 1980.

[33] Y. Mori and W. Nakayama, "Study on forced convective heat transfer in curved pipes: (1st report, laminar region)," *International Journal of Heat and Mass Transfer*, vol. 8, no. 1, pp. 67 – 82, 1965.

[34] Y. Mori and W. Nakayama, "Study of forced convective heat transfer in curved pipes (2nd report, turbulent region)," *International Journal of Heat and Mass Transfer*, vol. 10, no. 1, pp. 37–59, 1967.

[35] M. Poppe and H. Rögener, "Berechnung von rückkühlwerken," *VDI-Wärmeatlas*, vol. 111, pp. 1–15, 1991.

[36] J. Kloppers and D. Kröger, "A critical investigation into the heat and mass transfer analysis of counterflow wet-cooling towers," *International Journal of Heat and Mass Transfer*, vol. 48, no. 34, pp. 765 – 777, 2005.

[37] J. C. Kloppers, *A critical evaluation and refinement of the performance prediction of wet-cooling towers*. PhD thesis, Stellenbosch: University of Stellenbosch, 2003.

[38] K. M. Chehayeb, G. Prakash Narayan, S. M. Zubair, and J. H. Lienhard V, "Use of multiple extractions and injections to thermodynamically balance the humidification dehumidification desalination system," *International Journal of Heat and Mass Transfer*, vol. 68, pp. 422–434, 2014.

[39] G. P. Thiel, J. A. Miller, S. M. Zubair, and J. H. Lienhard V, "Effect of mass extractions and injections on the performance of a fixed-size humidification de-humidification desalination system," *Desalination*, vol. 314, pp. 50 – 58, 2013.

[40] F. Bosnjaković, *Technical thermodynamics*. Holt, Rinehart and Winston, 1965.